Journal of Applied Polymer Science

Preparation and characterization of thermoplastic water-borne polycarbonate-based polyurethane dispersions and cast films

Magdalena Serkis, Rafał Poręba, Jiří Hodan, Jana Kredatusová, Milena Špírková
Institute of Macromolecular Chemistry AS CR, Heyrovsky Sq.2, 162 06 Praha 6, Czech Republic
Correspondence to: M. Špírková (E-mail: spirkova@imc.cas.cz)

ABSTRACT: Stable water-borne polyurethane dispersions (PUDs) were prepared from bifunctional aliphatic polycarbonate-based macrodiol, 2,2-bis(hydroxymethyl)propionic acid (DMPA), 1,6-diisocyanatohexane, 1,4-butanediol (BD), and triethylamine. Water-borne dispersion particles are thus solely formed from self-assembled linear PU chains. Both PUDs and PUD-based films were characterized with regards to the concentration of DMPA (ionic species content) and BD (hard-segment content). Average particle size of PUDs decreased and their long-term stability increased with increasing DMPA and decreasing BD concentration. Functional properties of cast films made from PUDs are substantially influenced by the character of the original colloidal particle dispersions. The swelling behavior of the films, their surface morphology, and mechanical properties are more influenced by DMPA than BD contents. At DMPA concentrations higher than 0.2 mmol g^{-1} of the solid mass of polyurethane, distinct self-organization of individual nanoparticles into fibril-like structures was detected by atomic force microscopy and scanning electron microscopy. PU films made from PUD containing high BD as well as high DMPA concentrations have the best utility properties namely sufficient tensile properties and a very low swelling ability. © 2015 Wiley Periodicals, Inc. J. Appl. Polym. Sci. **2015**, *132*, 42672.

KEYWORDS: films; microscopy; nanoparticles; nanowires and nanocrystals; polyurethanes; structure–property relations

Received 15 April 2015; accepted 28 June 2015
DOI: 10.1002/app.42672

INTRODUCTION

Organic solvent-borne polymer dispersion systems used for surface coatings were widely produced and used in the past.[1,2] However, the evaporation of volatile organic compounds (VOCs) is the main problem for this type of applications. To reduce coating costs and eliminate VOCs to the atmosphere, organic solvents were replaced by water, the most environmentally friendly and cheapest medium.[3–5] Currently, aqueous polyurethanes have successfully filled up the applications areas previously reserved for organic solvent-borne polyurethanes. Because of the excellent adhesion to the substrate surface, high abrasion, and fouling resistance, the water-borne PUDs are now frequently used as flexible coatings for textile, wood, leather, and metal applications.[6–8] The size of the particles is a very important parameter because it controls the range of practical applications. Small particles are desired when a thorough and deep penetration of the dispersion into porous material is necessary. However, when a rapid drying is essential, relatively large particles are preferred.[9]

Water-borne PUDs are relatively complex systems, the behavior of which differ significantly from that of polyurethane elastomers (PUE), even though the basic components (i.e., macrodiol, chain extender, and diisocyanate) are very similar or in some cases the same as for PUE formulations. Unlike the solid PUEs, the water-borne PUDs are typical aqueous colloidal systems. Although all polyurethanes possess a number of highly polar urethane groups, they are basically hydrophobic and therefore they precipitate in water. There are two methods how to improve dispersibility of these materials in aqueous media: (i) using an external emulsifier or (ii) incorporating hydrophilic ionic groups into the polyurethane backbone. The main advantage of ionic group introduction into the polyurethane backbone is better stability of the charged polyurethane dispersions than that of systems containing the external emulsifiers.

The size of PU nanoparticles can be controlled by different factors. It strongly depends on temperature, rate of mixing, soft segment molecular weight, ionic group concentration, and the degree of neutralization.[4,9,10] It has been found that the chain hydrophilicity, which depends mainly on the number of ionic species (either cationic or anionic) in the molecular chain, decisively influences the particle size.[9] The hydrophobicity of the soft segment component[5,11] plays also a role, but its effect is much less pronounced.

Polyurethanes prepared from bifunctional diisocyanates, macrodiols (MD), and chain extenders (low-molecular weight diols) are linear block copolymers composed of soft (SS) and hard

(HS) segments. These products exhibit the thermoplastic behavior and have been used for a long time as elastomeric construction materials and soft coatings.[12] Their pronounced thermoplastic nature allows for easy processing, shaping, and forming by industrial processes like injection molding or extrusion. Also the simplicity of recycling and re-processing (compared to chemically cross-linked PU thermosets, more robust to recycling) belongs to their great benefits. Polyether-, polyester-, or polybutadiene-based macrodiols of MW 1000–5000 are frequently used as the components of soft segment which secure the flexibility of PU chains.[11–14] The hard segments acting as physical cross-linking sites reinforcing the PU chain are formed by the reaction of diisocyanates and low-molecular weight diols. It has been found that PUDs obtained from hydroxyl-based chain extenders are more flexible than those based on the corresponding amine based extender.[15]

Polycarbonate-based (PC) polyols which constitute the soft segments are a relatively new class of materials in the field of polyurethanes.[6,12,13,16–19] They are known to provide good weathering, fungi, and hydrolysis resistance and are at the same time highly biocompatible materials.[16] Until now, just a few studies of polycarbonates used as the soft segment components for the PUD preparation have been published.[6,16–19] However, in all these studies, the multifunctional chain extenders such as ethylenediamine, diethylenetriamine, or hydrazine were used which gave rise to branched or chemically cross-linked polymer structures.[8,17–21]

To our knowledge, no research has been performed on the preparation of thermoplastic water-borne PUDs based on PC macrodiol and bifunctional butane-1,4-diol as chain extender despite the fact that this type of PUs represents very attractive materials. To obtain the linear system, bifunctional butane-1,4-diol (BD), previously commonly applied in preparation of elastomers, was used as a chain extender. For the same reason 1,6-diisocyanatohexane (HDI) was used as a linear, aliphatic isocyanate compound. This choice of reactants secures the synthesis of recyclable PU materials*.

This article deals with the preparation and characterization of thermoplastic water-borne PUDs and cast films made from water-borne PUDs. The effect of polymer composition on the characteristics of the dispersions, mainly on the average particle size and long-term stability, is presented. The relationship between the properties of dispersions and resulting PU films, such as morphology, water absorption resistivity, and mechanical properties, is discussed and based the best candidates for practical use are subsequently selected.

*Unlike PU films made from "classical" thermoplastic PU elastomers, all PU films made from water-borne PUDs are fully soluble in polar solvents (acetone, tetrahydrofuran) at laboratory temperature. Acetone used for recycling of PUDs may be a technical solvent, which reduces the costs of re-processing. Moreover, after water addition into these PU solutions and after organic-solvent removal, PU dispersions in water are re-formed. They can be thus re-used in the same manner as original water-borne PUDs.

EXPERIMENTAL

Materials

Commercially available, aliphatic polycarbonate macrodiol (PC, trademark T4672) with the average molar mass around $M_n \sim 2770$ g mol^{-1} (detected by SEC/GPC) was kindly provided by Asahi Kasei Chemical Corporation, Tokyo, Japan. T4672 consists of butylene, C4 and hexylene, C6 units (C6/C4 molar ratio is 7 : 3) connected by carbonate groups and it is end-capped by hydroxyl groups. For the structure, see Figure 1. 1,6-HDI, butane-1,4-diol (BD), 2,2-bis(hydroxymethyl)propionic acid (DMPA), and triethylamine (TEA) were obtained from Sigma–Aldrich. Dried acetone (max. 0.0075% H_2O) was supplied by Merck KGaA, Darmstadt, Germany. Dibutyltin dilaurate (DBTDL, purchased from Sigma–Aldrich) in the form of the 10 wt % solution in Marcol oil (mixture of liquid saturated hydrocarbons) was used as a catalyst.

Dispersion Synthesis

Because of high viscosity of polycarbonate diol, which was used as the soft segment component, all reaction steps (including pre-polymerization) were performed in acetone solutions. The main difference between our polymerization process and the common procedure based on diamines consists in the fact that the chain extension is performed before the dispersion step. This modification prevents the reaction between unreacted NCO groups and water.[11] In the standard procedure of preparation PUDs based on polycarbonate macrodiols with diamines as chain extenders, the neutralization step is performed prior to chain extension.[18,21] Because we used diol, which is less reactive than diamine, we could perform the reaction with 1,4-butanediol before the neutralization. This type of synthesis was used by Nanda and Wicks,[11] who reported the preparation of PUDs based on polyesters diols and 1,4-butanediol as a chain extender. To minimize the reaction of diisocyanates with water which competes with the reaction of hydroxyl groups from diols and could cause a considerable decrease of PU molecular weight,[9,22] a very dry acetone with water content lower than 0.0075 wt % was used. In addition, the organo-tin catalyst (dibutyltin dilaurate) was used to accelerate the urethane-forming reaction with aliphatic diisocyanates and suppress the side reactions with water even more.[23] The main advantage of acetone is that a relatively low content of DMPA is necessary to produce stable dispersion.[11] The synthesis of PUD consisted of four subsequent steps; pre-polymerization, chain extension, neutralization, and dispersion formation by phase inversion process. A simplified preparation procedure is given in Figure 1.

Polycarbonate macrodiol, DMPA, and acetone were placed into a round bottom 100 cm^3 flask equipped with a magnetic stirrer, condenser, and temperature controller, and thoroughly mixed at room temperature to obtain a homogenous solution and a uniform mixture of monomers. The amount of acetone was in all cases 45 wt % of the total mass of the reaction mixture. Subsequently, HDI and the catalyst (0.05 mol % per mol of NCO groups) were added and mixed at the rate of 700 rpm. Then the reaction proceeded at 60°C for 6 h, until a constant NCO content was achieved (checked by FTIR analysis). To avoid the competitive reaction between hydroxyl groups of BD and water,

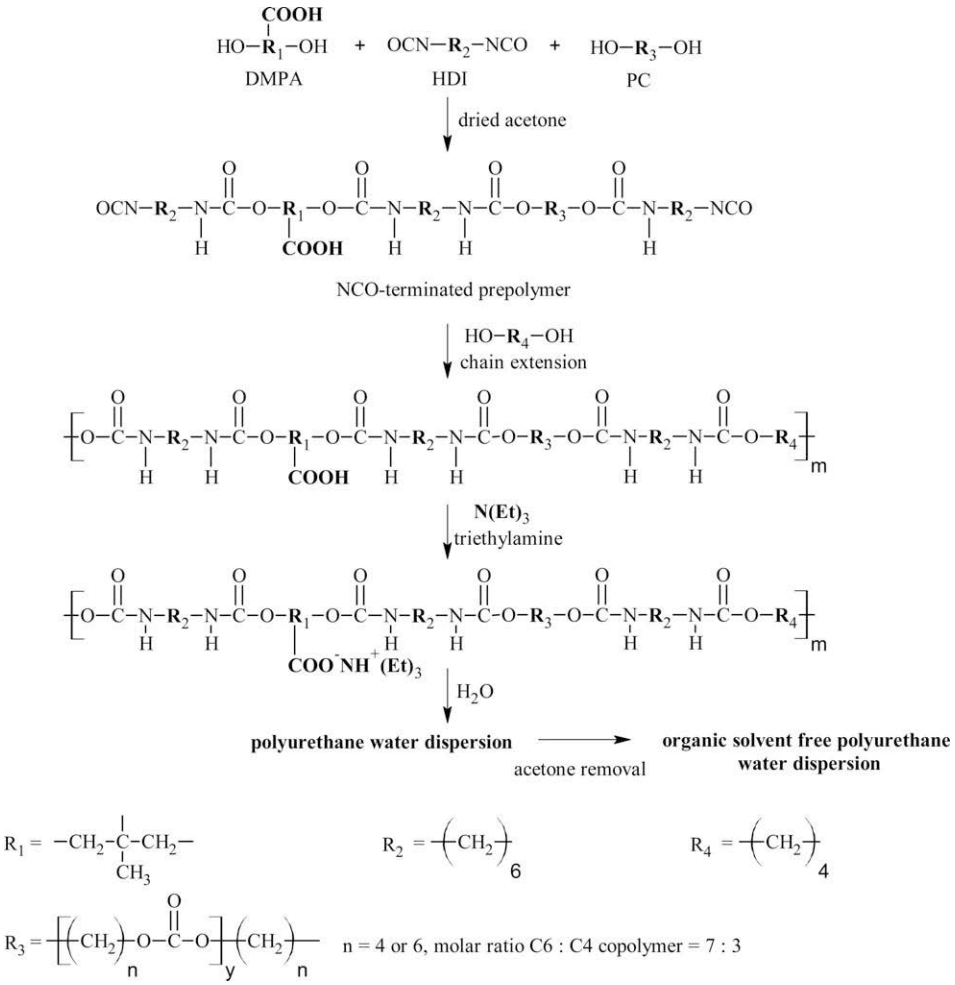

Figure 1. Simplified preparation procedure of the aqueous PU dispersions.

the chain extension reaction preceded the dispersion formation step. The amount of the chain extender (BD in this case) was set to maintain a constant value of the isocyanate index ($r = [NCO]/[OH]_{total} = 1.05$; $[OH]_{total} = [OH]_{PC} + [OH]_{DMPA} + [OH]_{BD}$). The chain extension reaction proceeded for 2 h at 60°C, followed by neutralization of the carboxylic groups by an addition a tertiary amine (TEA) to the polymer solution for 30 min at 55°C, both under constant rate of mixing of 700 rpm. The polymer solution was cooled to room temperature where after water was gradually added with a constant rate of 1 ml min^{-1} using a medical syringe. After acetone removal using rotavap under reduced pressure at room temperature, organic, solvent-free PU water dispersions were obtained. The solid content of polymer in the water dispersion was kept constant in all systems and was equal to 35 wt %.

Film Preparation

All films were prepared by casting the PU dispersions onto Teflon plates followed by slow water evaporation at room temperature for 5 days[†]. To remove residual water, the films were dried at 50°C for 20 h and subsequently for 1 h at 50°C under vacuum. The final film thickness was controlled by the volume of dispersion used for unit area of the Teflon plate; the final film thickness was in all cases 500 μm ± 25 μm. Obtained films were transparent, they became slightly opaque at increased BD/PC and decreased DMPA/PC ratios.

Methods of Characterization

Gel Permeation Chromatography. The molecular masses, M_n, M_w and polydispersity index, M_w/M_n were determined by gel permeation chromatography (GPC) (Deltachrom pump, Watrex Comp., autosampler Midas, Spark Instruments, two columns with PL gel MIXED-B LS [10 μm]). The eluent was tetrahydrofuran (THF) at flow-rate 0.5 ml min^{-1}. The injection-loop volume was 0.1 ml. Measurements were performed with triple viscosity/concentration/light-scattering detection. The set was connected with a light-scattering photometer DAWN DSP-F (Wyatt Technology) measuring at 18 angles of observation, a modified differential viscometer Viscotek model TDA 301 (without internal light scattering and concentration detectors) and a differential refractometer Shodex RI 71. The data were processed by the Astra and triSEC softwares.

[†]A modified procedure, that is, film preparation at 50°C immediately after dispersion casting led to deteriorated surface characteristics. For details, see Figure 6 in Surface Analysis of PU Films Prepared by PUD Casting section.

Dynamic Light Scattering. Dynamic light scattering (DLS) measurements were performed using an ALV CGE laser goniometer consisting of a 22 mW HeNe linear polarized laser operating at a wavelength of 632.8 nm, an ALV 6010 correlator, and a pair of avalanche photodiodes operating in pseudo cross-correlation mode. The samples were loaded into 10 mm diameter glass cells and maintained at 25 ± 1°C. Data were collected using ALV Correlator Control software and the counting time of 30 s. To avoid multiple light scattering, all samples were diluted 100 times before measurement.[24] The measured intensity correlation functions $g_2(t)$ were analyzed using REPES algorithm (incorporated in the GENDIST program)[25] giving the distributions of relaxation times shown in equal area representation as $\tau A(\tau)$. The mean relaxation time or relaxation frequency ($\Gamma = \tau^{-1}$) is related to the diffusion coefficient (D) of the nanoparticles as $D = D = \frac{\Gamma}{q^2}$ where $q = \frac{4\pi n \sin(\theta/2)}{\lambda}$ is the scattering vector, n is the refractive index of the solvent, and Θ is the scattering angle. The hydrodynamic diameter (D_H) or the distributions of D_H were calculated[26] using the well-known Stokes–Einstein relation:

$$D_H = \frac{k_B T}{3\pi\eta\ D}$$

where k_B is the Boltzmann constant, T is the absolute temperature, and η is the viscosity of the solvent.

Electrophoretic Light Scattering. Electrophoretic light scattering (ELS) measurements were used to determine the average zeta potentials (ζ) of the nanoparticles using the Zetasizer NanoZS instrument (Malvern Instruments, UK). The equipment measures electrophoretic mobility (U_E) and converts each value to ζ-potential (mV) using Henry's equation:

$$\zeta = \frac{3\eta\ U_E}{2\ \epsilon\ f(ka)}$$

where ε is the dielectric constant of the medium. The parameter $f(ka)$ is the Henry's function which has been calculated through Smoluchowski approximation $f(ka) = 1.5$. The measurements were performed at 25 ± 1°C and each reported ζ-potential value is the average of 10 subsequent measurements.

Differential Scanning Calorimetry. Thermal behavior was measured by Pekin-Elmer DSC 8500 calorimeter with nitrogen purge gas (20 $cm^3\ min^{-1}$). Indium was used as a standard to calibrate the instrument for temperature and heat flow. About 10 mg of each sample was encapsulated in hermetic aluminum pan. Differential scanning calorimetry (DSC) was performed in a cycle heating–cooling–heating from −80°C to 200°C at 10°C min^{-1}. Before and after each of the ramps two minutes of isothermal plateaux were inserted.

Swelling. Swelling experiments were performed at room temperature by immersing the specimens of dry cast films (~0.3 g) into deionized water for the overall time of 16 weeks. The swelling degree was expressed in percentage of the mass increase and calculated according to the equation:

$$\%\ \text{swelling} = \frac{w - w_0}{w} \times 100\ \%$$

where w_0 is the initial weight of the dry film and w is the weight of film in the swollen state.

The percentage weight loss Δw is the weight difference between the weights of dry films before and after swelling, original w_0 and final w_f calculated according to the equation:

$$\Delta w = \frac{w_0 - w_f}{w_0} \times 100\ \%$$

Atomic Force Microscopy. Investigation of the topography and heterogeneity relief of PU films was conducted by atomic force microscopy (Dimension Icon, Bruker), equipped with an SSS-NCL probe (Super Sharp Silicon™—SPM-Sensor from Nano-Sensors™ Switzerland with spring constant 35 N m^{-1} and resonant frequency ≈170 kHz). To investigate PU nanoparticles a freshly peeled out mica (flogopite, $KMg_3(Si_3Al)O_{10}(OH)_2$) surface was covered by dilute water PUD solution (c = ~1 mg ml^{-1}). After water evaporation, the samples were dried in a vacuum oven at ambient temperature for 12 h. The measurements were performed under ambient conditions using tapping mode atomic force microscopy (AFM) technique. The scans covered the sizes from 1 × 1 to 50 × 50 μm^2.

Scanning Electron Microscopy. The microstructure of the films was measured by scanning electron microscopy (SEM) using Vega Plus TS 5135 from Tescan, Czech Republic. Before SEM analysis, the films were sputtered with 4 nm Pt layer using vacuum sputter coater SCD 050 (Balzers, Czech Republic).

Tensile Tests. Tensile properties of the cast films were measured using an Instron model 5800 (Instron Limited, UK) according to test method ISO 527 at room temperature with a cross-head speed of 10 mm min^{-1}. The specimens were prepared according to given standard procedure ISO 527-2/5B. The used dimensions of each specimen were: length 35 mm, length and width of the narrowed part: 12 and 2 mm, and thickness 0.5 mm. Mechanical characteristics such as Young modulus E, stress-at-break σ_b and elongation-at-break ε_b were obtained from the tensile curves. Toughness was expressed as the energy to break the sample per volume unit. Reported values were the averages of at least five measurements. Presented tensile curves were taken from the measurements closest to each calculated average value.

RESULTS AND DISCUSSION

Stable water-borne PU dispersions composed exclusively of linear aliphatic chains have been prepared and characterized. The effect of composition (DMPA and BD contents) on the average particle size and ζ-potential, that is, on characteristics that reflect and pre-determine the long-term stability of PUDs, and on their functional properties such as water-absorption resistivity, surface morphology, and tensile properties of the cast PU films made from PUDs have been investigated and discussed.

For a smooth discussion, all samples are marked by codes. The code consists of three letters: either PUD (which stands for polyurethane dispersion), or PUF (which means polyurethane film cast from the relevant PUD). The letter code is followed by two numbers. The first gives the BD-to-PC molar ratio and the

Table I. Sample Codes and Composition of PU Dispersions

Code PUD[a] A–B	BD (mmol g^{-1})[b]	DMPA (mmol g^{-1})[b]	PC (mmol g^{-1})[b]	HDI (mmol g^{-1})[b]	TEA (mmol g^{-1})[b]
PUD 2.5-1	0.74	0.31	0.29	1.40	0.31
PUD 2-1	0.61	0.32	0.31	1.31	0.31
PUD 1-1	0.34	0.34	0.33	1.08	0.35
PUD 0.8-1	0.27	0.35	0.34	1.04	0.36
PUD 0.5-1	0.17	0.36	0.35	0.94	0.36
PUD 0.5-0.4	0.19	0.16	0.38	0.79	0.15
PUD 0.5-0.2	0.20	0.08	0.40	0.72	0.09

[a] PUF A–B: identification of film prepared from PUD of given composition A = BD/PC; B = DMPA/PC.
[b] Concentration expressed per gram of the solid mass of polymer.

second indicates the DMPA-to-PC molar ratio. As mentioned above, two parameters controlling PU compositions were varied and therefore two series of samples with either constant ionic group content (DMPA) or short diol (BD) content were prepared. Sample codes and compositions are given in Table I, in first to sixth column. Because the BD and HDI products contain groups which can form hydrogen bonds, the variation of BD content allow for the regulation of the number of physical crosslinks.[13] Conversely, polymer hydrophilicity of PUDs is controlled by the number of ionic species derived from the DMPA component. From this point of view, the series of PUDs and PUFs with constant ratio DMPA-to-PC (second number) shows the dependence of PU samples on the hard-segment contents while the series with constant BD-to-PC (first number) depicts the dependence of PUD or PUF samples on the contents of ionic groups.

Molecular Weights of Synthesized PUs

The molecular weights were determined by GPC. Dry samples were dissolved in THF in concentration 1 mg cm^{-3}. The results, based on the polystyrene calibration, are listed in Table II. The M_n values of samples containing various BD concentrations (PUD A-1 series) are similar. It is obvious that different amounts of DMPA influence M_n. Decreasing DMPA concentration leads to higher M_n.

Average Particle Size and Long-Term Stability of PUD

Particle size of PU dispersions is a result of the complex processes influenced by reaction conditions such as temperature, rate of mixing, type and concentration of ionic group and chain extender, type of macrodiol and diisocyanate, and the degree of neutralization of the ionic groups. The dispersions are formed by step-wise PU chain polymerization followed by a self-assembly of individual PU chains into the nanometer-size formations in the dispersion step. The complex chemistry of the preparation process requires that the reaction conditions suitable for the reproducible preparation of PUDs with desired functional properties have to be found and optimized. To tune the reaction conditions, FTIR was used to determine the minimum time necessary for the total isocyanate group conversion in the pre-polymerization and chain-extension reaction steps.

Table II. Molecular Weights of Prepared PUDs

Code	M_n (kg mol^{-1})	M_w (kg mol^{-1})	M_w/M_n
PUD 2.5-1	15.3	29.8	1.95
PUD 2-1	12.5	28.4	2.27
PUD 1-1	11.9	27.3	2.30
PUD 0.8-1	12. 2	28.5	2.34
PUD 0.5-1	12.9	30.5	2.36
PUD 0.5-0.4	22.7	48.2	2.12
PUD 0.5-0.2	28.9	58.1	2.01

After the study and validation of all individual steps, the process of the reproducible PUD preparation was set as follows: (i) pre-polymerization for 4 h at 60°C, (ii) chain-extension for 2 h at 60°C, (iii) neutralization for 0.5 h at 55°C, and (iv) finally a 30 min dispersion process at 55°C. All consecutive steps were conducted under stirring at the constant speed of 700 rpm.

The study of the influence of PUD composition on the average size of the nanoparticles was performed for samples with fully neutralized carboxylic groups with triethylamine to suppress complicating polyelectrolyte effects at low ionic strength.[5] As the conditions of preparation were identical for all PUD samples, the differences in average particle size and ζ-potential detected by the dynamic and ELS analyses are due to differences in PUD compositions. The effect of BD concentration (the series PUD A-1, with constant DMPA-to PC ratio) and the DMPA concentration (the series PUD 0.5-B, with constant BD-to-PC ratio) on the *z*-average particle size and on ζ-potential of the samples is presented in Figure 2.

The results are in accordance with literature data[27] and show that the average particle size decreases considerably with increasing DMPA content. The main reason consists in increased solubility of considerably charged polyelectrolyte chains rich in DMPA, that shifts the self-assembly towards dissociation and formation of smaller associates. Two general effects control the solubility of polyelectrolyte chains. The first one is entropic and reflects the increase in translational entropy of counterions, which are released in bulk aqueous medium.[28] The second effect is caused by changes in the solvation and in water structure after the dissociation and ion pairs and separation of individual ions. Both $-COO^-$ and $NH^+(C_2H_5)_3$ are large, so called "water structure-breaking" ionic groups and hence the changes in their solvation lead to the decrease of the

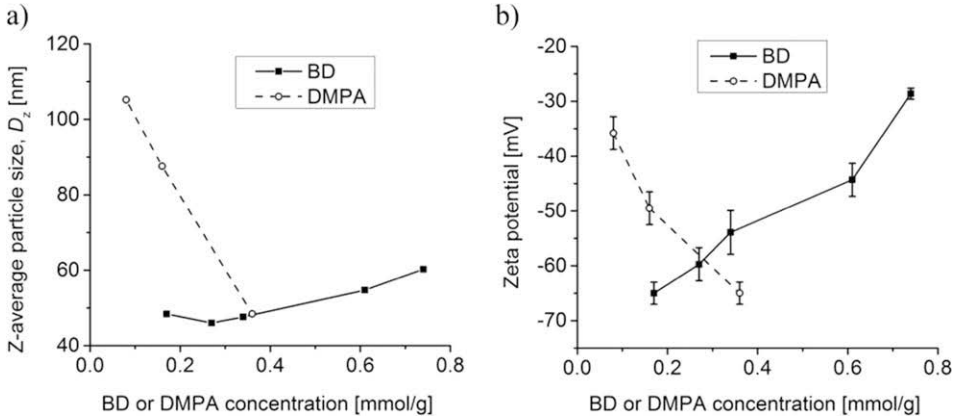

Figure 2. The influence of BD and DMPA concentrations on the *z*-average particle size (left) and ζ-potential (right). BD and DMPA concentration values are given in Table I, second and third column.

Gibbs function of the system.[29] One more effect contributes to the dissociation of particles with increasing DPMA content. The number of ionized —COO^- groups in associates formed by DMPA-rich samples is high and the electric charges are relatively close to each other. Therefore, the electrostatic repulsion is strong, which promotes the dissociation of associates. However, the effect is more complex. The charge of multiply ionized and relatively small nanoparticles (i.e., small for the total bare charge) is in a large extent compensated by counterions which "condense" on charged nanoparticles and lose their translational entropy. In summary, the dissociation of charged polyelectrolyte associates is due in main part to complex entropy reasons.[28] One more (quite trivial) factor contributes to the dependence of sizes of self-assembled nanoparticles on the DPMA content. Data in Table II show that molecular weights of single chains that in aqueous media self-assemble in nanoparticles depend on chemical composition and appreciably increase with decreasing DPMA content. The data further show that the average particle size increases with higher chain stiffness[5] which grows with increasing BD concentrations. This understandable effect is, of course less pronounced (45–60 nm; series PUD A-1) than that of DMPA (48–105 nm; the series PUD 0.5-B). In summary, the number of ionic species affects the self-assembly more significantly than the content of hard segments [for details see Figure 2(a) and Table III].

The values of ζ-potential reflect the efficiency the electrostatic stabilization of dispersed particles in polar liquids (particularly in aqueous media) and control the long-term stability of prepared dispersions[‡]. It is generally accepted that particle suspensions are stable if the absolute value of ζ-potential exceeds 30 mV (i.e., more positive than +30 mV or more negative than −30 mV).[30,31] All prepared PUDs which contain pendant anionic groups in DMPA units exhibit negative ζ-potentials. The influence of the content of ionic groups (DMPA) and hard segments (BD) on the ζ-potential is shown in Figure 2(b). As expected, the content of DMPA strongly influences absolute values of ζ-potential, which increases with increasing DMPA content. It is noteworthy, that the ζ-potential decreases considerably with BD content. This is caused mainly by the fact that the size of self-assembled particles increases with increasing content of BD (as explained above) and hence the charge spreads on a larger surface and the surface charge density is lower as compared with compact particles formed by PUs, which are poor in BD.

As almost all absolute values of ζ-potential are higher than 30 mV, the dispersion can be considered as long-term stable, which was proven experimentally by the stability tests, that is, by storing them at laboratory temperature (23 ± 2°C) for more than 1 year. All dispersions, with the only exception, which was the sample PUD 2.5–1 containing the highest amount of BD, with the value—(29 ± 1) mV, remained stable for more than 1 year. The stability of PUD 2.5–1 was limited and the particles spontaneously coagulated in 5 months.

To summarize this part, the stable water-borne dispersions (formed exclusively by linear PU chains) with *z*-average particle size between 45 and 105 nm were prepared using butane-1,4-diol as the chain extender and 2,2-bis(hydroxymethyl)propionic acid as the anionic species. Increasing DMPA concentration

Table III. Sample Codes, *z*-Average Particle Size, Size-Dispersity Index (PDI), and ζ-Potential of PU Dispersions

Code PUD A–B	*z*-Average particle size, D_z (nm)	PDI[a]	ζ-Potential (mV)
PUD 2.5–1	60.2 ± 0.5	0.20	− (29 ± 1)
PUD 2–1	54.7 ± 1.3	0.29	− (44 ± 3)
PUD 1–1	47.6 ± 0.4	0.13	− (54 ± 4)
PUD 0.8–1	46.0 ± 0.5	0.07	− (60 ± 3)
PUD 0.5–1	48.4 ± 0.2	0.09	− (65 ± 2)
PUD 0.5–0.4	87.6 ± 0.7	0.06	− (50 ± 3)
PUD 0.5–0.2	105.2 ± 10	0.26	− (36 ± 3)

[a] Size-dispersity index was estimated using the cumulant analysis of the autocorrelation functions.

[‡]The system is stable when the repulsive forces between the particles are sufficient enough to overcome their attraction and thus prevent their aggregation. Insufficient number of the ionic species will results in particle aggregation and subsequent sedimentation.

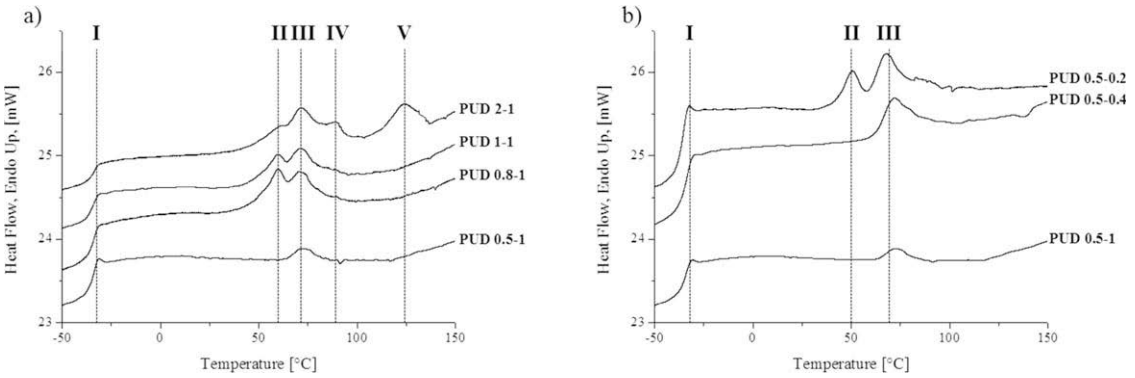

Figure 3. The DSC curves of PUDs-based films containing: (a) various amount of BD, (b) various amount of DMPA. Temperature regions I–V are drawn by the dotted lines.

Table IV. Thermal Properties of PUDs Based Films

Code	HSC_{BD}[a] (wt %)	HSC_{DMPA}[b] (wt %)	T_g[c] (°C)	T_r[d] (°C)	$(T_m)_s$[e] (°C)	$(\Delta H_m)_s$[f] (J g^{-1})
PUD 2-1	16.9	10.0	−34	61	71	11
PUD 1-1	9.6	11.0	−34	60	71	8
PUD 0.8-1	7.6	11.3	−34	60	73	8
PUD 0.5-1	5.2	11.6	−35	-	73	1
PUD 0.5-0.4	5.9	4.9	−34	-	71	4
PUD 0.5-0.2	5.6	2.5	−36	51	67	7

[a] HSC_{BD}—hard segment content derived from BD = $(m_{HDI\ used\ for\ BD} + m_{BD})/(m_{HDI} + m_{BD} + m_{PC} + m_{DMPA}) \times 100$.
[b] HSC_{DMPA}—hard segment content derived from DMPA = $(m_{HDI\ used\ for\ DMPA} + m_{BD})/(m_{HDI} + m_{BD} + m_{PC} + m_{DMPA}) \times 100$.
[c] T_g—glass transition temperature of the soft segments.
[d] T_r—relaxation temperature of the soft segments.
[e] $(T_m)_s$—melting temperature of the soft segments.
[f] $(\Delta H_m)_s$—melting enthalpy of the soft segment.

results in smaller and more stable water dispersions while increasing BD concentration leads to slightly larger and less stable dispersions. The synthesized PU dispersions exhibit suitable functional properties and can be used for preparation of free-standing films, coatings, or adhesives. In this study, the first possibility, that is, the use of stable water PUDs as starting materials for the preparation of cast free-standing PU films was addressed. The chapters of the article that follow focus on results obtained by the characterization and analyses of PU films. At the end of this paragraph, we would like to emphasize that while the behavior of charged PU chains and associates in aqueous media corresponds to the polyelectrolyte regime, in next parts of the study, the thermo-mechanical behavior of bulk films reflects the properties of materials in the ionomer regime.[28] It is why we use the term polyelectrolyte in the beginning of the article and ionomer in the later parts.

Differential Scanning Calorimetry

To investigate the thermal behavior of PUDs, such as melting and organization of crystalline domains, DSC measurements were performed. Row data and the effects of the soft and hard segment content are shown in Figure 3, the thermodynamic characteristics evaluated from DSC curves are listed in Table IV. The DSC thermograms generally show one glass transition temperature (I) at around −34°C and four endothermic peaks (II–V). The second (II) and third (III) peaks at temperatures between 51 and 73°C reflect the thermal behavior of soft segments. The second endothermic region (II) is related to relaxation of the soft segments in the interphase, whereas the third peak (III) is attributed to the melting of highly organized (crystalline) parts formed by the soft phase. The positions of both peaks do not change at relatively high BD content [Figure 3(a)]. It means that the physical cross-links do not significantly affect the motion of soft segments. The intensities of the endotherm peaks are the highest for the BD and DMPA ratios close to 1 (PUD 0.8–1 and PUD 1–1). The difference is visible for the sample with the lowest BD and simultaneously the highest DMPA amount (PUD 0.5–1), where the peak II disappears and intensity of the peak III is the weakest. This is probably due to the fact that BD content approaches the low limit, below which the interaction of ionic groups from DMPA dominates over the effect of hydrogen bonds formed by BD units. It suggests that presence of ionic groups hinders the motion chains[32] and crystallization of PC[§]. The same trend is observed in Figure 3(b) presenting samples from series PUF 0.5-B. The melting enthalpy values of soft segments $(\Delta H)_m$ in region

[§] Auxiliary DSC experiments of model PUs prepared without any BD revealed that endothermic peak III systematically diminished (or even disappeared) if DMPA content gradually increased.

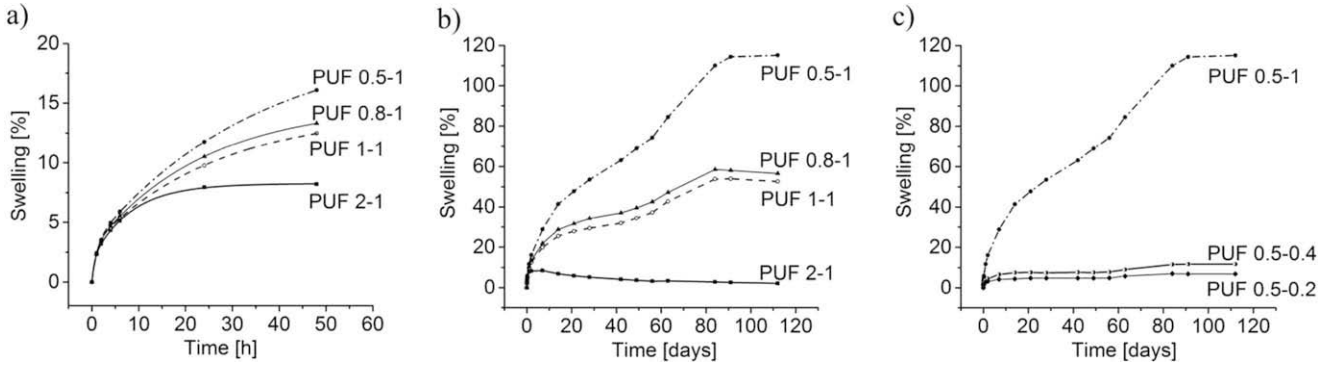

Figure 4. The effect of BD (PUF A-1 series: a, b) and DMPA concentrations (PUF 0.5-B series, c) on swelling properties. Time dependence of the swelling (a) for time up to 50 h, and (b,c) for time up to 16 weeks.

III increase with decreasing DMPA content and indicate better arrangement of chains poor in DMPA.

Multiple melting peaks IV and V at temperatures higher than 85°C occur only for the sample containing the highest HSC_{BD} value (PUD 2–1). They can be attributed either to the presence of highly organized hard-segment domains present in the different crystalline forms[13] or they can be associated with the mixing transition of the soft and hard segments.[33]

Swelling Behavior

The sensitivity and resistivity of cast PU films against water is a paramount criterion for most coating or adhesive applications.[1] The swellability of cast PU films increases with increasing hydrophilicity of polymer chains,[5,9] that is, in the studied samples, with growing DMPA content. Other factors such as the soft-segment type, molecular weight or the chain extender type and functionality also affect the water resistivity of coating materials.[27,34] The effects of BD [PUF A-1 series, Figure 4(a,b)] and DMPA contents [PUF 0.5-B, Figure 4(c)] on the degree of swelling (DS) were investigated on the timescale of hundreds of days.

Figure 4 shows that the initial rate of swelling (up to 5 h) almost does not depend on the sample composition. The mass increase (~3 wt %) at this stage is more likely the result of physical binding of water molecules onto the film surface than the diffusion inside the film. This type of polyurethane–water interaction is highly probable because the hydrophilic ionic groups are regularly distributed within the polyurethane chain and therefore also on the film surface. After 5 h, the rates of swelling of individual samples start to differentiate from each other and depend on the film composition. After 60 h, the maximum differences in the swelling degree reach 10 wt % of water [see Figure 4(a)], which represents almost 100% of the relative swelling. As the ratio of DMPA to PC is kept constant in the PUF A-1 series (see Table I for the compositions), the comparison of curves in Figure 4(a,b) shows that water resistivity of cast films increases with the hard-segment content. As already mentioned, the influence of DMPA content on the water resistivity is antagonistic to that of BD: the resistivity to swelling increases with decreasing DMPA content [Figure 4(c)] which is in accordance with literature data.[35] At low DMPA contents, up to 0.16 mmol g^{-1} (PUF 0.5–0.2 and PUF 0.5–0.4), DS did not exceed 12 wt % within the 16 weeks of conducted measurements. However, for the sample with a high DMPA content (PUF 0.5–1), large DS of 115 wt % was obtained after 16 weeks. It can therefore be concluded that DMPA content of about 0.2 mmol g^{-1} represents a threshold value below which the PU films behave as hydrophobic and highly water resistant materials. Below this the PU films are characterized by relatively high swelling resistivity in comparison to PUDs-based films prepared from isophorone diisocyanates and poly(tetra-methylene adipate glycol), where the percentage swelling in water is in a range from 48 to 92 wt %.[36]

With respect to long time (quasi-equilibrium) swelling properties, the prepared PU films can be divided into three categories: little swelling films (PUF 2–1, PUF 0.5–0.2, and PUF 0.5–0.4) which attain only a low quasi-equilibrium DS of about 10 wt %, medium swelling films (PUF 0.8–1 and PUF 1–1) with intermediate DS about 55 wt % and highly swelling films (PUF 0.5–1) which attain high DS of about 115 wt %. The weight

Table V. Swelling Properties of PU Films

Code PUF A-B	Swelling maximum (wt %)	Swelling after 16 weeks (wt %)	Time for maximum swelling* or quasi-equilibrium	Weight loss by swelling Δw (wt %)
PUF 2-1	8.5	2.2	7 days*	3.9
PUF 1-1	53.7	52.5	12 weeks*	3.4
PUF 0.8-1	58.5	56.5	12 weeks*	4.3
PUF 0.5-1	115.1	115.1	13 weeks	4.1
PUF 0.5-0.4	11.7	11.7	13 weeks	1.2
PUF 0.5-0.2	7.01	7.0	12 weeks	1.2

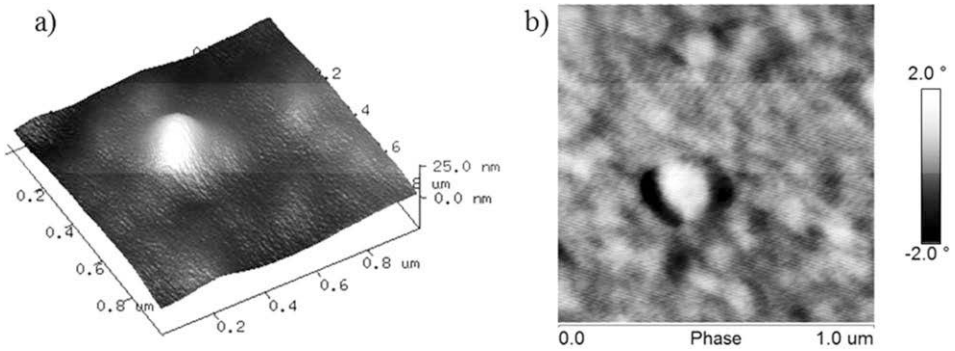

Figure 5. AFM 1 μm × 1 μm images: (a) 3D height, (b) 2D phase of one separated PU nanoparticle from PUD 0.5–0.4.

differences of dry samples before and after swelling were also measured. It was found that they are always fairly low. Lower values (ca. 1 wt %) were obtained for films made from bigger particles while films made from smaller particle lose about 3–4 wt % of the mass, not depending on the attained DS; see Table V, the fifth column.

In the following chapter, the swelling experiments will be further correlated to results of surface analyses (SEM and AFM).

Surface Analysis of PU Films Prepared by PUD Casting

Surface structure belongs to the most important features of films and coatings. Therefore, surface morphology of the PU films was analyzed by two microscopy techniques: atomic force microscopy (AFM) and scanning electron microscopy (SEM). However, before studying the films that are formed by a complex process, during which individual polymer chains from different nanoparticles reorganize and mutually interpenetrate, we studied the deposition of individual nanoparticles on the surface from very diluted solutions.

For the study of the deposition of PU particles on the surface by AFM, we have selected the hydrophilic atomically smooth freshly peeled-out mica surface. The dip-coating technique, consisting in a fast immersion of small mica sheet in a dilute solution followed by fast drying, was used to deposit individual particles. Figure 5 shows one isolated polymer nanoparticle deposited from the diluted aqueous PUD 0.5–0.4 solution. The section analysis of the spherical particle revealed its diameter of about 170 nm. When compared with DLS measurements (particle size 87.6 nm), the size of the deposited particle seems to be larger. This is caused by the pancake deformation of the flexible PU particle upon its deposition on the hydrophilic surface. Because different forces act on the PU nanoparticle in the aqueous dispersion and on the mica surface, it is usually impossible to compare particle sizes obtained from DLS directly. However, it has been shown that AFM is a useful technique for

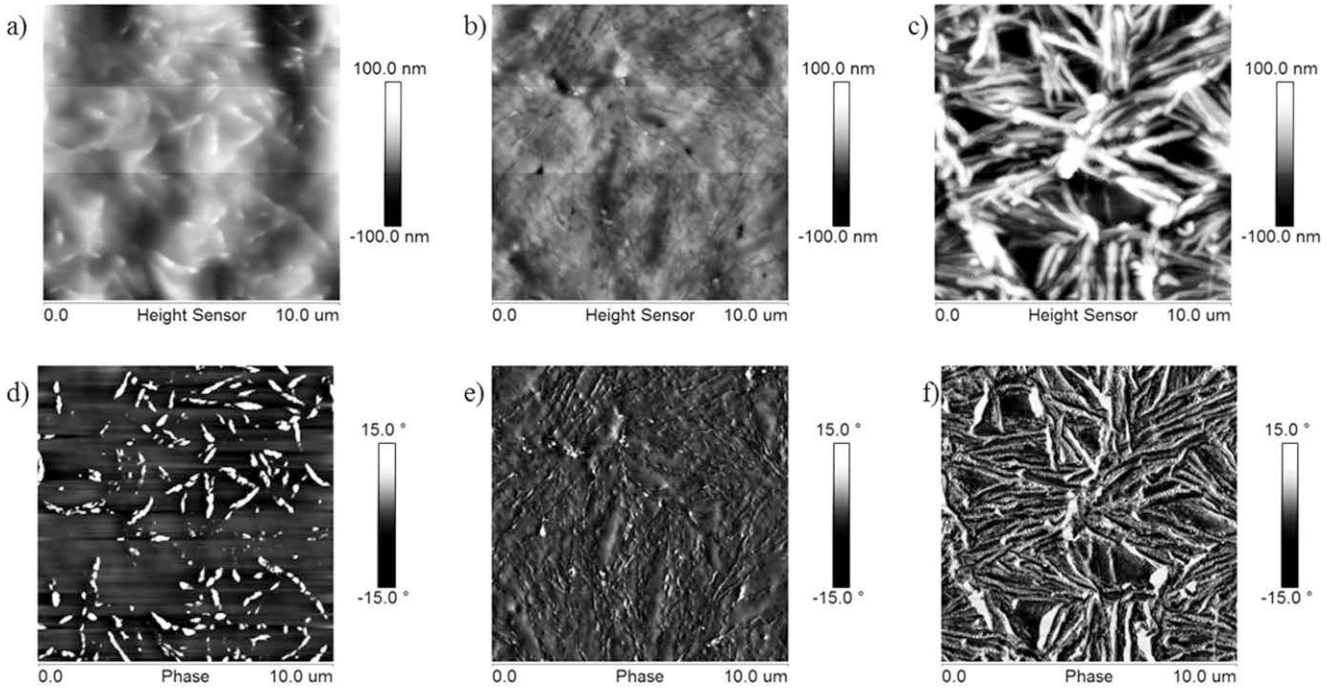

Figure 6. AFM 2D 10 μm × 10 μm (a–c) height, (d–f) phase images of PUF 0.5–0.4 sample prepared by: (a, d) drying at ambient temperature, (b, e) fast water evaporation, (c, d) slow water evaporation and following heating.

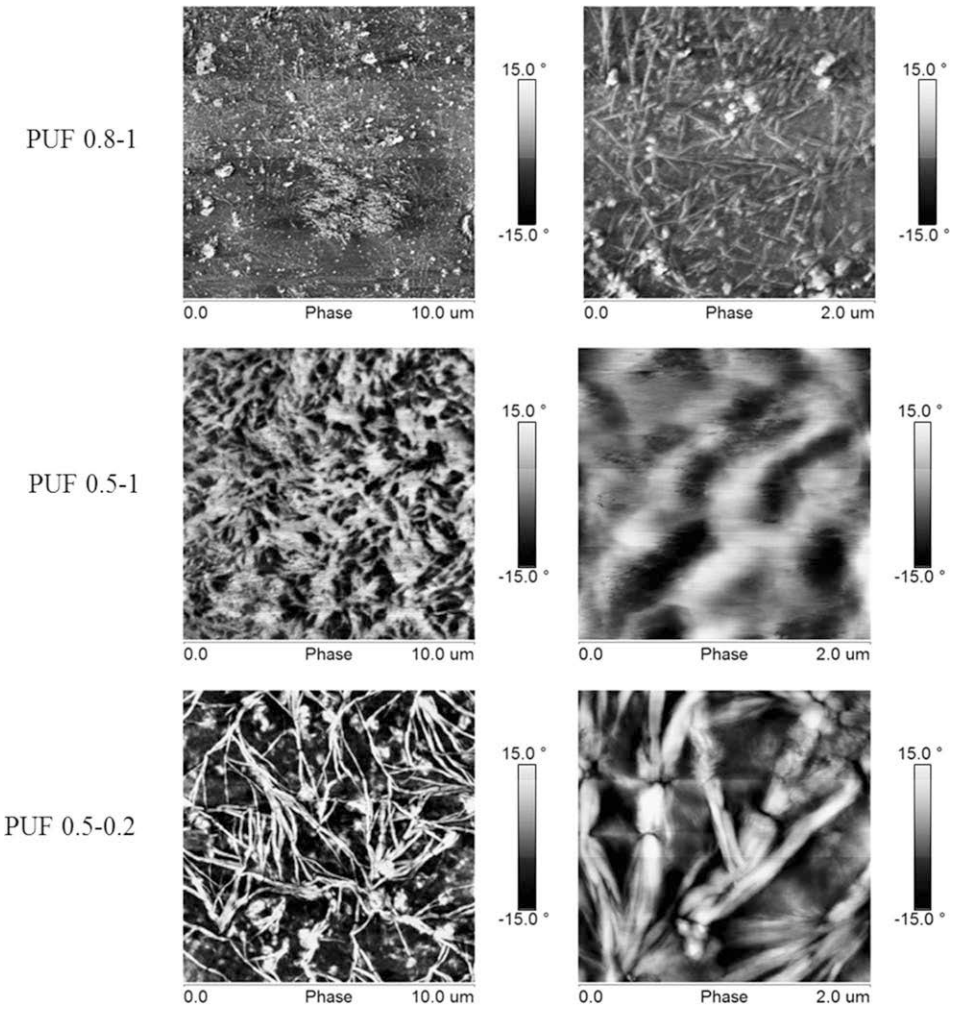

Figure 7. 2D phase AFM images of the cast PUDs films. Scan size 10 μm × 10 μm left, 2 μm × 2 μm right.

investigation of shapes and size distributions of various nanoparticles, including PU nanoparticles.[37,38]

AFM is a powerful tool for checking film surface regularity on the nanometer scale. Three PU samples (PUF 0.5–0.4) of identical composition, but prepared at different rates of water removal during the dispersion thickening and film formation, were analyzed by this method. Figure 6(a,d) shows the height and phase images of films prepared by drying at ambient temperature for 5 days. The slow procedure resulted in randomly oriented rod-like hard domains, which appear at the images as the brightest regions. The results of the second procedure, when the sample was directly heated at 50°C (well above T_g) for 24 h, are presented in Figure 6(b,e). This modification of the preparation procedure, which does not provide enough time for the organization of hard segments within soft phase due to too fast water evaporation, leads to highly disordered morphology of the film surface. To optimize the preparation of films, PUD 0.5–0.4 was dried first at ambient temperature for 5 days and then heated at 50°C ($T_g = -34$°C). Casting the films well above the glass transition temperature at which the polymer chains are highly mobile, results in more regular organization of hard segments. Figure 6(c,f) shows the morphology of the sample prepared by the third method. In this case highly organized and regularly arranged rod-like patterns connected with each other were observed in the AFM image. This indicates that the organization of hard segments depends not only on the rate of water evaporation but also on the casting temperature.

AFM was further used for studies of the effect of different groups content (particularly ionic groups and those that allow the formation of H-bonds) on surface morphology. We found that in all cases, the crystallization of soft segments, described in Differential Scanning Calorimetry section, influences significantly the microphase separation and consequently the surface morphology. Figure 7 compares several selected cast films. Very similar morphology was observed for samples containing different BD contents (series PUF A-1), which suggests that BD did not display significant H-bonding influence on the film morphology. This finding is consistent with DSC data which indicate (e.g., PUF 0.8–1) that hard segments are separated from soft phase depending on the HSC_{BD} concentration (see Table VI). The packing behavior could be caused by the high level of the superstructured organization of hard segments,[39] made

Table VI. Tensile Properties of Cast PU Films Prepared from PUDs of Different Composition: BD—Dependence (PUF A-1 Series) and DMPA—Dependence (PUF 0.5-B Series)

Sample	Young's modulus E (MPa)	Tensile strength σ_b (MPa)	Elongation-at-break ε_b (%)	Energy-to-break (mJ mm^{-3})
PUF 2-1	26.7 ± 0.7	3.7 ± 0.2	288 ± 11	11.2 ± 0.7
PUF 1-1	8.3 ± 0.2	1.4 ± 0.1	208 ± 19	3.5 ± 0.4
PUF 0.8-1	5.9 ± 0.1	1.0 ± 0.1	190 ± 10	2.4 ± 0.2
PUF 0.5-1	3.5 ± 0.1	0.7 ± 0.1	172 ± 7	1.5 ± 0.1
PUF 0.5-0.4	5.5 ± 0.2	1.3 ± 0.1	132 ± 8	1.7 ± 0.1
PUF 0.5-0.2	13.9 ± 0.8	1.8 ± 0.1	128 ± 13	2.4 ± 0.3

from symmetric diisocyanate (HDI) and symmetric BD, together with the high tendency to ordering of carbonate units in soft segments. The study also shows that the content of ionic groups has significant effect on the morphology and microphase separation (observed by AFM). When HSC_{DMPA} content decreases (series 0.5-B), the microphase separation also decreases, which is demonstrated by more homogenous structure of PUD 0.5–1. These observations are consistent with conclusions drawn from DSC results [Figure 3(a)] and support the correctness of the interpretation. Because the charged groups mutually repel, their effect on the compactness of the structure is opposite than that of hydrogen bonds. This may explain more tightly ordered structure of sample containing the lowest HSC_{DMPA} concentration (PUD 0.5–0.2). Similar results were obtained by Sami *et al.*[40] in system without DMPA, where the effect of hydrogen bonds resulted in formation of tightly ordered structure.

2D AFM height images and SEM top images of the surface relief of the PUF 0.5–0.4 cast film are compared in Figure 8. Almost identical magnifications of the images were used in both methods. Both microscopic techniques show similar microstructures where the aforementioned fibril-like structures on the film surface can be easily identified. In both cases, the width of the fibrils is in the range of 80–120 nm. Hollow dips, which retain continuous film surface [Figure 8(c)], can be detected by both techniques. Their presence is presumably the result of water exclusion from the polymer mass during film formation. Swelling experiments (Swelling Behavior section) revealed that this particular sample is very hydrophobic. Gradual water separation results in the formation of stable micrometer-size droplets included in the arising polymer film subsequently evaporated leaving the dip structures on the film surface.

SEM analysis was further used for determination of the effect of the hard-segment concentration on surface film morphology. Microscopic images of cast film surfaces at different BD concentrations (PUF A-1 series)[¶] are shown in Figure 9. Although PUF 0.5–1 [Figure 9(a)] with the lowest BD content exhibits the most homogenous structure, PUF 2–1 with the highest BD content [Figure 9(c)] contains numerous, randomly distributed hollow dips of different sizes. The diameter and average depth of several of the hollow structures were estimated by AFM section analysis and divided into small (1/0.1 μm), medium (2/0.3 μm), and large (5/1 μm) sized features. Number and size of the hollows clearly increase proportionally with increasing BD concentration and therefore the hard-segment content. This can be explained by the fact that samples with higher BD contents easier nucleate in solution. When water is evaporating, particles collide with each other, causing a creation of the porous structure. Conversely, swelling experiments revealed that the hydrophilicity or hydrophobicity of the films has crucial influence on the surface homogeneity of the cast films. The most hydrophilic PUF 0.5–1 has the most homogeneous surface relief while the very hydrophobic PUF 2–1 is distinguished by the highest number of micrometer-size hollow dips. Therefore, formation of the pores may be also caused by more complicated water exclusion process from the hydrophobic polymer mass during film formation. Despite the enlarged porous surface area of PUD 2–1 sample [Figure 9(c)] compared to the other films of the PUF A-1 series, this sample shows the lowest swelling tendency (Table V).

Tensile Properties

The influence of DMPA and BD content on the Young's modulus E, stress-at-break (tensile strength) σ_b, and elongation-at-break ε_b of the cast films were evaluated. The results are summarized in Table VI. As the components used for the PU samples preparation were bifunctional, the resulting cast films were thermoplastic in nature. This is a great advantage because it provides for the reuse and recycling of synthesized samples by various easy available methods, like the injection molding or extrusion. Nevertheless, the absence of chemical cross-lings has a detrimental effect on mechanical properties, which are worse than those of similar chemically cross-linked PU compounds, for example, of those cross-linked by tetrafunctional amines.[35,41]

Two aspects influencing the mechanical properties were investigated: (i) BD concentration (PUF A-1 series) and (ii) the effect of DMPA content (PUF 0.5-B series). Tensile curves of the two series of samples are shown in Figure 10.

The results can be summarized as follows: increasing amount of BD leads to gradual increase of E (Table VI, the second column). This behavior, which has been found in many PU systems,[13,42] is directly related to the hard-segment-promoted increase of sample compactness. Simultaneous increase in tensile strength, elongation at break, and toughness is observed for the

[¶]The unstable dispersion PU 2.5–1 was not used for the film formation.

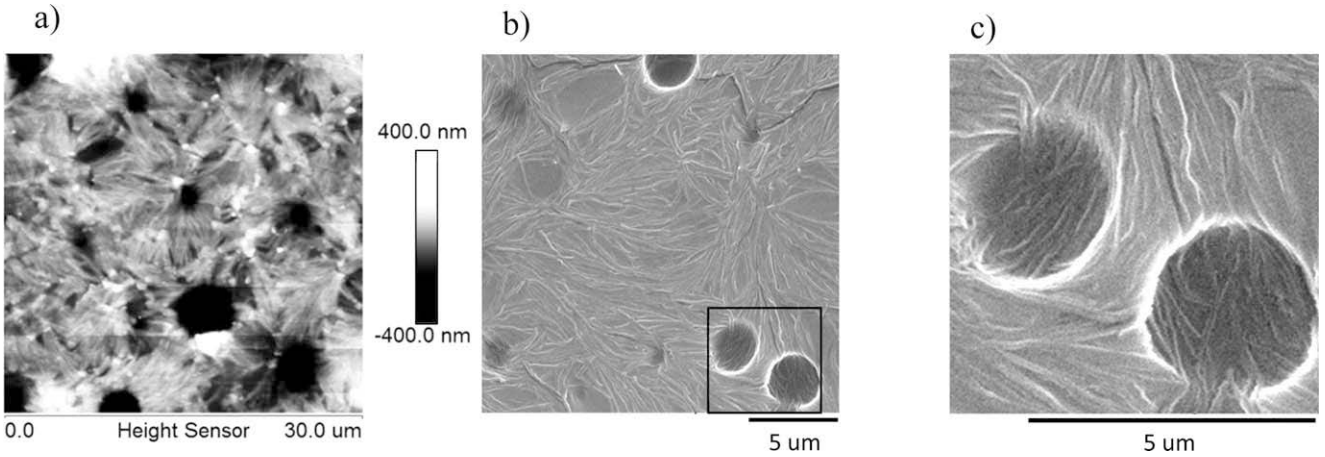

Figure 8. The microstructure of PUF 0.5–0.4: (a) 2D height AFM image (30 μm × 30 μm), (b) SEM image (magnification ×7000), and (c) SEM image (magnification ×30,000).

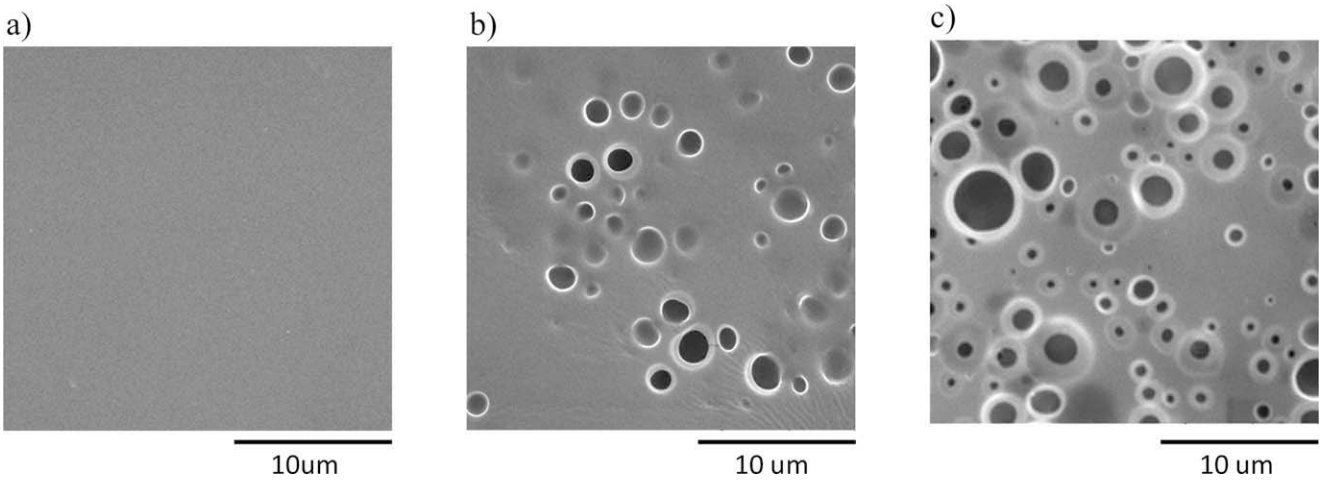

Figure 9. SEM images of PUDs-based films with different BD content (PUF A-1 series): (a) PUF 0.5–1, (b) PUF 1–1, and (c) PUF 2–1 at magnification ×5000.

whole series: PUF A – 1, with the best mechanical properties found for PUF 2 – 1.

The effect of DMPA concentration (PUF 0.5-B series) on the tensile properties is shown in Figure 10(b). Simultaneous increase of E, σ_b, and the energy-to-break and at the same time decrease of ε_b can be seen with the decreasing concentration of the anionic groups (DMPA) [Tables I and III and Figure 10(b)]. The two tensile characteristics, namely σ_b and ε_b, show opposite trends which contradicts the results for films based on both (a) PU dispersions of chemically cross-linked systems (where the

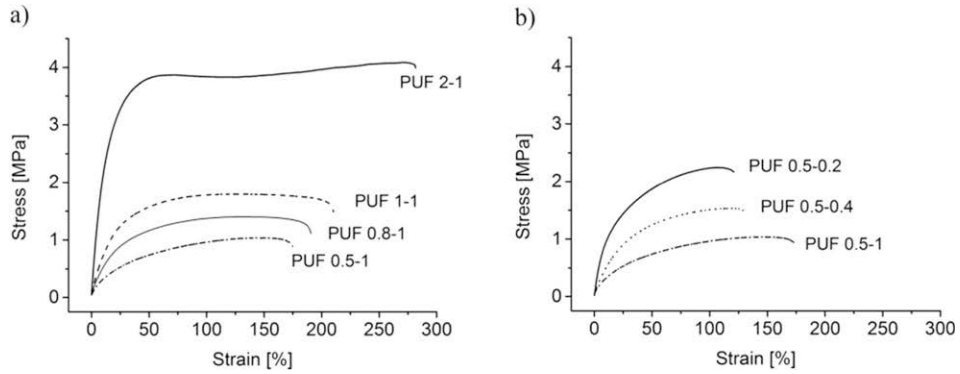

Figure 10. Tensile curves of cast PU films (a) at different BD concentrations (PUF A-1 series), and (b) at different DMPA concentrations (PUF 0.5-B series).

increase of DMPA content resulted in σ_b increase and ε_b decrease[9]) and (b) related starting materials such as PC macrodiol, HDI, and BD prepared by bulk polymerization.[13,43]

The most important factor influencing the PUD composition and average particle size in the PUD 0.5-B series is clearly the DMPA content. It can be assumed that the increase of the anionic group number and also the decrease of average particle size of the dispersions lead to somewhat looser structures, with Coulombic forces overwhelming the hydrogen bonding interactions in the hard segments. All charged nanoparticles are self-assembled entirely from linear PU chains. The packing of the particles and resulting compactness of the films are dependent on the average particle size and their anionic strength. Although smaller, highly charged particles give less tight and less compact materials, bigger and less charged particles form stronger films at low hard-segment contents.

The highest energy-to-break is observed for PUF 2–1 in PUF A-1 and for PUF 0.5–0.2 in the PUF 0.5-B series. Both films are also distinguished by sufficient water resistance (see Swelling Behavior section for details) but they differ in the average size of the dispersion particles (Table III). Both formulations (PUF 2–1 and PUF 0.5–0.2) are excellent candidates for top coating materials which can be applied in both internal and external conditions.

CONCLUSIONS

Stable novel water-borne dispersions based on linear PU chains containing only the aliphatic components such as polycarbonate-based macrodiol, DMPA, HDI, and BD were prepared and characterized. The average particle size (between 45 and 105 nm) decreases with increasing DMPA content, but is only slightly influenced by the amount of chain extender (BD) in the polymer. The absolute values of ζ-potential (between -29 and -65 mV) decrease with ascending DMPA and descending BD contents. The long-term stability tests confirmed that all these dispersions are stable for the minimum period of 1 year. The only exception is the dispersion of the sample with the highest BD content (with the lowest absolute value of ζ-potential -29 mV), the stability of which was found to be limited to 5 months only.

Surface morphology, swelling degree, and tensile properties of the cast films made from polyurethane dispersions were found to depend strongly on the dispersion composition, mainly on the content of the anionic groups as given by DMPA concentration. Three swelling categories were detected: low degree of swelling of about 10 wt %, intermediate with about 55 wt %, and finally high degree of approximately 115 wt %. The surface of films with relatively high (>0.1 mmol g^{-1}) DMPA content shows the self-assembly of particles on the nanometer and micrometer scale arranged into irregular interlined fibril-like structures as detected by AFM. Although the length of fibril-like structure is on the micron unit level, its width is in tens of nanometers. The surface structures and morphologies of individual samples also differ on both the micrometer and millimeter scale depending of the composition, as detected by SEM. The micrometer-size pores are detectable on the surface of hydrophobic PU films, giving a rough design to the material on the micrometer scale. However, on the millimeter level the surface appears relatively regular. Mechanical properties are substantially influenced by the composition of the given dispersions. Tensile strength, elongation-at-break, and energy-to-break increase with increasing BD contents, but increasing DMPA contents leads to higher elongation-at-break but lower tensile strength and energy-to-break. Summarizing the conclusions concerning the functional properties from the practical point of view, samples PUF 0.5–0.2 and especially PUF 2–1 seem the best candidates for the use as internal or external topcoat materials.

ACKNOWLEDGMENTS

The authors wish to thank the financial support of the Grant Agency of the Czech Republic (Czech Science Foundation, project No. 13–06700S).

REFERENCES

1. Brock, T.; Groteklaes, M.; Mischke, P. European Coatings Handbook, Vincentz Verlag: Hannover, **2000**, p 67.
2. Chattopadhyay, D. K.; Raju, K. V. S. N. *Prog. Polym. Sci.* **2000**, *32*, 352.
3. Cakić, S. M.; Stamenković, J. V.; Djordjević, D. M.; Ristić, I. S. *Polym. Deg. Stab.* **2009**, *94*, 2015.
4. Nanda, A. K.; Wicks, D. A.; Madbouly, S. A.; Otaigbe, J. U. *J. Appl. Polym. Sci.* **2005**, *98/6*, 2514.
5. Kim, B. K. *Colloid Polym. Sci.* **1996**, *274*, 599.
6. Cakić, S. M.; Ristić, I. S.; Marinović-Cincović, M.; Špírková, M. *Int. J. Adhes. Adhes.* **2013**, *41*, 132.
7. Król, P. *Prog. Mater Sci.* **2007**, *52*, 915.
8. Chen, T. K.; Chui, J. Y.; Shieh, T. S. *Macromolecules* **1997**, *30*, 5068.
9. Kim, B. K.; Lee, J. C. *Polymer* **1996**, *37*, 469.
10. Lee, D. K.; Tsai, H. B.; Tsai, R. S. *J. Appl. Polym. Sci.* **2006**, *102*, 4419.
11. Nanda, A. K.; Wicks, D. A. *Polymer* **2006**, *47*, 1805.
12. Špírková, M.; Poręba, R.; Pavličević, J.; Kobera, L.; Baldrian, J.; Pekarek, M. *J. Appl. Polym. Sci.* **2012**, *126*, 1016.
13. Poręba, R.; Špírková, M.; Brožová, L.; Lazić, N.; Pavličević, J.; Strachota, A. *J. Appl. Polym. Sci.* **2013**, *127/1*, 329.
14. Noble, K. L. *Prog. Org. Coat.* **1997**, *732*, 131.
15. Delpech, M. C.; Coutinho, F. M. *Polym. Test.* **2000**, *19*, 939.
16. Lee, D. K.; Yang, Z. D.; Tsai, H. B.; Tsai, R. S. *Polym. Eng. Sci.* **2009**, *49*, 2264.
17. Garcia-Pacios, V.; Jofre-Reche, J. A.; Costa, V.; Colera, M.; Martin-Martinez, J. M. *Prog. Org. Coat.* **2013**, *76*, 1484.
18. Cakić, S. M.; Špírková, M.; Ristić, I. S.; B-Simendić, J. K.; M-Cincović, M.; Poręba, R. *Mater. Chem. Phys.* **2013**, *138*, 277.
19. Lee, D. K.; Tsai, H. B.; Yang, Z. D.; Tsai, R. S. *J. Appl. Polym. Sci.* **2012**, *126*, E275.

20. Madbouly, S. A.; Otaigbe, J. U. *Prog. Polym. Sci.* **2009**, *34*, 1283.
21. Garcia-Pacios, V.; Costa, V.; Colera, M.; Martin-Martinez, J. M. *Prog. Org. Coat.* **2011**, *71*, 136.
22. Barrére, M.; Landfester, K. *Macromolecules* **2003**, *36*, 5119.
23. Špírková, M.; Kubín, M.; Dušek, K. *J. Macromol. Sci.* **1987**, *A24*, 1151.
24. Štěpánek, P. *J. Chem. Phys.* **1993**, *99*, 6384.
25. Jakeš, J. *Czech. J. Phys.* **1988**, *38*, 1305.
26. Štěpánek, P.; Koňák, Č. *Polymer* **1984**, *21*, 195.
27. Kim, B. K.; Lee, J. C. *J. Polym. Sci., Part A: Polym. Chem.* **1996**, *34*, 1095.
28. Dobrynin, A. V.; Rubinstein, M. *Prog. Polym. Sci.* **2005**, *30*, 1049.
29. Kelly, C. P.; Cramer, C. P.; Truhlar, D. G. *J. Phys. Chem. B* **2006**, *110*, 16066.
30. Ostolska, I.; Wiśniewska, M. *Colloid Polym. Sci.* **2014**, *292*, 2453.
31. Lee, J.; Kim, M.; Hong, C. K.; Shim, S. E. *Meas. Sci. Technol.* **2007**, *18*, 3707.
32. Dietrich, D.; Keberle, W.; Witt, H. *Angew. Chem. Int. Edit.* **1970**, *9*, 40.
33. Saiani, A.; Rochas, C.; Eeckhaut, G.; Daunch, W. A.; Leenslag, J. W.; Higgins, J. S. *Macromolecules* **2004**, *37*, 1411.
34. Hourston, D. J.; Williams, G.; Satguru, R.; Padget, J. D.; Pears, D. *J. Appl. Polym. Sci.* **1998**, *67*, 1437.
35. Lee, J. S.; Kim, B. K. *Prog. Org. Coat.* **1995**, *25*, 311.
36. Lee, Y. M.; Lee, J. C.; Kim, B. K. *Polymer* **1994**, *35*, 1095.
37. Matějíček, P.; Humpolíčková, J.; Procházka, K.; Tuzar, Z.; Špírková, M.; Hof, M.; Webber, S. E. *J. Phys. Chem.* **2003**, *107*, 8232.
38. Sultan, M.; Islam, A.; Gull, N.; Bhatti, H. N.; Safa, Y. *J. Appl. Polym. Sci.* **2015**, *132*, 41706.
39. Yilgor, I.; Yilgor, E.; Wilkes, G. L. *Polymer* **2015**, *58*, A1.
40. Sami, S.; Yildirim, E.; Yurtsever, M.; Yurtsever, E.; Yilgor, E.; Yilgor, I.; Wilkes, G. L. *Polymer* **2014**, *55*, 4563.
41. Nanda, A. K.; Wicks, D. A.; Madbouly, S. A.; Otaigbe, J. U. *J. Appl. Polym. Sci.* **2005**, *98*, 2514.
42. Korley, L. T. J.; Pate, B. D.; Thomas, E. L.; Hammond, P. T. *Polymer* **2006**, *47*, 3073.
43. Špírková, M.; Pavličević, J.; Strachota, A.; Poręba, R.; Bera, O.; Kaprálková, L.; Baldrian, J.; Šlouf, M.; Lazić, N.; B-Simendić, J. *Eur. Polym. J.* **2011**, *47*, 959.

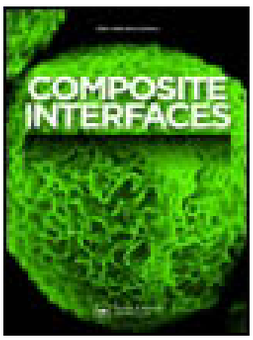

Composite Interfaces

ISSN: 0927-6440 (Print) 1568-5543 (Online) Journal homepage: http://www.tandfonline.com/loi/tcoi20

Organic–inorganic nanocomposite films made from polyurethane dispersions and colloidal silica particles

Magdalena Serkis, Milena Špírková, Jana Kredatusová, Jiří Hodan & Radovan Bureš

To cite this article: Magdalena Serkis, Milena Špírková, Jana Kredatusová, Jiří Hodan & Radovan Bureš (2016): Organic–inorganic nanocomposite films made from polyurethane dispersions and colloidal silica particles, Composite Interfaces, DOI: 10.1080/09276440.2016.1124666

To link to this article: http://dx.doi.org/10.1080/09276440.2016.1124666

Published online: 11 Jan 2016.

COMPOSITE INTERFACES, 2016
http://dx.doi.org/10.1080/09276440.2016.1124666

Taylor & Francis
Taylor & Francis Group

Organic–inorganic nanocomposite films made from polyurethane dispersions and colloidal silica particles

Magdalena Serkis[a], Milena Špírková[a], Jana Kredatusová[b], Jiří Hodan[b] and Radovan Bureš[c]

[a]Nanostructured Polymers and Composites Department, Institute of Macromolecular Chemistry AS CR, Prague, Czech Republic; [b]Polymer Processing Department, Institute of Macromolecular Chemistry AS CR, Prague, Czech Republic; [c]Informatics Computers and Applied Mathematics Department, Institute of Materials Research, Slovak Academy of Sciences, Kosice, Slovak Republic

ABSTRACT

Polyurethane/silica nanocomposites were prepared by solution blending of polyurethane water dispersion (PUD) based on polycarbonate macrodiol with colloidal silica aqueous sol LUDOX TMA. Because of mixing PUDs made from linear polyurethane with the nanofiller, only physical polymer/filler type of interface formed by hydrogen bonds was obtained. As a result the materials were possible to reuse after dissolution in acetone followed by dispersion in water. The effect of colloidal silica content on mechanical, thermal, morphological, and swelling properties of obtained films was tested by tensile test, dynamic mechanical thermal analysis, thermogravimertic analysis, scanning electron microscopy, atomic force microscopy, and swelling analyses. The nanocomposites were classified in three groups differing in the internal structure and functional properties: organic matrix filled with inorganic nanofiller (up to 10 wt% of silica), bicontinous systems (25 and 32 wt% of silica) and inorganic matrix filled with polyurethane (50 and 60 wt% of silica). Only small amount of colloidal silica (up to 10 wt%) improves thermo-mechanical properties, smoothes the materials, and suppresses extent of swelling without changing of the films transparency.

ARTICLE HISTORY
Received 11 August 2015
Accepted 20 November 2015

KEYWORDS
Polyurethane dispersion; colloidal silica; composites; morphology; mechanical properties

1. Introduction

Polyurethanes (PU) containing polycarbonate polyols (PCDs) as a soft phase become more and more common.[1,2] In comparison with polyether- or polyester-based polyurethanes they have better mechanical properties and they are more resistant to UV–light, hydrolysis, heat, and oxidative processes. PCDs are produced by the reaction of alkane diol and dialkyl carbonates and there are used as biocompatible materials with suitable flexibility at low temperature.[3,4] They are mainly used as elastomers, but, due to excellent hydrolytic and oxidative stability, they are also more and more popular in a form of colloidal nanoparticles (PU dispersions and PUDs), being utilized as coatings, films, and adhesives.[5,6] The main

CONTACT Magdalena Serkis serkis@imc.cas.cz; Milena Špírková spirkova@imc.cas.cz

problem for solvent-borne polyurethane coatings is emission of organic solvents to the atmosphere, which was a motivation for development of polyurethane water dispersions. Waterborne polyurethanes are polymer chains dispersed in water, due to incorporation of internal emulsifiers (ionic, e.g. involving carboxylic groups) into polyurethane backbone. [7–10] A disadvantage of carboxylic groups present in a polymer chain is a possibility of hydrolysis and a deterioration of thermal and mechanical properties.[11] One of the common method to improve PU systems (being in the form of elastomers, plastics, foams, or dispersions) is using them in organic–inorganic (O–I) nanocomposite synthesis.[12,13]

O–I nanocomposites became very popular, especially in the last two decades.[14–16] Their popularity is caused mainly from the simplicity in tuning of functional properties by the choice of organic and inorganic raw materials, their concentration, shape, preparation procedure, etc. Four main ways of O–I nanocomposite preparation are possible: (i) the addition of inorganic precursor into the organic polymer (e.g. use of the sol–gel process for the reinforcement of given polymer),[17] (ii) the addition of inorganic particles into the polymerizable mixture of monomers,[18] (iii) the use of the mixture of monomers and inorganic precursor – both matrices are formed subsequently in situ,[19] and (iv) the mixing of final organic polymer with inorganic nanoparticles.[20] All routes are used in practice, and their either benefits or limits depend on intended use.

Silica nanoparticles belong to very common and popular nanofiller in O–I nanocomposites due to excellent stability, high hardness, and low price.[15,21] It can be further modified on the surface that spreads their utility possibilities. Silica nanoparticles exist as a powder obtained from fumed silica or precipitated silica. However, colloidal silica is more popular than powder one due to perfectly round shape of particles, homogenously dispersed in water or alcohol.[22–24]

In principle, polyurethane/silica nanocomposites can be prepared by all four above-mentioned ways, but sometimes with specific conditions of the preparation depending on the intended practical use. According to which type of interaction is desirable, different methods of preparation PU/nanosilica composites exist. Most of them utilize chemical interactions between the nanofiller and polyurethane, obtained, for example, in sol–gel process. This method is a two-step network forming technique, firstly the hydrolysis and secondary polycondensation reaction of alkoxides. In sol–gel process silica precursor (e.g. TEOS) reacts with monomers or polymer and as a result a cross-linked polymer is obtained.[21,24]

In situ, polymerization process involves three steps: (i) pre-treatment of nano-additives with modifiers, (ii) dispersing of modified additives into monomers, and (iii) forming of nanocomposites *in situ* during the polymerization. This method is often used during preparation of PU/nanosilica composites, but the main problem accompanying the process is necessity of water removal from aqueous silica sol or transfer the silica into organic solvent during forming the nanocomposites.[23,24]

The simplest way of incorporating silica particles into polymer is direct mixing of the both components. There are two types of this method: (i) melt blending and (ii) solution blending.[24] Due to this way of preparation only hydrogen bonds and van der Waals forces are present between nanosilica particles and polyurethane matrix (nanoparticles formed from linear charged PU chains), that means the 3D-network structure is formed due to temporary physical bonds between both types of the nanoparticles. The main advantage of nanocomposites based on solely physical bonding is the simplicity of the reusing or recycling.

According to our knowledge there are only few publications, which consider the preparation and characterization of PUDs derived from PCDs [4,5,7–10,25] and all of them are cross-linked systems based on ethylenediamine or monohydrated hydrazine. In one study dedicated to PUDs [26] the sol–gel process with the participation of 3-aminopropyltrieth-oxysilane (APTES) has been used, which allowed to obtain the cross-linked-salinized PU.

Our previous study have presented linear system of PUDs based on polycarbonate macrodiol, diisocyanate-1,6-hexane, 2,2-bis (hydroxymethyl) propionic acid, and butane-1,4-diol.[27] Despite the fact that the dispersions were stable, mechanical properties of obtained films were limited. In order to study the impact of nanosilica content on the final (especially surface, mechanical, and thermal) functional properties, series of PU/silica nanocomposites differing on the silica content were prepared. The solution blending followed by slow and gradual water evaporation enabled the preparation of PU/silica nanocomposites being joint together just by physical bonds. To our knowledge, nanocomposites made from PUDs based on solely linear aliphatic PU chains and colloidal silica nanoparticles were not described yet.

2. Experimental

2.1. Materials

Aliphatic polycarbonate macrodiol (PC, trademark T4672) with molecular weight ca. 2770 g mol^{-1} was kindly provided by Asahi Kasei Chemical Corporation, Tokyo, Japan. Hexamethylene diisocyanate (HDI), 2,2-bis (hydroxymethyl) propionic acid (DMPA), 1,4-butanediol and triethylamine (TEA) were received from Sigma-Aldrich Co. Dried acetone (max. 0.0075 wt% H_2O) was supplied by Merck KGaA, Darmstadt, Germany. The catalyst constituted 10 wt% solution of dibutyltin dilaurate (DBTDL) (Sigma-Aldrich, Co.) in Marcol oil. Aqueous silica sol LUDOX TMA[1] was obtained from Aldrich Chemical Company, Inc., USA, as a 34 wt% suspension in deionized water. The characteristic values of the silica were as follow: molecular weight of 60.08 g mol^{-1}, specific surface area of 140 m^2 g^{-1}, pH of 7, and density of silica particles 2.37 g cm^{-3}.

2.2. Preparation of PU/silica nanocomposites

The detailed preparation of waterborne PU is described in our previous work.[27] In this paper, colloidal silica was added to PUD made from PC, HDI, DMPA, BD, and TEA. PUD containing BD-to-PC molar ratio equal to 0.5 and DMPA-to-PC equal to 0.4 was used as the organic matrix. This PUD was chosen because of the narrowest size dispersity index, PDI = 0.06, in comparison to other PUDs prepared and very good long-term stability, ca. 1 year. Other characteristics of the PUD were as follow: particle size of 88 nm, ζ-potential of –50 mV, M_n = 22.7 kg mol^{-1}, M_w = 48.2 kg mol^{-1}. For other details see [27].

PU/silica nanocomposites were prepared by solution blending method, as given in Figure 1. For this purpose PUD containing 32 wt% of PU in water was mixed with the aqueous silica sol using magnetic stirrer at the rate of 700 rpm for 1.5 h at room temperature. Samples containing from 5 to 60 wt% of the nanofiller were prepared, calculated on the dry weights of silica and polyurethane. The sample codes and compositions are given in Table 1. Neat polyurethane contained two types of hydrogen bonding: hard–soft segments (Figure 1(a)) and hard–hard segments (Figure 1(b)). As a result of mixing linear polymer

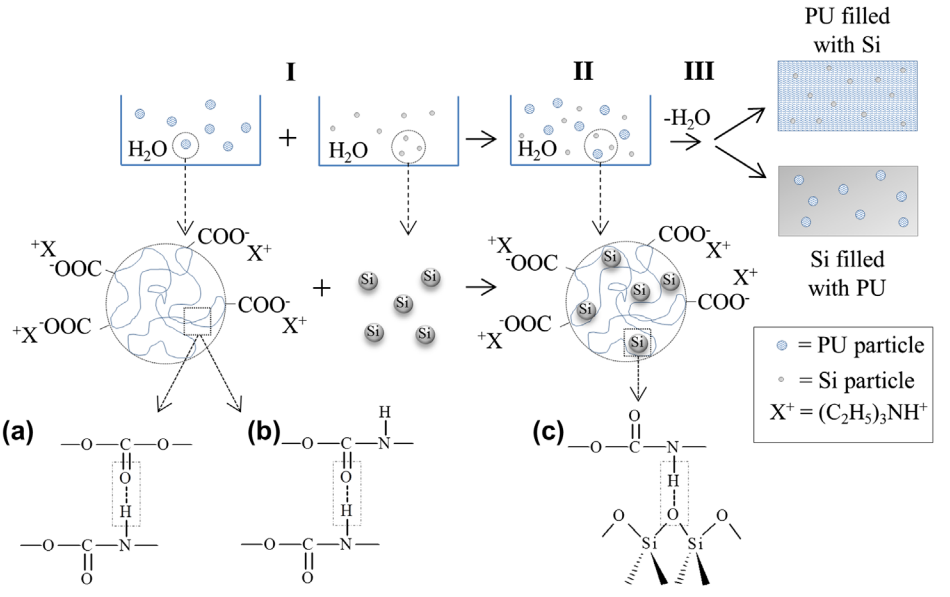

Figure 1. Scheme of preparation PU/nanosilica composites: (I) solution blending of PU and colloidal silica (Si) dispersed in water, (II) incorporation of Si particles between polymer chains, (III) obtaining of continuous film (different types depending on PU and Si concentration). Possibilities of hydrogen bonding in PU/nanosilica composites: (a) urethane–carbonate groups (hard–soft segments), (b) urethane groups (hard–hard segments), and (c) silica–urethane groups.

Table 1. Sample codes, code abbreviations (used solely in figures), and silica content in PU/silica nanocomposites.

Code	Code abbreviation	m^a_{TMA} (g)	m^a_{PU} (g)	Silica content (wt%)
TMA-0	0	0	5.99	0
TMA-5	5	0.29	5.50	5
TMA-10	10	0.56	5.50	9.3
TMA-25	25	1.83	5.47	25
TMA-32	32	1.92	4.08	32
TMA-50	50	5.48	5.48	50
TMA-60	60	3.61	2.40	60

m^a – mass of dry silica and dry polyurethane.

with silica particles, new physical cross-links were created (Figure 1(c)). PU/silica dispersions in water were cast on Teflon plates. After drying the samples for 5 days at room temperature and then at 50 °C for 20 h, continuous films were obtained. Film thickness (~500 μm) was controlled by the amount of nanoparticle–water mixture used for unit area of the Teflon mold. The ease of use of this system was the same environment-friendly medium (water) and a good chance of homogeneous mixing for both types of particles. The greatest advantage of these materials was possibility of recycling. Due to solubility of obtained films in acetone, they can be easily suspended in water and used again for films formation. In our previous study,[27] we have observed the same thing, however here we concluded that addition of colloidal silica did not deteriorate the materials recyclability.

2.3. Methods of characterization

2.3.1. Tensile characterization

Static and mechanical properties were measured on Instron model 6025/5800R (Instron Limited, UK) equipped with 100 N load cell, at room temperature with a cross-head speed of 10 mm min^{-1}. Dumbbell-shaped specimens corresponded to the ISO 527-2/5B type: total specimen length 35 mm, length, and width of the narrowed part: 12 and 2 mm, thickness 0.5 mm. Selected tensile characteristics were determined: Young's modulus E (modulus of elasticity, given in MPa), tensile strength σ_b (maximum stress before braking the material, given in MPa), elongation-at-break ε_b (percentage increase in length before the sample break), and toughness (energy-to-break the sample per volume unit, given in mJ mm^{-3}). Reported values were the averages of at least five measurements. Presented tensile curves were taken from the measurements the closest to each calculated average value.

2.3.2. Dynamic mechanical thermal analysis

Dynamic mechanical thermal analysis (DMTA) was measured by ARES-G2 from TA instruments. An oscillation frequency of 1 Hz, deformation in a range from 0.01 to 3.5%, the heating rate of 3 °C min^{-1} from −100 to +180 °C were applied. The geometry of standard specimens was: 25 × 6 × 0.5 mm^3. Storage modulus (G'), loss modulus (G''), and loss factor ($\tan \delta = G''/G'$) were measured.

2.3.3. Thermogravimetric analysis

Thermogravimetric analyses (TGA) of the samples (10–15 mg) were performed on Pekin-Elmer Pyris 1 TGA. The analyses were carried out in temperature from 30 to 700 °C under nitrogen flow of 30 ml/min at 10 °C min^{-1}. TGA curves were determined. T_{onset}, $DTGA_{max}$, and $W_{R600\ °C}$ were investigated as well.

2.3.4. Optical microscopy

Films appearance and transparency were investigated by surface analysis of the material using stereo microscope at magnification 1×. Dried samples were measured at the same field by NIKON SMZ18 equipped with objective P2-SHR Plan Apo 0.5×. There was not needed any additional sample preparation before the measurement.

2.3.5. Scanning electron microscopy

Scanning electron microscopy (SEM) was used for general determination of samples morphology, both the surface and the cross section in magnification range from 500× to 15,000×. Dried films were broken in liquid nitrogen. Measurements were carried out by Vega Plus TS 5135 (Tescan, Czech Republic). Before SEM analysis samples were sputtered with 4 nm Pt layer using vacuum sputter coater SCD 050 (Balzers, Czech Republic).

2.3.6. Atomic force microscopy

Analysis of the surface morphology of PU/silica films and colloidal silica dispersity in the polymer matrix were performed by atomic force microscopy (AFM) (Dimension Icon, Bruker), equipped with the SSS-NCL probe (Super Sharp SiliconTM – SPM-Sensor from NanoSensors™ Switzerland; spring constant 35 N m^{-1}, resonant frequency ≈ 170 kHz), using tapping mode AFM technique. The scans covered sizes from 1 × 1 μm to 10 × 10 μm. The

Table 2. Tensile properties of PU/nanosilica films.

Sample code	Young's modulus, *E*, (MPa)	Stress-at-maxload, (MPa)	Elongation-at- maxload (%)	Stress-at-break, σ_b, (MPa)	Elongation-at-break, ε_b, (%)	Energy-to-break (mJ/mm^3)
TMA-0	8	2.0	84	1.4	94	1.5
TMA-5	12	2.0	87	1.4	108	1.8
TMA-10	15	1.9	83	1.3	110	1.9
TMA-25	41	1.8	36	1.0	107	1.8
TMA-32	62	1.4	22	0.6	84	1.1
TMA-50	552	7.6	2.8	2.3	33	1.3

AFM images of film surfaces and the fractured areas after previous freeze – fracturing in liquid nitrogen conditions were measured. The evaluation of the roughness surface parameters R_q, R_a, and R_{max} were based on areas 5 × 5 μm.

2.3.7. Swelling and solubility in water

Water swell was measured by immersing the films in water at room temperature for 20 weeks. After the residual water was wiped from the sample surfaces with filter paper, the weight of swollen films was measured immediately. The water swelling of the samples was calculated by measuring its mass increase as a function of time, by the following equation:

$$\%\ \text{Swelling} = \frac{w - w_0}{w_0} \times 100\% \tag{1}$$

where w_0 is mass of the dry film, w is mass of the film after being measured in water over a certain period of time.

After the immersion in water by 20 weeks, the samples were dried in 50 °C for 20 h. The percentage weight loss, Δw, was calculated according to the equation:

$$\Delta \text{w} = \frac{w_0 - w_f}{w_0} \times 100\% \tag{2}$$

where w_f is the weight of dried film after immersing in water.

3. Results and discussion

Series of thermoplastic PU/nanosilica films differing in the content of inorganic nanofiller (from 5 to 60 wt%) were prepared by mixing of the polymer matrix with colloidal silica. Depending on the composition they differed in appearance and consistence. Due to variety of the materials, tensile properties were tested at first.

3.1. Tensile properties

Tensile properties of PU/nanosilica films depend significantly on the silica amount. Table 2 summarizes the Young's modulus (E), stress-at-break (σ_b), elongation-at-break (ε_b), and energy-to-break (toughness). As the samples are distinguished by the complex elastic–plastic character, elongation at maximal stress value (marked as elongation-at-maxload and stress-at-maxload) are the part of Table 2. Figure 2(a) shows tensile characteristics of

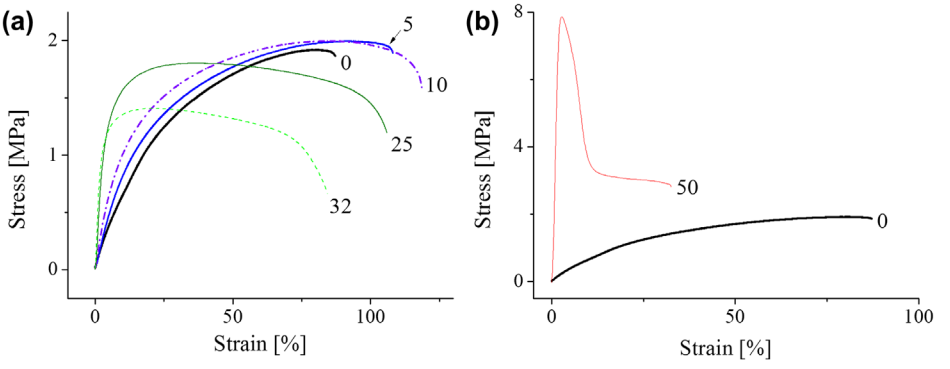

Figure 2. Stress–strain curves of cast PUD/nanosilica films: (a) colloidal silica concentration up to 32 wt% and (b) pure matrix and sample containing 50 wt% of silica amount (code abbreviations are given in Table 1).

films containing up to 32 wt% of silica. Tensile curves of pure PU matrix, TMA-0, and the sample with the silica loading of 50 wt%, TMA-50 are given in Figure 2(b).

Three groups featuring different tensile characteristics can be observed. (i) The neat matrix and films with 5 and 10 wt% of the nanofiller have elastomeric-like behavior. In samples TMA-5 and TMA-10 continuous polyurethane matrix is filled with ceramic-type nanomaterial, which causes slight improvement of mechanical properties. This can be explained by the effective stress transfer from the polymer matrix to the silica particles. (ii) Samples TMA-25 and TMA-32 represent bicontinuous system, where the material becomes tough plastic with elastic limit given by the yield strength at very low elongation (up to 10%). There is an increasing in number of places where no polymer between silica particles is available for energy dissipation, compared to the first group. The nanofiller in this case impairs elasticity referring to the polyurethane matrix. (iii) In case of TMA-50, the continuous phase is silica, filled with dispersed polyurethane. As a result, obtained material is hard, visible at the first part of curve, and typical for ceramic. After crossing the yield strength, plastic behavior derived from the organic polyurethane part is visible. Sample TMA-60 was too brittle for tensile measurements.

3.2. Dynamic mechanical thermal analysis

The temperature dependences of the storage modulus (G') and loss factor (tan δ) for PU/nanosilica films containing different amount of the nanofiller are shown in Figure 3. The storage modulus G' of the films (Figure 3(a)) increases as silica content is increasing due to reinforcing of the organic matrix by the inorganic filler and blocking relaxation of polyurethane chains by silica particles. Moreover, it is visible that melting temperature of the nanocomposite materials increases with the increasing filler concentration, which can be explained by higher amount of hydrogen bonds between PU matrix and silica nanoparticles.

The maxima on tan δ curves $(\tan \delta)_{max}$, show the glass transition temperature, T_g (α-relaxation peak) identical for all samples, around –31 °C (Figure 3(b)). The glass transition temperature depends on many factors, such as loading, size, and concentration of a filler and dispersion condition.[24] No significant changes in T_g for neat PU matrix and PU/silica

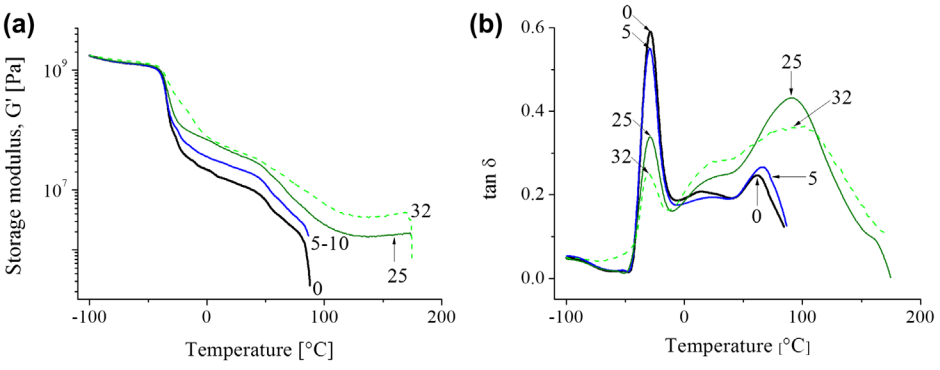

Figure 3. The temperature dependences of: (a) storage modulus, G′, (left) and (b) loss factor, tan Δ, (right) of PU/nanosilica composites. Code abbreviations are given in Table 1.

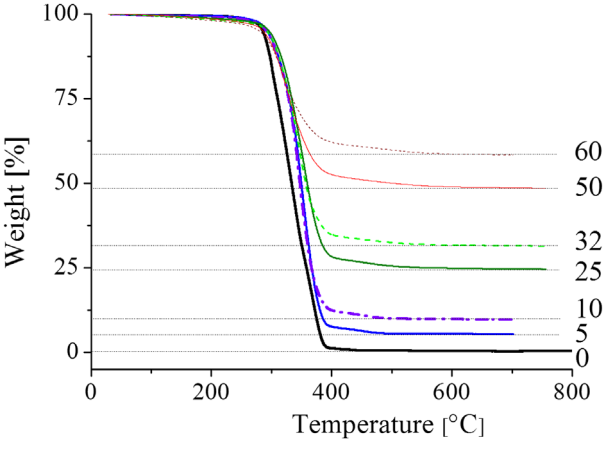

Figure 4. TGA curves of PU-based films containing different silica content. Code abbreviations are given in Table 1.

nanocomposites occurred as a result of weak, physical interactions between the filler and polymer matrix. The presence of nanosilica thus changes only the packing of polyurethane chains, but does not change their stiffness.

Increase in silica amount causes blocking of PU chains mobility and as a result, the chains are released at higher temperatures. In case of sample containing 32 wt% of silica (TMA-32) different trend in tan δ vs. temperature is visible, caused by the increase in the amount of silica/silica interface in comparison to silica/matrix. The difference in the bicontinous film behavior was also confirmed by tensile tests (see Chapter 3.1). Sample TMA-10 showing similar behavior to TMA-5 was deleted from Figure 3(a) and (b) due to clarity of the plots. Films containing 50 and 60 wt% of silica were too brittle for DMTA measurements.

3.3. Thermogravimetric analysis

TGA was used to study the effect of colloidal silica content on the PU/silica nanocomposites. TGA curves are shown in Figure 4. Obtained data are summarized in Table 3. In

Table 3. Parameters obtained from TGA measurements for the PU/nanosilica films.

Code	T_{onset} (°C)	$DTGA_{max}$ (°C)	$W_{R600\,°C}$ (%)
TMA-0	274	335	0.5
TMA-5	276	350	5.4
TMA-10	278	344	9.8
TMA-25	281	353	24.9
TMA-32	279	346	31.7
TMA-50	270	325	48.9
TMA-60	273	319	58.6

T_{onset} – thermal degradation onset temperature, $DTGA_{max}$ – maximum of derivative TGA, $W_{R600\,°C}$ – residue at 600 °C in nitrogen atmosphere.

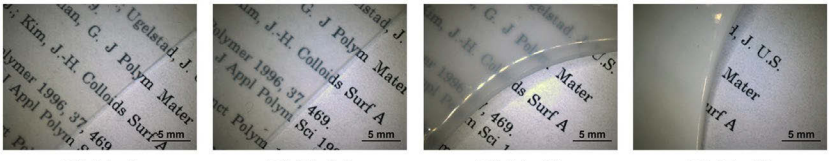

TMA-5 TMA-32 TMA-50 TMA-60

Figure 5. Optical microscopy images (magnification 1×) of films containing 5, 32, 50, and 60 wt% of silica, respectively.

general, the TGA curve of neat polyurethane has two thermal decomposition stages. There are attributed to removal of residual water and decomposition of hard and soft segments in polyurethane.[28] The films modified by colloidal silica have the same trend and there is no additional stage in comparison with the matrix. However, the decomposition of PU/nanosilica stage is shifted to higher temperatures. It is caused by shielding effect of the filler,[29] which reduce mass transport rate. Moreover, incorporation of silica particles into polymer matrix decreases mobility of PU chains. The nanofiller acts as a mass transport barrier for the volatile products, which are generalized during thermal stability of PUD-based films. The TGA thermograms (Figure 4) and Table 3 (4th column) show silica residues, which amount is precisely equal to the nanofiller concentration in PU/nanosilica films. It provides that organic polyurethane parts were completely oxidized, whereas $W_{R600\,°C}$ is the inorganic filler residue.

3.4. Optical microscopy characterization

Transparency is one of very important property of coating materials, which gives information about possibility of the light transmission trough a sample. However, addition of silica particles often increases the nanocomposite opaqueness because of light scattering caused by silica particles.[26]

Figure 5 shows optical microscopy images of selected samples containing various concentrations of the nanofiller. The materials transparency was tested by measuring of the films located on the same background. It is clearly visible that samples are transparent till 32 wt% of silica loading, which suggest that in these cases nanofiller is well dispersed in the matrix (see Figure 8). This result shows a real possibility of using PU/silica nanocomposites as transparent materials.

The films became more opaque with increasing of silica amount, till completely white sample containing 60 wt% of the nanofiller. This phenomenon is caused not only by creation of silica agglomerates, but also by increasing samples porosity, which will be discussed in the SEM section (Chapter 3.5).

3.5. Scanning electron microscopy

It was found that mechanical and thermal properties of PU/silica nanocomposites depend significantly on nanosilica content. In order to correlate their microstructure with the other functional properties, both film surfaces and surfaces of cross sections for broken samples were measured by SEM. Representative micrographs of PU/nanosilica films are shown in Figure 6.

In accordance to mechanical analysis (Chapters 3.1 and 3.2) the samples can be divided into three groups.

The first group contains neat matrix (TMA-0) and samples with inorganic core surrounded by organic polymer shell (TMA-5 and TMA-10). This part of films is represented in Figure 6 on the top. At the surface there are visible rod-like structures, simultaneously all fibrils are connected with each other. The cross-section analysis of these films, which offers the view into the bulk characteristics, presents homogenous structure.

The samples containing higher silica amount (TMA-25 and TMA-32) belong to the second group, named bicontinous materials. The surface micrographs show that rods are separated, which is a result of blocking and disordering of PU chains by silica particles,

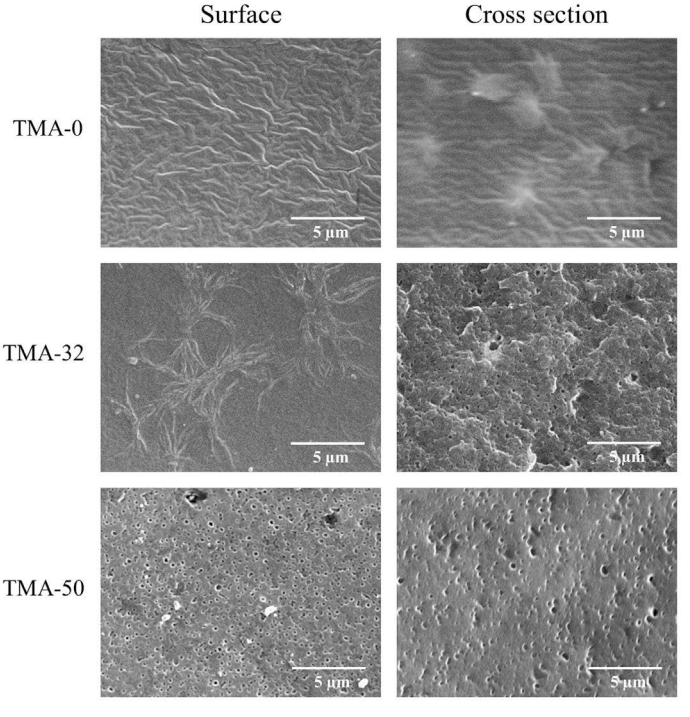

Figure 6. Surface (left) and cross-section (right) SEM images of PU/nanosilica films (magnification 10,000 ×).

but polymer-like morphology is still visible in these cases. However, freeze-fractured areas present porous structure. This behavior may be explained by increasing the number or intensity of hydrogen bonding between PU molecules and nanosilica particles. The porosity accumulates internal stress and makes the material weaker (see tensile test measurements in Chapter 3.1).

To the third group belong samples with the highest nanofiller concentration (TMA-50 and TMA-60), representing silica filled with PU. Both surface and cross-section analysis show high number of pores in the structure, typical for ceramic materials. The porosity causes deformation of the brittle films and makes materials appear white (see Figure 5). Due to low magnification, no individual silica nanoparticles are visible, however.

3.6. Atomic force microscopy

AFM was used in order to study the size and shape of silica particles and influence of the nanofiller content on changes in microstructure of obtained films. Height images show surface morphology, whereas phase images reflect a contrast between different sample components, that is heterogeneity.

The particle size of LUDOX TMA colloidal silica was reported by the manufacturer as 22 nm, however DLS measurements yield a value of approximately 39 nm. The particles were well dispersed in deionized water (zeta potential of –37 mV). The surface of pure TMA previously dried at 50 °C for 20 h is presented in Figure 7. Rounded particles are closely packed next to each other. High distribution of particle size, in a range from 35 to 70 nm was measured by NanoScope Analysis software, via section analysis. Dried colloidal silica is tough, brittle, and highly cracked material.

More detailed morphology of PU/nanosilica films previously characterized by SEM (see Chapter 3.5) was obtained by AFM. The same samples measured by the both microscopic techniques are shown in Figure 8. The microstructure of samples containing the lowest silica amount (TMA-0, TMA-5 and TMA-10) is represented by TMA-0 and shown on the top, confirming the SEM results (cf. with Figure 6, top). The surface analysis of the second group (TMA-25 and TMA-32) shows structure of separated roads, which corresponds to the SEM image (Figure 6, middle). In this case the concentration of the filler is so low that silica particles are not visible on the films surfaces because they are covered by PU layer.

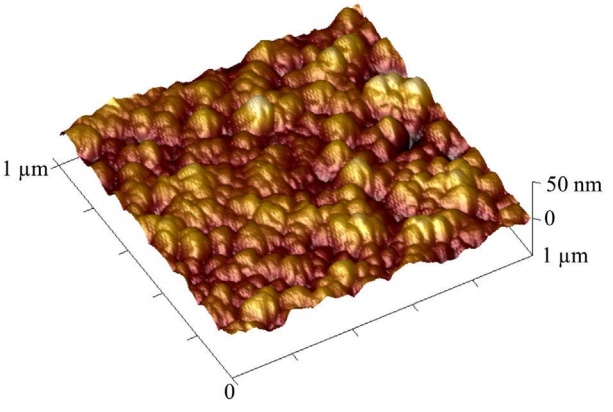

Figure 7. 3D AFM height image of dry TMA, scan size 1 × 1 µm.

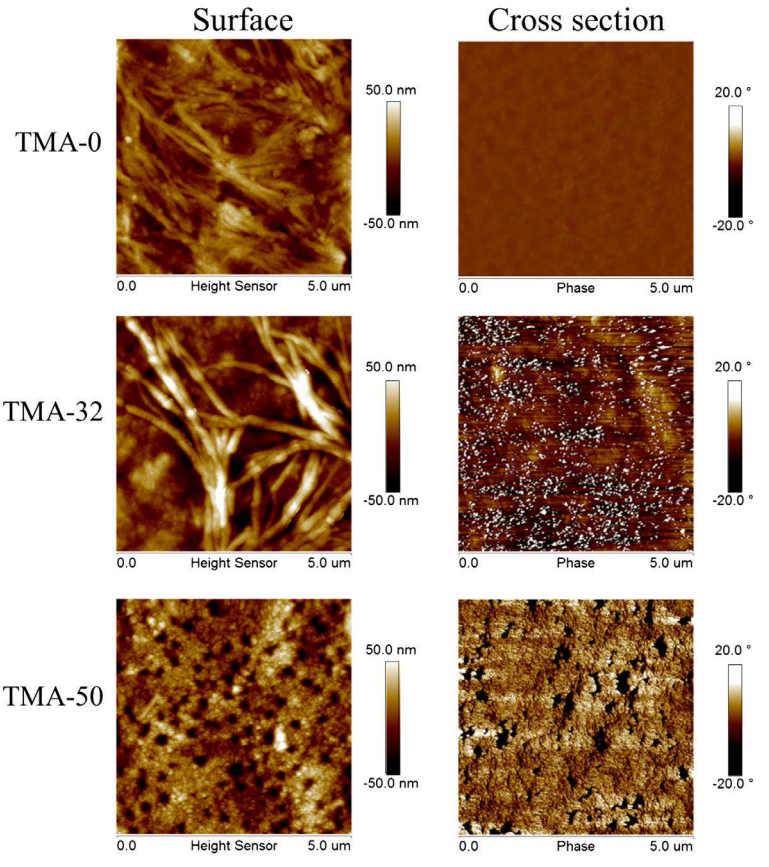

Figure 8. 2D AFM images (5 × 5 μm) of PU/nanosilica films: height images of film surfaces (left) and phase images of cross sections (right). Sample TMA-0 (top) represents the first group, TMA-32 (middle) the second group and TMA-50 (bottom) the third group of PU/nanosilica films.

The freeze fractured cross sections show the lighter spots reflect to the harder silica particles, whereas the softer polymer phase appears darker. As observed, even with quite high nanofiller loading (TMA-32), the particles are evenly distributed though the sample. The micrographs of the films containing the highest silica concentration (TMA-50 and TMA-60, third group, Figure 8, bottom) present visible silica agglomerates, both at surfaces and cross sections. In these cases separated parts of PU are surrounded by the nanofiller, which means that silica shell is located around the polymer core. This material is hard ceramic I-O system (see Chapters 3.1 and 3.2). In summary, AFM, SEM, and optical microscopy images demonstrate the influence of the nanofiller in the PU/silica films on their surface and bulk morphologies and can also explain the differences in sample properties measured by other techniques.

The roughness values of PU/nanosilica film surfaces were determined. All data, based on areas 5 × 5 μm are reported in Table 4. Low nanofiller amount (TMA-5 and TMA-10) makes the films smoother. The reduction in surface roughness could be understood on the basic of incorporation of small silica particles between bigger polymer molecules, which complements cavities on the materials surfaces. The roughness parameters become higher

Table 4. Surface roughness of neat and silica-filled PUs.

Code	Surface area (μm²)[a]	R_q (nm)[b]	R_a (nm)[c]	R_{max} (nm)[d]
TMA-0	25.4	22	18	142
TMA-5	25.2	14	11	80
TMA-10	25.1	15	12	97
TMA-25	25.3	26	21	143
TMA-32	25.8	24	19	169
TMA-50	26.5	25	19	193
TMA-60	27.1	36	29	245

[a]Surface area: the total area of experimental sample surface.
[b]R_q: the root-mean square roughness – standard deviation of the *Z* values within the given area.
[c]R_a: the mean roughness – arithmetic average of the absolute values of the surface height deviations measured from the mean plane.
[d]R_{max}: the max height – maximum vertical distance between the highest and lowest data points in the image following the planefit.

with the increase in silica amount, which proves that the nanocomposite structure starts to change. The highest roughness parameters are obtained for films containing the highest nanofiller concentration (TMA-50 and TMA-60). These samples are the most porous (see Figure 6) and silica particles protrude from the film surfaces (see Figure 8). As a result of deep depressions that characterize pores and high hills caused by the nanofiller, the materials become rougher.

3.7. Swelling behavior

Water interactions with polymers may cause some undesirable effects, such as plasticization, deterioration of mechanical properties, microcrack, and craze formation and degradation of the matrix/filler interfaces. These changes depend on the level of interactions between polymer and water molecules. Because of small molecular size of water, it can spread into nanometer size-free volume between polymer chains, forcing them apart.[30] Therefore, water sorption and solubility of polymers should be as low as possible.

The swelling in water was determined as the mass increasing over a period of time; the results are shown in Figure 9 and summarized in Table 5. Water sorption of neat PU-based film (TMA-0) is caused by hydrophilicity corresponding to DMPA content, built into the polyurethane chain. The amount of sorbed water decreases with increasing colloidal silica content in case of films containing up to 10 wt% of the nanofiller (sample TMA-10 is not presented at the plot because of almost identical swelling behavior-like TMA-5). In these compact samples as a result of creation hydrogen bonds between silica and PU, lower swellability is observed. It can be explained by less vacants possible for water molecules accommodation, which are already occupied by silica particles, as compared to pure PU film (TMA-0). Samples TMA-5 and TMA-10 are characterized by fast swelling over a short time of immersion in water. After one day (Table 5, 4th column) the weight decreased, however. The swelling maximum in PU/silica nanocomposites is lower only for sample TMA-5, compared to pure PU (Table 5, 2nd column) but after 20 weeks, two samples (TMA-5 and TMA-10) have lower swelling values than neat matrix (TMA-0).

Increasing of silica amount causes increasing of films porosity, shown in the cross-section SEM images (Figure 6), which enhances water transport. There are only slight changes between neat PUD-based film (TMA-0) and TMA-25, probably because the blocking silica effect, which reduces swellability, is in equilibrium with hydrophilic influence of colloidal

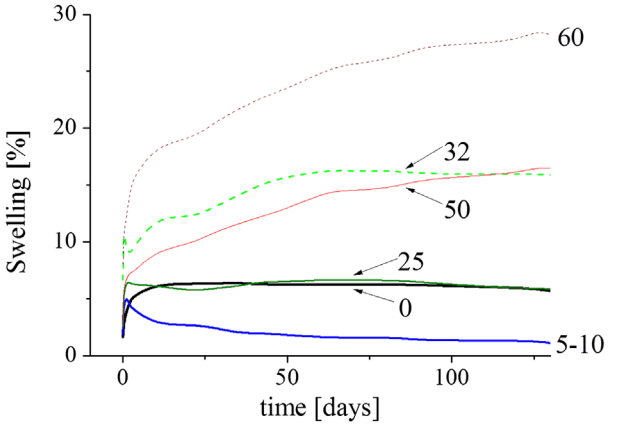

Figure 9. Influence of colloidal silica content on swelling properties of PU/silica nanocomposites. Code abbreviations are given in Table 1.

Table 5. Swelling properties of PU/silica nanocomposite films.

Sample	Swelling maximum (%)	Swelling after 20 weeks (%)	Time for quasi equilibrium (days)	Weight loss after swelling, Δw (%)
TMA-0	6.4	5.6	35	2.6
TMA-5	5.2	1.0	1	3.1
TMA-10	6.3	1.6	1	3.2
TMA-25	6.7	5.8	63	4.5
TMA-32	16.3	15.8	63	4.7
TMA-50	16.6	16.4	126	4.9
TMA-60	28.7	27.9	126	4.3

silica. The swelling in water significantly increases in case of samples TMA-32, TMA-50, and TMA-60, which is a result of greater porous sample morphology.

The water solubility was determined according to weight loss after swelling, Δw. The results are summarized in Table 5. The weight loss slightly increased with increasing colloidal of silica amount, but the differences in weight loss are not significant, not exceeding 5 wt% in the maximum (Table 5, 5th column).

4. Conclusion

Novel PU/silica nanocomposites were studied on the basic of mechanical, thermal, surface, and swelling properties. The nanocomposite films were successfully prepared by solution blending of two types of nanoparticles dispersed in water followed by slow water evaporation. The organic part was formed from long-term stable polyurethane dispersion composed of colloidal PU particles of average diameter 88 nm being formed from linear all aliphatic polycarbonate-based PU chains. The inorganic part was commercial product, colloidal silica LUDOX TMA of average particle size 39 nm. The absence of chemical bonds between the nanoparticles enabled recycling of the films by dissolving in acetone and then dispersing in water. Physical type of PU/nanosilica interface improved the material properties. The set of analytical methods revealed substantially different character and diverse end-use properties of O–I nanocomposites depending on silica content.

The nanocomposite samples were divided into three groups. The first group contained O–I materials, where the organic polymer was reinforced by small amount of inorganic nanofiller (up to 10 wt% of silica). These samples were nonporous materials with polymer-like morphology. Comparing this group to the neat matrix, they had better mechanical properties, smoother surfaces, and lower swellability in water. The second group (silica content 25 and 32 wt%) was called bicontinous systems, where both polymeric-like and ceramic-like features were simultaneously observed. Mechanical and swelling properties were slightly deteriorated in comparison to the first group, but all nanocomposites containing up to 32 wt% of silica were transparent films with well-dispersed filler into the PU matrix. The third group covered the O–I films filled with the highest nanofiller amount (50 and 60 wt%). These materials were hard, but brittle polymer-mixed ceramic films. In all cases of prepared films improvement of thermal properties caused by shielding effect of silica was observed.

From the potential practical use, the best combination of functional (mechanical, thermal, swelling, and surface) properties have O–I nanocomposite films containing up to 10 wt% of silica. These systems could be used as smooth and transparent coatings for substrates of different origin (e.g. polymer, wood, metal, and glass). Moreover, because of water medium in the dispersions and films recyclability, obtained PU/silica nanocomposites are environment-friendly materials.

Note

1 LUDOX TMA is deionized to remove sodium present in alkali-stabilized colloidal silica, without addition of ammonia to stabilize TMA.

Acknowledgments

Magdalena Serkis would like to thank the Charles University, Faculty of Science for the opportunity to pursue her PhD study. In addition, the authors are grateful to Dr R. Poreba for helping with the preparation of PUDs, and for DMTA measurements performed by Mrs I. Vlasáková.

Disclosure statement

No potential conflict of interest was reported by the authors.

Funding

This work was supported by the Grant Agency of the Czech Republic (Czech Science Foundation) under project number 13-06700S.

References

[1] Špírková M, Pavličević J, Strachota A, et al. Novel polycarbonate-based polyurethane elastomers: composition–property relationship. Eur. Polym. J. 2011;47:959–972.
[2] Špírková M, Poręba R, Pavličević J, et al. Aliphatic polycarbonate-based polyurethane elastomers and nanocomposites. I. The influence of hard-segment content and macrodiol-constitution on bottom-up self-assembly. J. Appl. Polym. Sci. 2012;126:1016–1030.

[3] García-Pacios V, Costa V, Colera M, et al. Affect of polydispersity on the properties of waterborne polyurethane dispersions based on polycarbonate polyol. Int. J. Adhes. Adhes. 2010;30:456–465.
[4] Cakić SM, Ristić IS, Marinović-Cincović M, et al. The effects of the structure and molecular weight of the macrodiol on the properties polyurethane anionic adhesives. Int. J. Adhes. Adhes. 2013;41:132–139.
[5] Cakić SM, Špírková M, Ristić IS, et al. The waterborne polyurethane dispersions based on polycarbonate diol: effect of ionic content. Mater. Chem. Phys. 2013;138:277–285.
[6] García-Pacios V, Jofre-Reche JA, Costa V, et al. Coatings prepared from waterborne polyurethane dispersions obtained with polycarbonates of 1,6-hexanediol of different molecular weights. Prog. Org. Coat. 2013;76:1484–1493.
[7] Lee DK, Tsai HB, Tsai RS. Effect of composition on aqueous polyurethane dispersions derived from polycarbonatediols. J. Appl. Polym. Sci. 2005;102:4419–4424.
[8] Lee DK, Yang ZD, Tsai HB, et al. Polyurethane dispersions derived from polycarbonatediols and m-di(2-isocyanatopropyl)benzene. Polym. Eng. Sci. 2009;49:2264–2268.
[9] Lee DK, Tsai HB, Yang ZD, et al. Polyurethane dispersions derived from polycarbonatediols by a solvent-free process. J. Appl. Polym. Sci. 2012;126:E275–E282.
[10] García-Pacios V, Costa V, Colera M, et al. Waterborne polyurethane dispersions obtained with polycarbonate of hexanediol intended for use as coatings. Prog. Org. Coat. 2011;71:136–146.
[11] Sardon H, Irusta L, Aguirresarobe RH, et al. Polymer/silica nanohybrids by means of tetraethoxysilane sol–gel condensation onto waterborne polyurethane particles. Prog. Org. Coat. 2014;77:1436–1442.
[12] Bistričić L, Baranović G, Leskovac M, et al. Hydrogen bonding and mechanical properties of thin films of polyether-based polyurethane-silica nanocomposites. Eur. Polym. J. 2010;46:1975–1987.
[13] Cao X, Lee LJ, Widya T, et al. Polyurethane/clay nanocomposites foams: processing, structure and properties. Polymer. 2005;46:775–783.
[14] Hoffmann F, Fröba M. Silica-based mesoporous organic–inorganic hybrid materials. In: Rurack K, Martinez-Manez R, editors. The supramolecular chemistry of organic–inorganic hybrid materials. New Jersey, NJ: Wiley; 2010. p. 39–112.
[15] Špírková M, Poręba R, Brožová L. The influence of the size, shape and character of nanofillers of functional properties of polyurethane elastomers. In: Wang X, editor. Nanocomposites. Synthesis, characterization and applications. New York, NY: Nova Science; 2013. p. 259–289.
[16] Špírková M, Brus J. View from inside to the surface of nanocomposite coatings. In: Mittal V, editor. Polymer nanocomposite coatings. Florida, FL: Taylor & Francis; 2013. p. 125–165.
[17] Chen Y, Iroh JO. Synthesis and characterization of polyimide/silica hybrid composites. Chem. Mater. 1999;11:1218–1222.
[18] Bourgeat-Lami E, Lang J. Encapsulation of inorganic particles by dispersion polymerization in polar media – 1. Silica nanoparticles encapsulated by polystyrene. J. Colloid Interface Sci. 1998;197:293–308.
[19] Lim JS, Hong SM, Kim DK, et al. Effect of isocyanate-modified fumed silica on the properties of poly(butylene succinate) nanocomposites. J. Appl. Polym. Sci. 2008;107:3598–3608.
[20] Chan CM, Wu JS, Li JX, et al. Polypropylene/calcium carbonate nanocomposites. Polymer. 2002;43:2981–2992.
[21] Wang G, Ma GZ, Hou CY, et al. Preparation and properties of waterborne polyurethane/nanosilica composites: a diol as extender with triethoxysilane group. J. Appl. Polym. Sci. 2014;131.
[22] Chen GD, Zhou SX, Gu GX, et al. Modification of colloidal silica on the mechanical properties of acrylic based polyurethane/silica composites. Colloids Surf., A. 2007;296:29–36.
[23] Zhang SW, RenLiu Jiang JQ, et al. Facile synthesis of waterborne UV-curable polyurethane/silica nanocomposites and morphology, physical properties of its nanostructured films. Prog. Org. Coat. 2011;70:1–8.
[24] Zou H, Wu SS, Shen J. Polymer/silica nanocomposites: preparation, characterization, properties, and applications. Chem. Rev. 2008;108:3893–3957.

[25] Liu N, Zhao YH, Kang MQ, et al. The effects of the molecular weight and structure of polycarbonatediols on the properties of waterborne polyurethanes. Prog. Org. Coat. 2015;82:46–56.
[26] Zhou HF, Wang H, Tian XY, et al. Effect of 3-Aminopropyltriethoxysilane on polycarbonate based waterborne polyurethane transparent coatings. Prog. Org. Coat. 2014;77:1073–1078.
[27] Serkis M, Poręba R, Hodan J, et al. Preparation and characterization of thermoplastic waterborne polycarbonate-based polyurethane dispersions and cast films. J. Appl. Polym. Sci. 2015;132:42672.
[28] Li XJ, Hu J, Sun DX, et al. Nanosilica reinforced waterborne siloxane-polyurethane nanocomposites prepared via "click" coupling. J. Coat. Technol. Res. 2014;11:517–531.
[29] Hamdani S, Longuet C, Perrin D, et al. Flame retardancy of silicone-based materials. Polym. Degrad. Stab. 2009;94:465–495.
[30] Ito S, Hashimoto M, Wadgaonkar B, et al. Effects of resin hydrophilicity on water sorption and changes in modulus of elasticity. Biomaterials. 2005;26:6449–6459.

Progress in Organic Coatings 101 (2016) 342–349

Contents lists available at ScienceDirect

Progress in Organic Coatings

journal homepage: www.elsevier.com/locate/porgcoat

Nanocomposites made from thermoplastic waterborne polyurethane and colloidal silica. The influence of nanosilica type and amount on the functional properties

Magdalena Serkis[a,*], Milena Špírková[a,*], Jiří Hodan[b], Jana Kredatusová[b]

[a] Nanostructured Polymers and Composites Department, Institute of Macromolecular Chemistry AS CR, Heyrovsky Sq. 2, 162 06 Prague 6, Czech Republic
[b] Polymer Processing Department, Institute of Macromolecular Chemistry AS CR, Heyrovsky Sq. 2, 162 06 Prague 6, Czech Republic

ARTICLE INFO

Article history:
Received 13 April 2016
Received in revised form 20 June 2016
Accepted 9 July 2016

Keywords:
Polymer-matrix composites (PMCs)
Mechanical properties
Microstructures
Thermal analysis

ABSTRACT

Novel waterborne polyurethane/silica nanocomposites were prepared via blending of two aqueous dispersions. Polyurethane water dispersion (PUD) was synthesized from polycarbonate diol (PC), 1,6-diisocyanatohexane (HDI) and butane-1,4-diol (BD) in order to provide solely linear character of PU chain. Two types of commercial colloidal silica, Ludox AS and Ludox TMA, differing in the size, shape and type of counter ions were used. The nanocomposites were made from negatively charged PUD and aqueous nanofiller sol at concentrations 5, 32 and 50 wt% of nanosilica. The films were obtained after slow drying of the water mixtures and characterized by AFM, SEM, tensile testing, DMTA, TG and water uptake measurements. It was found that all films are thermoplastics materials, reinforced by hydrogen bonds between silica particles and the polymer matrix, soluble in organic solvents and possible to re-production of PUD. Ludox AS was smaller than TMA and revealed better improvement of PUD-based films due to higher physical cross-linking density. It was observed that film containing 32 wt% of silica Ludox AS showed ten-times increasing Young's modulus with slight improvement of elongation at break and two-times higher melting temperature in comparison to the neat PU matrix. Moreover sample with 5 wt% of AS nanofiller loading revealed excellent water resistance (swelling 0.8%). The obtained PU/silica nanocomposites have promising applications in recyclable environment-friendly waterborne coatings.

1. Introduction

Thermoplastic polyurethanes (TPUs) are linear segmented block copolymers with mechanical performance of rubber, but upon heating can be melt-processed. A combination of high elasticity, high tensile strength and excellent abrasion has allowed TPUs to be used in footwear, tubing, films, sheets and many other applications [1–3]. However, thermoplastics unlike thermoset elastomers do not create chemical networks. The possibility of strengthening TPUs is creation of hydrogen-bonded networks which are much weaker than chemical cross-links. In order to obtain superior properties of TPUs various types of fillers, such as organoclay, carbon nanofiber, silicon carbide, carbon black and ZnO nanoparticles have been used in PU nanocomposites [4–6].

Different types of silica fillers, such as silica sol [7] and nanosilica particles [8] have found use in preparation of nanocomposites with TPUs due to improvement of their physical and chemical properties. The low cost and possible surface modifications of colloidal silica make it an interesting candidate for various applications; Ludox silica spheres have been widely used in clay suspensions [9,10], bioapplications [11] and composites with polymers, for example polyamides [12,13], poly(vinyl alcohol) [14], poly(vinyl acetate) [15], poly(ethylene oxide) [16], polysiloxane epoxides [17,18] and polyurethanes [19,20].

Environmental friendly polyurethane water dispersions (PUDs) have been increasingly used due to their nontoxicity and non-flammability. Referring to properties which may be obtained for PUDs, some of their defects can be reduced by preparation of PUD/silica nanocomposites. Although films prepared from cross-linked PUD/silica composites comprise a large group of materials, they cannot be melt-processed or dissolved in organic solvents. According to our knowledge there are a few publications describing composites of linear waterborne polyurethanes with silica [21–23]. One of these uses polycarbonate diols [21], but all those PUDs

* Corresponding authors.
E-mail addresses: serkis@imc.cas.cz (M. Serkis), spirkova@imc.cas.cz (M. Špírková), hodan@imc.cas.cz (J. Hodan), kredatusova@imc.cas.cz (J. Kredatusová).

http://dx.doi.org/10.1016/j.porgcoat.2016.07.021
0300-9440/

Table 1
Properties of Ludox AS and TMA colloidal silica and PUD.

	Counter ion	Silica [wt%]	pH		Particle size [nm]			Zeta potential [mV] [5]
			[1]	[2]	[1]	[3]	[4]	
AS	NH_4^+	40	9.1	9.02	22	22–25	34	−41
TMA	Na^+	34	4–7	7.32	22	22–54	39	−37
PUD	$NH_4^+(Et)_3$	–	–	8.25	–	–	88	−50

Given by: [1] the manufacturer, [2] pH meter, [3] AFM, [4] DLS, [5] ELS.

are based on 5-isocyanato-1-(isocyanatomethyl)-1,3,3-trimethylcyclohexane (IPDI); HDI is used in these systems for the first time.

Our previous research was focused on the preparation and detailed characterization of waterborne TPUs, prepared from PC, BD and HDI [22]. In the preliminary study [20] we reported on thermal, mechanical and swelling profile upon addition of hydrophilic colloidal silica Ludox TMA. In the both cases we obtained re-cycling PU films soluble in organic solvents, which became again PUDs after water addition. In this paper differences between PUD nanocomposites with two types of hydrophilic anionic colloidal silica: Ludox AS and TMA were investigated. These two nanofillers differ in pH of the sol and used counterions for stabilization. More information can be found in Table 1 and in the chart with product description [25]. The differences between compatibility of silica spheres AS and TMA with PU matrix in various nanofiller concentrations were presented in this study. Further, we investigated the influence of the silica type and amount on morphology, mechanical, thermal and water resistance of obtained nanocomposite films.

2. Experimental

2.1. Materials

Aliphatic PC[1], trademark T4672 with molecular weight ca. 2770 g mol^{-1} was kindly provided by Asahi Kasei Chemical Corporation, Tokyo, Japan. HDI, BD, *N*,*N*-diethylethanamine (TEA) and 2,2-bis (hydroxymethyl) propionic acid (DMPA), were obtained from Sigma-Aldrich Co. Dried acetone (max. 0.0075 wt% H_2O) was recived from Merck KGaA, Darmstadt, Germany. The catalyst was prepared as 10 wt% solution of dibutyltin dilaurate (DBTDL) (Sigma-Aldrich, Co.) in Marcol oil. Two types of aqueous silica sol Ludox: AS and TMA were obtained from Aldrich Chemical Company, Inc., USA. In Ludox AS the used counter ion was ammonium, in the case of Ludox TMA sodium was the counter ion [25,26]. The characteristic values are presented in Table 1.

2.2. Preparation procedure

The PUD was prepared according to our previously published procedure [24] from: PC, HDI and DMPA. The components were dissolved in acetone and reacted to obtain NCO-terminated prepolymer. Then, after chain extension by BD, TEA was used to neutralize the carboxylic groups in DMPA. In the last step water was gradually added and acetone was removed from PUD. In this paper PUD containing DMPA-to-PC molar ratio equal to 0.4 and BD-to-PC equal to 0.5 was used as the organic matrix. The features of the PUD are presented in Table 1 and [24].

PU nanocomposites with two types of colloidal silica were prepared by blending of two aqueous dispersions[2], as shown in Fig. 1. In prepared nanocomposites new physical crosslinks were created by hydrogen bonds between PU and the nanofiller. Two types of physical interactions were possible: between silanol groups of silica and (i) urethane groups in hard and soft segments (see Fig. 1) or (ii) the carbonyl groups of the polycarbonate diol-based soft segments (for simplification not shown here). Samples containing 5, 32 and 50 wt% of AS or TMA and the neat matrix were prepared. The last step was casting the mixtures on Teflon plates and dying at first at room temperature for 5 days and next at 50 °C for 20 h. The nanocomposite codes describe type and content of colloidal silica, for example the sample containing 5 wt% of TMA is marked with the code TMA-5.

2.3. Methods of characterization

2.3.1. Dispersion characterization

Starting materials for films preparation (neat PUD and silica dispersions) given in Table 1 were characterized as follows: the *pH* was determined using Hanna Instrument pH 213 Microprocesor pH Meter, dynamic light scattering (DLS) measurements were performed by ALV CGE laser goniometer, electrophoretic light scattering (ELS) measurements were carried out by Zetasizer NanoZS instrument (Malvern Instruments, UK).

2.3.2. Film characterization

The morphology was investigated by *Scanning electron microscopy* (SEM) TS 5153 (Tescan, Czech Republic). Before the measuring the samples were sputtered with 4 nm Pt layer using vacuum sputter coater SCD 050 (Balzers, Czech Republic). Dispersity of silica particles into PU matrix and analysis of the nanocomposite microstructures were carried out by *Atomic force microscopy* (AFM) (Dimension Icon, Bruker), equipped with the SSS-NCL probe, Super Sharp SiliconTM–SPM-Sencor from NanoSensors^{TM} Switzerland with spring constant 35 Nm^{-1} and resonant frequency of 170 kHz. The measurements were performed by tapping mode AFM technique. The roughness parameters R_a, and R_{max} were evaluated from areas 10 μm × 10 μm. Static mechanical properties were measured by Instron model 6025/5800R (Instron Limited, UK) according to test method ISO 527-2/5 B at room temperature. Dumbbell shaped specimens (total specimen length of 35 mm, length and the width of the narrowed part: 12 and 2 mm, thickness 0.5 mm), and cross-head speed of 10 mm min^{-1} were used for the analysis. *Dynamic mechanical thermal analysis* (DMTA) was carried out by ARES-G2 from TA instruments at oscillation frequency 1 Hz, the heating rate of 3 °C min^{-1} from −100 to +180 °C and deformation in a range between 0.01–3.5%. The geometry of standard specimens: 25 mm × 6 mm × 0.5 mm. *Thermograwimmetric analysis* (TG) of obtained materials was measured by Pekin-Elmer Pyris 1 TGA. A sample mass of 10–15 mg was heated from 30 to 700 °C, under nitrogen flow of 30 ml min^{-1} at constant heating rate 10 °C min^{-1}. *Water uptake* was carried out by immers-

[1] The formula of PC: 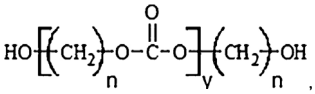 , where n = 4 or 6, molar ratio C6:C4 copolymer = 7:3

[2] For more details about preparation of the nanocomposites see [23].

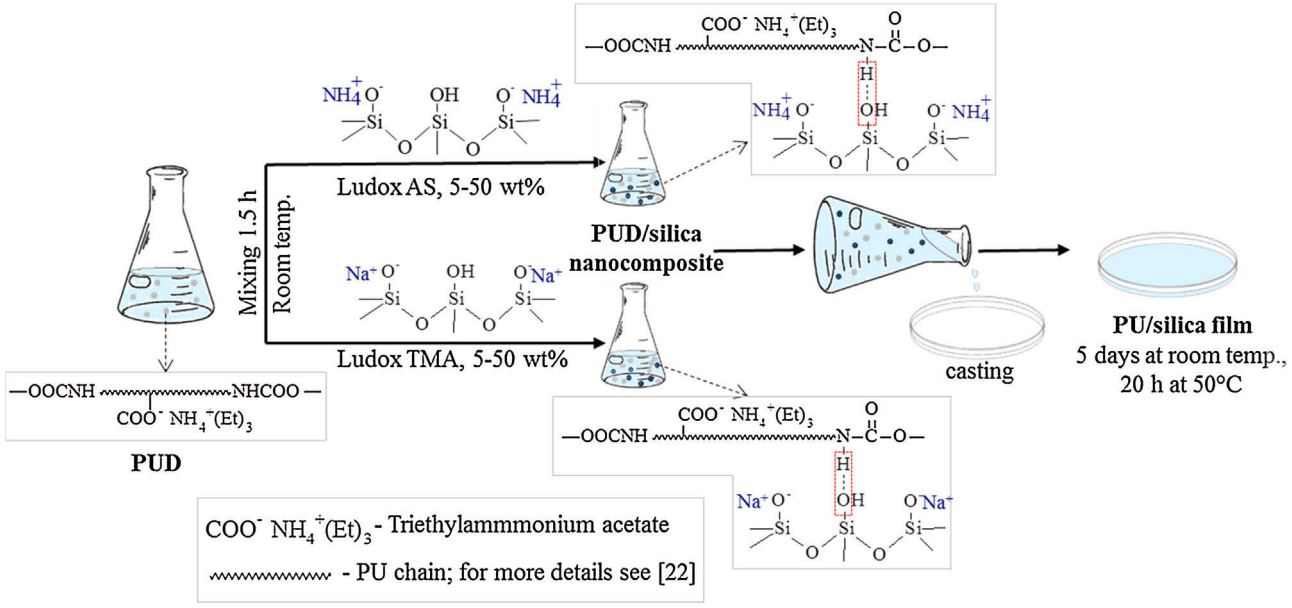

Fig. 1. Nanocomposite PUD/silica preparation process.

ing the dry films into deionized water for 20 weeks and immediate weighting of swollen samples after removal of the residual water by filter paper. The swelling degree was calculated by the following equation:

$$\%\text{swelling} = \frac{w - w_0}{w_0} \times 100\%$$

where w_0 is the initial weight of the dry film and w is the weight of film in the swollen state. After the immersion in water by 20 weeks, the samples were dried in 50 °C for 20 h. The percentage weight loss was calculated according to the equation:

$$\Delta w = \frac{w_0 - w_f}{w_0} \times 100\%$$

where w_f is the weight of dried film after immersing in water.

3. Results and discussion

3.1. Morphology characterization

A combination of two microscopic techniques, AFM and SEM was used to determine microstructure of film surfaces and their cross-sections. According to these methods, size, shape, dispersity of silica particles and porosity of the films were investigated.

3.1.1. Characterization of silica nanoparticles

AFM images of neat silica and the nanofiller particles in PU matrix were shown in Fig. 2. The phase contrast, which describes interaction between measured material and the tip and provides information about variations in sample properties and adhesion between the probe and surface [27,28] was applied. Using the same experimental parameters and sharpness of the tip allowed us to compare Fig. 2a)–c) and Fig. 2d)–i) in the same color contrasts. In order to determine the size and shape of Ludox AS and TMA, they were dried before the measuring. Both types of the nanofiller particles differ in shape and size (see Fig. 2a) and b). AS nanoparticles are hexagonal and create honeycomb structure, whereas TMA are oval-shaped. Distribution of particle size was measured by NanoScope Analysis software via particle analysis for AS in a range from 22 to 25 nm and TMA between 22 and 54 nm.

Investigation of silica particles dispersity in PU matrix was carried out by AFM analysis of previously freeze-fractured films. Phase images of broken nanocomposite samples at the same color scale are shown in Fig. 2d)–i). Polymer matrix appears dark, while the nanofiller particles are bright spots. From the same color contrast it is visible that softer material appears lighter, which may suggest that TMA is harder than AS.

In nanocomposites containing 5 or 32 wt% of silica loading, quite well filler dispersity was observed. However some places with aggregates of the nanofiller particles are caused by better affinity between silica particles than silica and matrix. Significant differences in nanocomposites containing 50 wt% of silica were observed. Sample AS-50 demonstrated highly packed nanofiller particles with very small amount of dark field, corresponding to PU, in size up to 50 nm and depth 25 nm. In the structure of TMA-50 high number of pits in size of 150 nm and depth 60 nm was observed. It suggests that in this sample PU matrix is blocked by TMA in lower degree than AS. This makes TMA-50 preserving some of the matrix properties.

3.1.2. Comparison of AFM and SEM surface analysis

In order to investigate surface morphology, results obtained from the both microscopic techniques were compared. SEM images with AFM pictures on the left upper corner are shown in Fig. 3. AFM height images, which reflect samples topography, were used as pictures providing information similar to SEM. Used scale bar is referring to both images, which facilitates the comparison.

In the case of PU matrix-based film (Fig. 3 upper left corner) fibril-like structure was observed by the both methods. Addition of 5 wt% colloidal silica smoothed the sample surfaces. This effect was more evident in TMA-5, both in the macroscopic images, as well as in the roughness parameters (Table 2). The microscopic results prove that in the cases of low nanofiller concentrations (5 wt%) silica particle size does not have the main influence on the film roughness.

Higher filler loading (32 wt%) in the both cases caused more rough surface, but silica particles were still covered by the polymer. Sample AS-32 featured matrix-like structure due to better compatibility of AS with the polymer because of smaller Ludox AS nanoparticles in comparison to Ludox TMA, which provides higher physical cross-linking density between the nanofiller and PU. How-

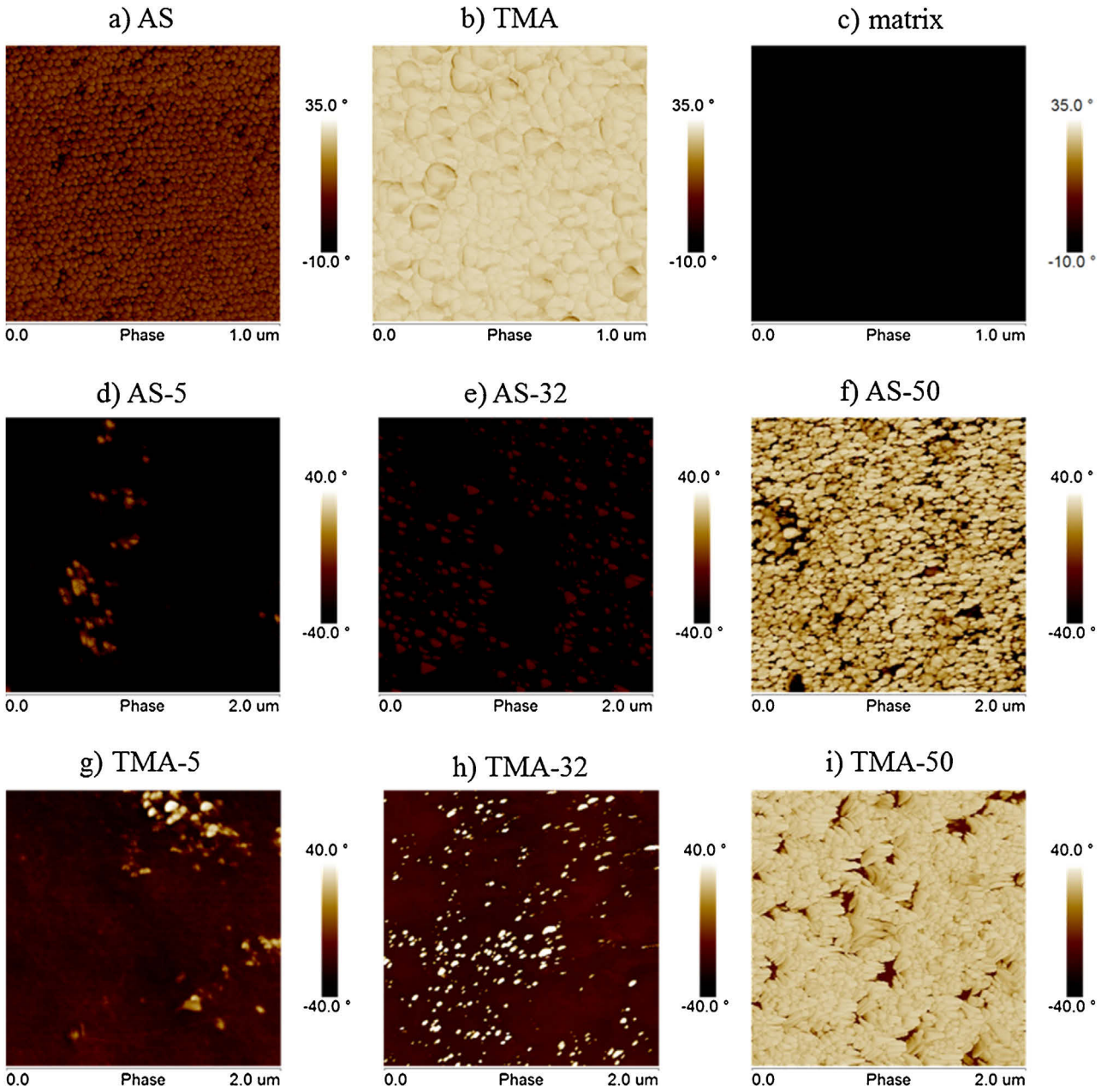

Fig. 2. Cross section Phase AFM images of: a) AS b) TMA pure silica and c) neat PU matrix (1 μm × 1 μm) and d)–i) PU/silica nanocomposite films (2 μm × 2 μm).

Table 2
Roughness values and tensile properties of PU/silica nanocomposite films.

Sample code	R_a [nm][a]	R_{max} [nm][b]	Young's Modulus, E, [MPa]	Stress at break, δ_b, [MPa]	Elongation at break, $\varepsilon_{b,}$ [%]	Energy to break [mJ/mm^3]
Matrix	23	255	8 ± 0.5	1.4 ± 0.2	94 ± 9.7	1.5 ± 0.2
AS-5	18.3	273	13 ± 0.7	1.4 ± 0.1	112 ± 6.2	1.9 ± 0.2
AS-32	59.3	744	85 ± 8.4	1.3 ± 0.1	116 ± 10.0	2.3 ± 0.2
AS-50	56.3	489	435 ± 43.2	5.8 ± 0.5	15 ± 1.4	0.3 ± 0.1
TMA-5	14.5	140	10 ± 0.9	1.4 ± 0.2	108 ± 10.4	1.8 ± 0.2
TMA-32	28.0	207	62 ± 6.1	0.6 ± 0.1	84 ± 8.5	1.1 ± 0.1
TMA-50	33.5	270	552 ± 55.4	2.3 ± 0.4	33 ± 6.1	1.3 ± 0.20

[a] R_a – the mean roughness (arithmetic average of the surface height deviations).
[b] R_{max} – the max height (maximal vertical distance between the highest and the lowest points).

ever fibrils were very sharp, clearly protruding from the surface. It was visible in the roughness values and as the highest color contrast in the AFM picture, where brightest parts are the highest and the darkest are the lowest. Nanocomposite film containing the second filler type (TMA-32) presented separated fibrils on the surface, but general smoothness was better than in the case of AS-32. When the highest filler concentration was used (50 wt%), silica protruded above the film surfaces. For AS-50 highly rough morphology, with-

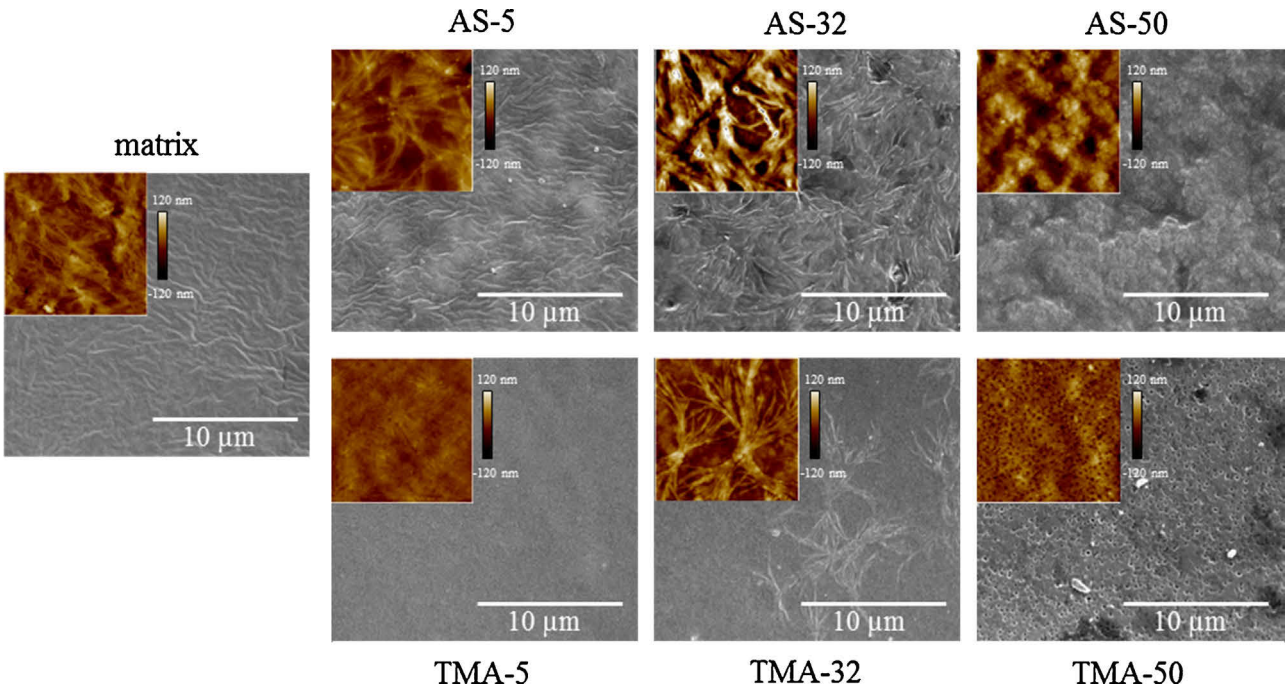

Fig. 3. Surface SEM (magnification 7000×) and 10 µm × 10 µm Height AFM (upper left corner) micrographs of PU/silica nanocomposite films.

out visible pores was observed. Sample TMA-50 was characterized by high porosity (size ~200 nm), but the depth pores was around 60 nm, which resulted in lower roughness values compared to AS-50.

3.2. Static mechanical properties

Fig. 4 shows tensile test curves of the nanocomposite films containing different types and concentrations of silica particles. The corresponding mechanical properties are summarized in Table 2. Samples containing up to 5 wt% of silica behaved as elastomers, without a yield point. In the nanocomposites AS-5 and TMA-5 Young's modulus increased from 8 MPa to 13 and 10 MPa, respectively. Surprisingly increasing of elongation at break was observed after addition of the nanofillers. This improvement of mechanical properties may be explained by better stress transfer from soft matrix to rigid silica due to creation of hydrogen bonding between the nanofiller and PU [29]. Also slight difference between fracture strain of AS-5 and TMA-5 can be caused by larger contact area between smaller AS particles, which enables higher density of hydrogen bonds.

Films with 32 wt% of silica loading behaved as plastic polymers. Significant enhancement was observed in sample AS-32 as ten-times increasing of Young's Modulus (85 MPa) compared to the neat matrix. Moreover in this case elongation at break was improved, as a result of increasing hydrogen bonding density between the nanofiller and PU. Also the energy to break was calculated from Fig. 4 by integrating the area below stress-strain curves. The highest value had AS-32 as the most resistant to fracture sample. It can be understood as better compatibility between PU matrix and Ludox AS in comparison to PU with Ludox TMA. Stress-strain properties of AS-32 reflect its morphology, where fibril-like structure of the polymer was unperturbed (Fig. 3) and the nanofiller particles were well dispersed in the matrix (Fig. 2). In contrast, deterioration of tensile strength (δ_b) and elongation at break (ε_b) were observed for TMA-32. The sample was more rigid than the neat matrix, but overall toughness decreased. The reduction of its mechanical resistance may be caused by improved phase separation between soft polymer and harder silica type. Stress-strain properties are confirmed by microstructure images of TMA-32 (Fig. 3), in which deterioration of PU morphology was clearly visible as separated rods.

For better visualization, static mechanical properties of pure matrix and nanocomposites with the highest silica loading were shown in separate image (Fig. 4b). It can be seen that samples containing 50 wt% of the nanofiller concentration are brittle polymers. In the both cases significant deterioration of elongation at break and toughness were observed. This behavior is related to aggregation of silica particles, visible in the AFM images (Fig. 2). In these cases aggregates act as defects and interactions between filler particles predominate over the silica-PU. Comparing stress-strain curves of the nanocomposites prepared from different silica types, AS-50 features more ceramic-like properties, with minimal matrix influence. This behavior may be caused by strong blocking of PU by high number of silica particles. However TMA-50 showed more plastic nature and elongation at break (33%) two-times more than AS-50. The stronger effect of PU may be explained by the sample morphology. In this film TMA particles create bigger agglomerates and thereby PU matrix occupies larger area, sufficient to affect the film properties. Moreover TMA-50 featured higher Young's modulus than AS-50, which may confirm that TMA particles are harder than AS.

3.3. Dynamic mechanical properties

The viscoelastic properties of PU/silica nanocomposite films were evaluated by dynamic mechanical thermal analysis (DMTA) to obtain the information of the glass transition temperature (T_g) and the storage modulus (G')[3]. Fig. 5a) shows DMTA storage modulus values as a function of temperature. Sharp range of T_g for AS-5 and TMA-5 can be understood as good compatibility of PU and silica. In the rubbery plateau region, at temperature exceeding 8 °C, increasing of G' for the nanocomposites was observed. Therefore silica acts as physical cross-linker. Melting of all samples confirmed

[3] Films with 50 wt% of the nanofiller were not measured because of too high fragility.

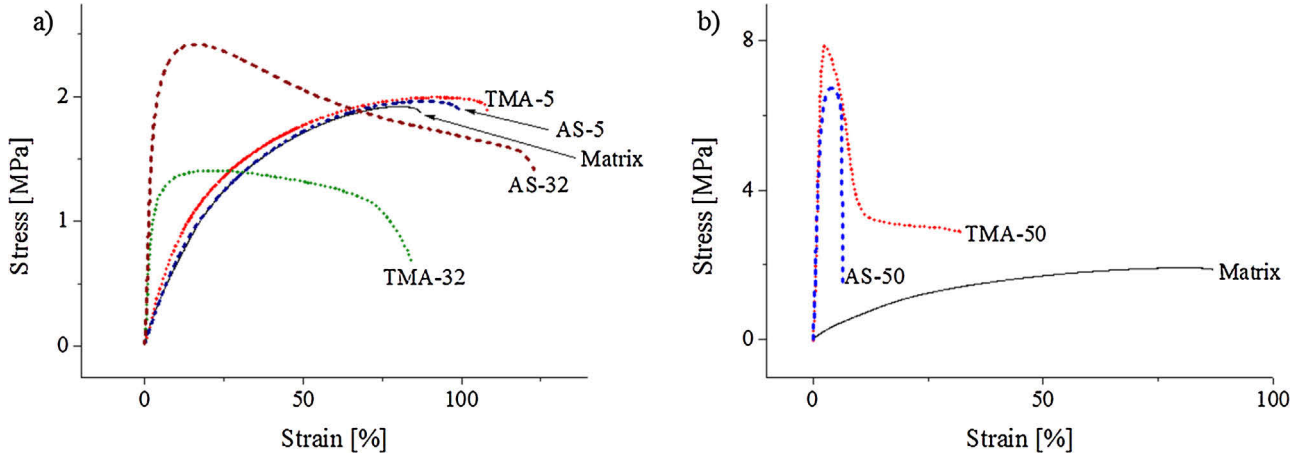

Fig. 4. Stress-strain curves of PU/silica films containing: a) up to 32 wt% of the nanofiller, b) neat matrix and the nanocomposites with 50 wt% of silica loading.

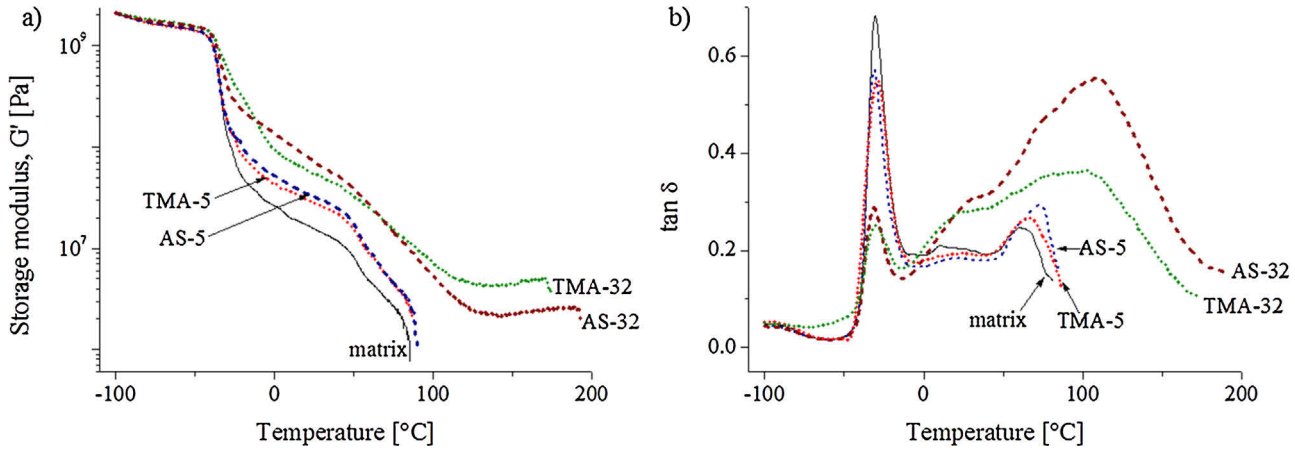

Fig. 5. The temperature dependence of: a) storage modulus, *G'* and b) loss factor, *tan δ* of PU/silica nanocomposite films.

their thermoplastic character. Nanocomposite films showed higher melting temperature (T_m) than the matrix due to increasing of hydrogen bonds density, which also demonstrates improvement of its thermal resistance. It was more visible for AS-32 (T_m = 192 °C) in comparison to TMA-32 (T_m = 174 °C)[4], which confirmed better compatibility of AS to PU.

Fig. 5b) displays the DMTA loss tangent (*tan δ*) as a function of temperature. The same T_g (around −31 °C)[5] for all films were detected from the maxima of *tan δ*. Generally, changes of T_g upon addition of nanofillers are caused by strong interactions between nanoparticles and polymer [30]. In our samples constant T_g confirms weak, physical bonding between silica and PU matrix. The second peak of *tan δ* is related to releasing of residual PU chains. Decreasing of T_g peak intensity and simultaneously increasing and shifting to higher temperatures of the second peak for samples AS-5 and TMA-5 were observed. It can be explained by blocking of polyurethane chains mobility by the nanofiller particles. Nanocomposite AS-32 showed the same behavior as AS-5, but more visible. It proves strong blocking of PU chains and releasing them in higher temperatures. Sample TMA-32 showed small additional peak before T_g, which suggests releasing of silica agglomerates and friction between the nanofiller particles and PU. This behavior confirms lower compatibility of TMA to the polymer, which was also observed by the microscopic methods and tensile test.

3.4. Thermogravimetric analysis

In order to examine the effect of colloidal silica on thermal stability of the nanocomposites, TG measurements were carried out. The DTG curves are shown in Fig. 6 and thermal properties of the samples are summed in Table 3. Two steps of mass loss, attributed to degradation of hard (I) and soft (II) segments in PU, were detected.

The beginning of thermal degradation is represented by $T_{5\%}$ and starts between 285 and 294 °C. The addition of colloidal silica shifts $T_{5\%}$ and $T_{10\%}$ to higher temperatures due to shielding effect of the nanofiller. According to Table 3, the first degradation step (I) takes place between 325 and 365 °C, whereas the second one (II) is in a range from 366 to 393 °C. The most significant shifting of I and II to higher temperatures was observed for nanocomposites containing silica AS. It was a result of increasing hydrogen bonds density between PU and the nanofiller. These physical cross-links need higher temperature to decompose. Even sample with the highest AS loading (AS-50) had better thermal stability than pure PU. It may be explained by AS-50 morphology (see Fig. 2), where small silica particles are separated from each other by thin polymer layer. In case of the second nanofiller type, TMA-50 showed deterioration of thermal properties in comparison to the neat matrix. This was caused by creation of big silica agglomerates visible in Fig. 2. The residual masses of the samples after complete degradation at

[4] T_m obtained from DCS measurements were 171 °C for AS-32 and 162 °C for TMA-32.

[5] According to DSC curves all samples had T_g between −37 and −40 °C.

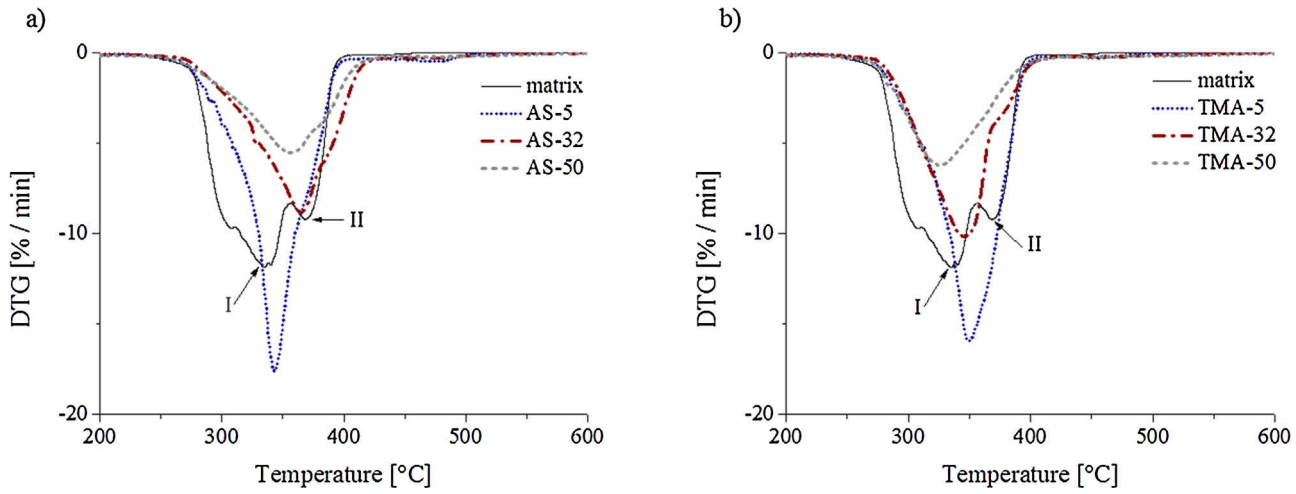

Fig. 6. DTG curves of PU with: a) Ludox AS, b) Ludox TMA silica nanocomposites as a function of the nanofiller concentration. Arrows indicate two stages of mass loss.

Table 3
Thermal and water uptake properties of PU/silica nanocomposites.

Sample code	$T_{5\%}$ [°C][a]	$T_{10\%}$ [°C][a]	DTG_{max} [°C][b]	Residue [wt%] at 600 °C	Swelling maximum [%]	Swelling after 20 weeks [%]	Mass loss after swelling, Δw [%]
Matrix	285	294	335/368	0.5	6.4	5.6	2.6
AS-5	289	304	344/374	6.9	3.7	0.8	3.3
AS-32	294	314	365/393	31.8	10.7	9.5	3.8
AS-50	285	311	357/388	49.2	14.6	14.6	3.9
TMA-5	293	307	350/366	5.4	5.2	1.0	3.1
TMA-32	292	307	346/380	31.7	16.3	15.8	4.7
TMA-50	285	303	325/-	48.9	16.6	16.4	4.9

[a] $T_{5\%}$, $T_{10\%}$ – the temperature at which the loss of 5 and 10% of the total sample mass was occurred, respectively.
[b] Maximum of derivative TG.

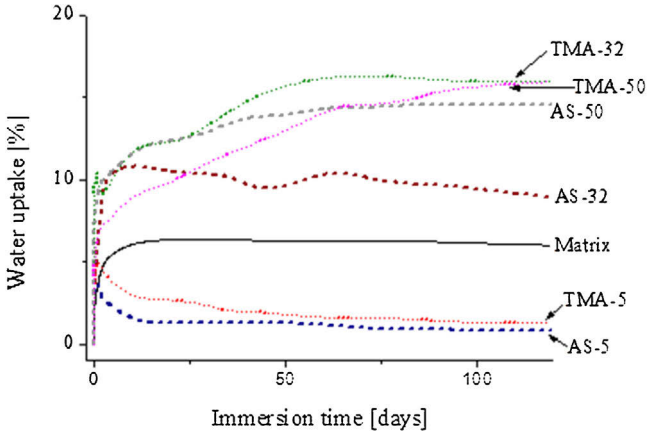

Fig. 7. Water uptake of the nanocomposites containing two types of colloidal silica at various concentrations.

600 °C are listed in Table 3. These data confirm the nanofiller mass percentage of PU/silica nanocomposites.

3.5. Water uptake and solubility

Water uptake of PU/silica nanocomposite films was tested and shown in Fig. 7 and Table 3. Significant enhancement of water resistance for films containing 5 wt% of the nanofiller loading was observed. Although silica is hydrophilic material, this behavior was caused by increasing of cross-linking density created by hydrogen bonding. The cross-links provides barrier to the migration of water molecules into the bulk by decreasing of the polymer chain free volume. Similar results were obtained for other PUD/silica nanocomposites [31,32]. The best improvement of water resistance showed AS-5, with minimal swelling value of 0.8%. This sample indicated the best balance between AS hydrophilicity and cross-linking density of the nanocomposite.

After swelling experiments the samples were dried to the constant mass. In the all cases small mass losses of the dried films were observed. Because pure PU matrix has segmented structure consisting of more hydrophobic and more hydrophilic fragments [24], a part of the polymer may be soluble in water. According to Table 3, 6th to 8th columns, the mass uptake increases with increasing nanosilica concentration due to hydrophilic nanofiller nature and increasing of porosity. On the other hand the mass loss practically does not depend on the silica content.

4. Conclusions

Series of nanocomposites based on water-borne PUD and Ludox AS or Ludox TMA were successfully prepared by solution blending method. The proper concentration of colloidal silica improves selected functional properties of the nanocomposites. Increasing of water resistance for 5 wt% nanofiller loading, improvement of functional properties for 32 wt% and improvement of thermal stability for 50 wt% silica were observed. Silica AS revealed better enhancement than TMA due to stronger physical cross-linking effect. It was found that samples containing 5 wt% of the nanofiller are elastomers, 32 wt% show plastic behavior and 50 wt% are brittle materials. However all films are thermoplastic, which makes them possible to re-processing by dissolution in organic solvents or injection molding method.

Acknowledgments

The work was financially supported by Grant Agency of the Czech Republic (Czech Science Foundation) under project number 13-06700S. The authors would like to thank Mrs. I. Vlasáková for DMTA measurements and Dr. R. Poręba for help with preparation of PUD matrix. In addition, Magdalena Serkis would like to thank the Charles University, Faculty of Science for the opportunity to pursue her PhD study.

References

[1] H.J. Qi, M.C. Boyce, Stress–strain behavior of thermoplastic polyurethanes, Mech. Mater. 37 (2005) 817–839.
[2] A. Eceiza, M.D. Martin, K. de la Caba, G. Kortaberria, N. Gabilondo, M.A. Corcuera, I. Mondragon, Thermoplastic polyurethane elastomers based on polycarbonate diols with different soft segment molecular weight and chemical structure: mechanical and thermal properties, Polym. Eng. Sci. 48 (2008) 297–306.
[3] A. Stribeck, F. Jokari-Sheshdeh, E. Pöselt, B. Eling, P.J. In'T Veld, G.J. Gerigk, A. Hoell, Machine prepared thermoplastic polyurethanes of varying hard segment content: morphology and its evolution in tensile tests, J. Polym. Sci. Polym. Phys. 53 (2015) 1213–1223.
[4] I.S. Gunes, F. Cao, S.C. Jana, Evaluation of nanoparticulate fillers for development of shape memory polyurethane nanocomposites, Polymer 49 (2008) 2223–2234.
[5] M. Špírková, A. Duszová, R. Poręba, J. Kredatusová, R. Bureš, M. Fáberová, M. Šlouf, Thermoplastic polybutadiene-based polyurethane/carbon nanofiber composites, Compos. Part B—Eng. 67 (2014) 434–440.
[6] J. Pavličević, M. Špírková, O. Bera, M. Jovičić, B. Pilić, S. Baloš, J. Budinski-Simendić, The influence of ZnO nanoparticles on thermal and mechanical behavior of polycarbonate-based polyurethane composites, Compos. Part B—Eng. 60 (2014) 673–679.
[7] O. Malay, O. Oguz, C. Kosak, E. Yilgor, I. Yilgor, Y.Z. Menceloglu, Polyurethaneurea-silica nanocomposites: preparation and investigation of the structure-property behavior, Polymer 54 (2013) 5310–5320.
[8] S. Cruz, L.A. Rocha, J.C. Viana, Enhanced printability of thermoplastic polyurethane substrates by silica particles surface interactions, Appl. Surf. Sci. 360 (2016) 198–206.
[9] D. Kleshchanok, V. Meester, C.E. Pompe, J. Hilhorst, H.N.W. Lekkerkerker, Effects of added silica nanoparticles on hectorite gels, J. Phys. Chem. B 116 (2012) 9532–9539.
[10] L. Bailey, H.N.W. Lekkerkerker, G.C. Maitland, Rheology modification of montmorillonite dispersions by colloidal silica, Reol. Acta 53 (2014) 373–384.
[11] G. Orts-Gil, K. Natte, D. Drescher, H. Bresch, A. Mantion, J. Kneipp, W. Österle, Characterisation of silica nanoparticles prior to in vitro studies: from primary particles to agglomerates, J. Nanopart. Res. 13 (2011) 1593–1604.
[12] P.S. Singh, V.K. Aswal, Characterization of physical structure of silica nanoparticles encapsulated in polymeric structure of polyamide films, J. Colloid Interface Sci. 326 (2008) 176–185.
[13] L. Zhang, E.S. Daniels, V.L. Dimonie, A. Klein, Mechanism for the formation of PNIPAM/PS core/shell particles, J. Appl. Polym. Sci. 131 (2014) 40124.
[14] P.S. Singh, V.K. Aswal, J. Kohlbrecher, Influence of hydrophilic silica nanoparticles to the conformation of hydrophilic polymer chain in dilute solution system, J. Colloid Interface Sci. 353 (2011) 52–60.
[15] V. Uricanu, J.R. Eastman, B. Vincent, Stability in colloidal mixtures containing particles with a large disparity in size, J. Colloid Interface Sci. 233 (2001) 1–11.
[16] R. Furlan, E.W. Simões, M.L.P. da Silva, L. Ramos, E. Fachini, Modeling of composite fiber production with silica nanoparticles dispersed in polyethyleneoxide, Polymer 48 (2007) 5107–5115.
[17] M. Špírková, J. Brus, L. Brožová, A. Strachota, J. Baldrian, M. Urbanová, J. Kotek, B. Strachotová, M. Šlouf, A view from inside onto the surface of self-assembled nanocomposite coatings, Prog. Org. Coat. 61 (2008) 145–155.
[18] M. Špírková, A. Strachota, L. Brožová, J. Brus, M. Urbanová, J. Baldrian, M. Šlouf, O. Bláhová, P. Duchek, The influence of nanoadditives on surface, permeability and mechanical properties of self-organized organic–inorganic nanocomposite coatings, J. Coat. Technol. Res. 7 (2010) 219–228.
[19] A. Rebati, M. Piñero, N. de la Rosa-Fox, L. Esquivias, Mechanical properties of organic-inorganic hybrid black coating of silica and polyurethane, Key Eng. Mater. 423 (2010) 161–165.
[20] M. Serkis, M. Špírková, J. Kredatusová, J. Hodan, R. Bureš, Organic-inorganic nanocomposite films made from polyurethane dispersions and colloidal silica particles, Compos. Interfaces 23 (2016) 157–173.
[21] J.-J. Chen, C.-F. Zhu, H.-T. Deng, Z.-N. Qin, Y.-Q. Bai, Preparation and characterization of the waterborne polyurethane modified with nanosilica, J. Polym. Res. 16 (2009) 375–380.
[22] P.J. Peruzzo, P.S. Anbinder, F.M. Pardini, O.R. Pardini, T.S. Plivelic, J.I. Amalvy, On the strategies for incorporating nanosilica aqueous dispersion in the synthesis of waterborne polyurethane/silica nanocomposites: effects on morphology and properties, Mater. Today Commun. 6 (2016) 81–91.
[23] B.K. Kim, J.W. Seo, H.M. Jeong, Properties of waterborne polyurethane/nanosilica composite, Macromol. Res. 11 (2003) 198–201.
[24] M. Serkis, R. Poręba, J. Hodan, J. Kredatusová, M. Špírková, Preparation and characterization of thermoplastic water-borne polycarbonate-based polyurethane dispersions and cast films, J. Appl. Polym. Sci. 132 (2015) 42672.
[25] Ludox—Technical Literature, E. I. du Pont de Nemorus and Company, Wilmington, DE, 1999.
[26] S. Sihler, A. Schrade, Z. Cao, U. Ziener, Inverse pickering emulsions with droplet sizes below 500 nm, Langmuir 31 (2015) 10392–10401.
[27] H. Wang, A.B. Djurišić, W.K. Chan, M.H. Xie, Factors affecting phase and height contrast of diblock copolymer PS-b-PEO thin films in dynamic force mode atomic force microscopy, Appl. Surf. Sci. 252 (2005) 1092–1100.
[28] D. Raghavan, X. Gu, T. Nguyen, M. VanLandingham, A. Karim, Mapping polymer heterogeneity using atomic force microscopy phase imaging and nanoscale indentation, Macromolecues 33 (2000) 2573–2583.
[29] S. Zhang, Renliu, J. Jiang, C. Yang, M. Chen, X. Liu, Facile synthesis of waterborne UV-curable polyurethane/silica nanocomposites and morphology, physical properties of its nanostructured films, Prog. Org. Coat. 70 (2011) 1–8.
[30] S. Zhang, J. Chen, D. Han, Y. Feng, C. Shen, C. Chang, Z. Song, J. Zhao, Effect of polyether soft segments on structure and properties of waterborne UV-curable polyurethane nanocomposites, J. Coat. Technol. Res. 12 (2015) 563–569.
[31] S. Zhang, Z. Chen, M. Guo, J. Zhao, X. Liu, Waterborne UV-curable polycarbonate polyurethane nanocomposites based on polydimethylsiloxane and colloidal silica with enhanced mechanical and surface properties, RSC Adv. 4 (2014) 30938–30947.
[32] H. Zhou, H. Wang, X. Tian, K. Zheng, Q. Cheng, Effect of 3-aminopropyltriethoxysilane on polycarbonate based waterborne polyurethane transparent coatings, Prog. Org. Coat. 77 (2014) 1073–1078.

Progress in Organic Coatings 106 (2017) 119–127

Contents lists available at ScienceDirect

Progress in Organic Coatings

journal homepage: www.elsevier.com/locate/porgcoat

Formation of linear and crosslinked polyurethane nanoparticles that self-assemble differently in acetone and in water

Magdalena Serkis-Rodzeń[a,*], Milena Špírková[a,*], Pavel Matějíček[b], Miroslav Štěpánek[b]

[a] Nanostructured Polymers and Composites Department, Institute of Macromolecular Chemistry AS CR, Prague, Czechia
[b] Department of Physical and Macromolecular Chemistry, Charles University in Prague, Czechia

ARTICLE INFO

Article history:
Received 10 January 2017
Received in revised form 1 March 2017
Accepted 1 March 2017

Keywords:
Polyurethane water dispersion
Nanoparticles
Self-assembly
Atomic force microscopy
Static light scattering
Dynamic light scattering

ABSTRACT

For the first time, stable water-borne polyurethane dispersions (PUDs) leading to mechanically strong polyurethane (PU) coatings were prepared without any chain extender. Elimination of this step and using of water-crosslinking gives promising applications of PUDs as biomaterials and production on an industrial scale. The PU system consists of polycarbonate macrodiol (PCD), (2,2-bis(hydroxymethyl)) propionic acid (DMPA), 1,6-diisocyanatohexane (HDI) and *N*,*N*-diethylethanamine (TEA). Fourier transform infrared spectroscopy (FTIR), dynamic mechanical thermal analysis (DMTA), static light scattering (SLS), dynamic light scattering (DLS) and atomic force microscopy (AFM) enabled the study of the assembly of the PU chains/nanoparticles into supramolecular structures in acetone and in water. In acetone, the self-assembly of isocyanate-terminated pre-polymer chains occurs in the form of either PU solutions (linear PUs) or PU dispersions (crosslinked PUs). Due to a phase inversion, spherical linear or water-crosslinked PU dispersions are formed after water addition. The isocyanate-to-total hydroxyl ratio is very important; a slight isocyanate (NCO) excess of 1.05 leads to linear rod-like nanoparticles in acetone followed by a core-shell structure after water addition. An isocyanate excess of 1.5 leads to compact sphere or micro-gel particles initially crosslinked by moisture in acetone, and the final crosslinking and phase inversion occurs after water addition. The chain lengths of the linear PUs and the mesh sizes in PU networks increase with the PCD:DMPA ratio. Thus, the design of PU nanoparticles with desired sizes, shapes and crosslink densities is possible. Unlike the substantially different shapes, sizes and compactness of PUs in acetone, all PUDs in water are spherical nanoparticles with an average diameter from 21 to 72 nm, a zeta potential from −40 to −65 mV and a size-dispersity index from 0.05 to 0.22.

1. Introduction

In recent years, polyurethane water dispersions (PUDs) have been extensively used to replace conventional polyurethanes (PUs) to eliminate the emission of organic solvents to the atmosphere. PUDs have found application as environmentally friendly coatings and adhesives in industrial and biomedical applications due to their excellent mechanical and chemical properties and good biocompatibility [1–4].

Different polyols can be used to prepare PUDs. Among them, polycarbonate diols (PCDs) represent a relatively new class. In comparison to polyester- or polyether-based PUDs, they are biocompatible biomaterials with better hydrolytic, thermal and mechanical resistance [1,5,6].

In addition to PCDs, which build so-called soft segments, other components are used in the synthesis of PUDs. The so-called hard segments are composed of isocyanate and low-molecular-weight chain extenders and enhances mechanical properties of the final PUs. Moreover, the incorporation of dihydroxylic acids provides dispersity of PU chains in water due to the presence of ionic groups. The most widely used is 2,2-bis(hydroxymethyl)propionic acid (DMPA), which acts not only as an internal emulsifier but also as a chain extender[6–8].

Among PUDs based on PCDs, mostly diamines and diols are used as chain extenders. García-Pacios et al. applied diethyleneglycol as a short diol and monohydrated hydrazine as a chain extender [1,2,5,7], while Cakić et al. [3,6], Liu et al. [9] and Lee et al. [10,11] used ethylene diamine. The disadvantages of amines are their unpleasant odors and toxicity. To minimize the toxic influence of the chain extenders, butane-1,4-diol (BD) was used in our

* Corresponding authors.
E-mail addresses: serkis@imc.cas.cz (M. Serkis-Rodzeń), spirkova@imc.cas.cz (M. Špírková).

http://dx.doi.org/10.1016/j.porgcoat.2017.03.003
0300-9440/

previous work [12–14] and by Fang et al. [15] Even though BD is safer than amines, it has a pronounced effect on the central nervous system [16].

To expand the application of PUDs as medical biomaterials, such as scaffolds for skin regrowth [17], in this work, we fully eliminated the chain extension step (see, e.g., Fig. 1, line 3, in Ref. [12]). This approach enabled the acquisition of materials with reduced toxicity, manufacturing cost and energy consumption. To the best of our knowledge, this is the first study describing novel stable PUDs based on PCDs without using any chain extender based on a short diamine or diol.

Due to incompatibility between the hard and soft segments in PUs, phase separation occurs and leads to various morphologies [18,19]. Therefore, PUDs can self-assemble and create different microstructures. Understanding the process of nanoparticle formation would be helpful for modification of the dispersions and improvement of their properties [20,21]. Although several studies describe the assembly of PUDs, they are mostly focused on already-reacted particles dispersed in water [20,22] or PU film formations [23]. There is only one publication that reports the self-organization of PU nanoparticles in the pre-polymerization stage [21]. However, despite the PUs being prepared without a chain extender, the paper reports an SCF simulation study describing nanoparticles already dispersed in water.

This article describes experimental research focused on the formation of PU nanoparticles in the initial pre-polymerization stage in acetone followed by the dispersion step (phase inversion) in water. The course of the two-step polymerization was monitored by infrared spectroscopy. We report on the self-assembly behavior of PU nanoparticles using AFM and light scattering methods. Here, we also compare the effect of water-crosslinking and the molar ratio of the reagents on the particle morphology and properties.

2. Experimental section

2.1. Materials

Commercial aliphatic PCD, trademark T4672, with a molecular weight M_w ~2770 g mol^{-1} (detected by GPC) was kindly provided by Asahi Kasei Chemical Corporation, Tokyo, Japan. DMPA, 1,6-diisocyanatohexane (HDI) and *N*,*N*-diethylethanamine (TEA) were received from Sigma-Aldrich. Dried acetone (max. 0.0075 wt% H_2O) was obtained from Merck KGaA, Darmstadt, Germany. Dibutyltin dilaurate (DBTDL, Sigma-Aldrich), 10 wt% solution in Marcol oil, was used as the catalyst.

2.2. Preparation procedure

PUDs were prepared via an acetone process without the chain extension step using varying PCD:DMPA molar ratios to control the amount of the soft and hard segments. The ratio [NCO]:$[OH]_{total}$ ($[OH]_{total} = [OH]_{PCD} + [OH]_{DMPA}$) was set either at 1.05 to obtain linear PUs or at 1.5 for water crosslinked PUs. The sample codes describe the type and molar ratio of the used components and are marked as PUx/y:z for nanoparticles dissolved/dispersed in acetone and PUDx/y:z for the polyurethane water dispersions. In these names, x indicates the ratio [NCO]:$[OH]_{total}$, whereas y:z is the PCD:DMPA molar ratio. For example, the sample PU1.5/1:2 is the acetone dispersion of nanoparticles containing a 1.5-fold excess of NCO groups with a PCD:DMPA ratio equal to 1:2, and PUD1.5/1:2 is the sample of identical composition dispersed in water. The preparation procedure of the PUDs and the possibility of water-crosslinking are given in Fig. 1, and the wt% of the components used for all samples is summarized in Table S1.

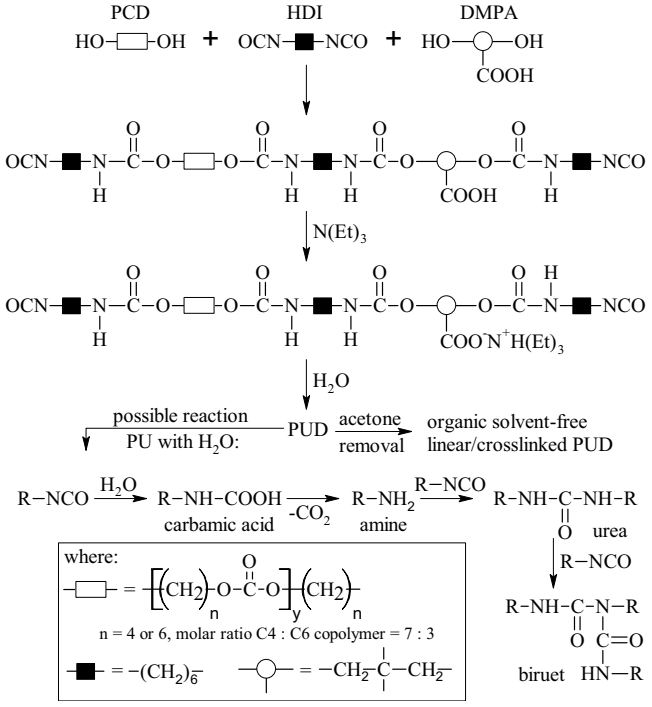

Fig. 1. Synthesis scheme of PUDs and possible reaction of PU with H_2O.

PCD, DMPA, HDI, the catalyst (0.05 mol of DBTDL per mol of NCO groups) and acetone were placed into a round bottom flask and mixed at a rate of 700 rpm at 60 °C for 4 h until a constant NCO content was reached. Then, TEA was added to fully neutralize the carboxylic groups and mixed for 30 min at 55 °C followed by the gradual addition of water. The latter step involves not only the phase inversion but also the reaction of water with unreacted NCO groups, if present. Organic solvent-free PUDs were obtained after acetone removal using a rotavap under reduced pressure.

2.3. Characterization techniques

Fourier transform infrared spectroscopy (FTIR) was used to monitor the isocyanate, urethane, urea and biuret bond formations in the PU nanoparticles. The FTIR spectra were obtained using a PerkinElmer Spectrum 100 spectrometer equipped with a universal ATR accessory with a diamond crystal.

Light scattering measurements of acetone solutions at the reaction step before water addition were carried out using an ALV instrument (ALV, Langen, Germany) consisting of a 633 nm He-Ne laser source, an ALV CGS/8F goniometer, an ALV High QE APD detector and an ALV 5000/EPP multibit, multitau autocorrelator. The refractive index increments, d n/d c, were measured using an Optilab T-rEX refractive index detector (Wyatt Technology Corporation) connected to a Cole-Parmer syringe pump at 0.123 for PU dispersions in acetone. Static light scattering (SLS) results were treated by the Berry method. Dynamic light scattering (DLS) data were evaluated by fitting the obtained normalized autocorrelation functions of the scattered light intensity to the second-order cumulant expansion and treated as dynamic Zimm plots. Details of the LS data analysis are given in the Supplementary results (equation S1).

Electrophoretic light scattering (ELS) measurements were used to determine the ζ-potentials of water PUDs from their electrophoretic mobilities using the Smoluchowski approximation. For this purpose, a Nano-ZS zetasizer (Malvern Instruments, UK) was

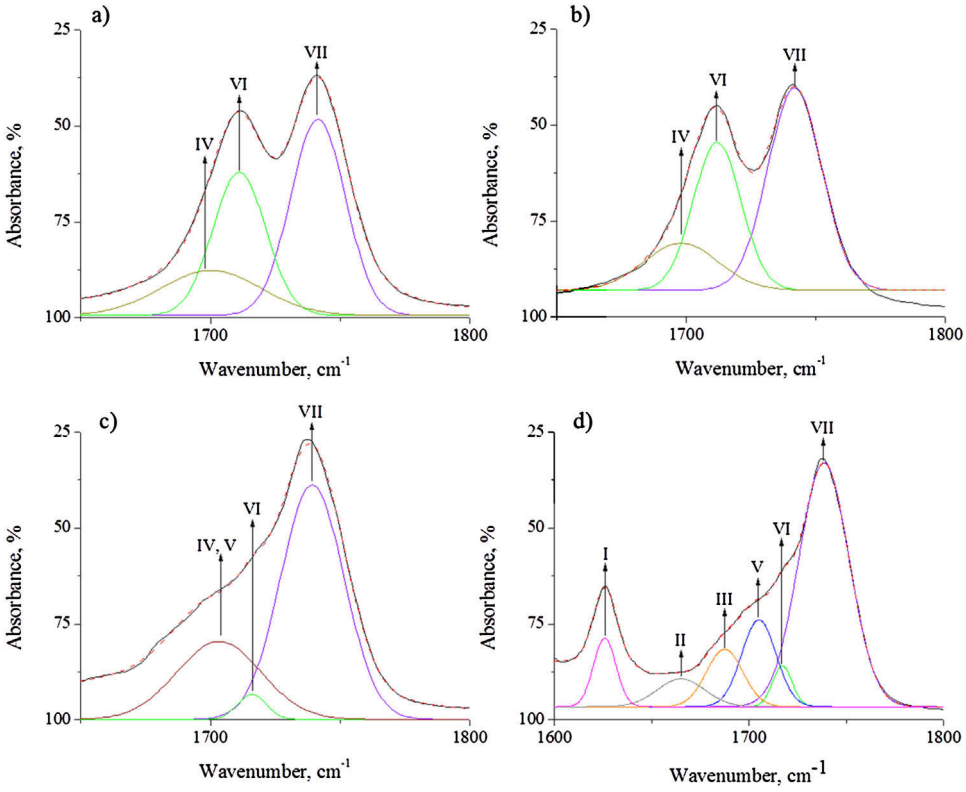

Fig. 2. Deconvoluted carbonyl region of the FTIR spectra of PU nanoparticles in acetone: a) PU1.05/1:1, b) PU1.5/1:1 and dried PUDs: c) PUD1.05/1:1, d) PUD1.5/1:1.

used. The obtained values were the average of three subsequent measurements; each measurement consisted of 15–100 runs.

An atomic force microscope (AFM, Dimension Icon, Bruker) equipped with an SSS-NCRL-20 probe (Super Sharp Silicon™ – SPM – Sensor with resonance frequency 146–236 kHz and force constant 21–98 N m^{-1}) was used to investigate the PU nanoparticle microstructures. The size and shape of particles were studied after deposition of PUs dissolved/dispersed in acetone or in water (~2 g L^{-1}) on freshly peeled mica surfaces (flogopite, $KMg_3AlSi_3O_{10}(OH)_2$). After acetone or water evaporation, the samples were dried in a vacuum oven at ambient temperature for 12 h.

3. Results and discussion

Stable PCD-based waterborne dispersions were successfully prepared without any chain extension step, resulting in mechanically strong PU films. This fact is very important for potential practical applications. To confirm the macrodiol uniqueness, PCD was replaced by other types of polyols of similar molar masses during the synthesis of the PUD1.05/1:1 sample. The results revealed that while the use of hydroxyl-terminated polybutadiene leads to the separation of the aqueous and organic phases, the application of polypropylene glycol leads to unstable dispersions and sticky films. Finally, polycaprolactone diol provides stable dispersions, but the obtained films are highly fragile.

The final PUDs are amphiphilic block copolymers consisting of alternating hydrophilic hard segments (HS) and hydrophobic soft segments (SS). The soft domains are formed by PCD to grant an elastomeric character to the PU chain. The hard segments, which act as reinforcing fillers, are composed of short DMPA chains and urethane groups originating from HDI and urea groups [24,25]. Series of PUDs differing in their component molar ratios were measured after two reaction steps: i) PU nanoparticles dissolved/dispersed in acetone after neutralization (PUx/y:z) and ii) final PUDs in water after acetone removal (PUDx/y:z). PUDs containing PCD:DMPA molar ratios of 1:2, 1:1 and 2:1 were prepared with NCO excesses equal to 1.05 and 1.5.

Table 1
FTIR spectra of PUs and PUDs in the carbonyl region.

Band number	ν, cm^{-1}	Assignment
I	1623–1626	Strongly bonded urea
II	1663–1664	Weakly bonded urea
III	1687–1694	Biuret + H-bonded carbonate
IV	1698–1699	Free urea
V	1702–1708	Free carbonate
VI	1711–1717	H-bonded urethane
VII	1738–1741	Free urethane

3.1. Fourier transform infrared spectroscopy (FTIR)

The molecular structure of each sample was analyzed by FTIR. To examine the formation of urethane, urea and biuret, the region between 1600 and 1800 cm^{-1} was examined. Several vibration bands overlap in the area of carbonyl stretching, which makes the spectra difficult to interpret. To recognize the main carbonyl peaks, i.e., the free and hydrogen-bonded C=O of urethane, urea, carbonate, carboxylic acid and biuret, deconvolution of this region was performed and is shown in Fig. 2, Fig. S2 and Table 1.

Samples containing the same molar ratio of DMPA to PCD and different NCO excesses were chosen as representatives for the investigation of the PU chemical structures at two steps of the reaction. Similar spectra for all PUs dispersed/dissolved in acetone (Fig. 2 a and b) were observed before water addition. In both cases, the deconvolution of the C=O region revealed peaks at approximately 1740 cm^{-1} (band VII) attributed to free C=O urethane groups, 1715 cm^{-1} (band VI) assigned to hydrogen-bonded urethane and 1699 cm^{-1} representing free urea [26–28]. These results demonstrate that in this step, urea as well as urethane is form-

ing as a product of the reaction between HDI and residual water present in the components, solvent and air. Moreover, comparison of PU1.05/x:y and PU1.5/x:y revealed that the peak at approximately 2270 cm^{-1} attributed to free isocyanate groups [26] was visible only in the samples containing 1.5 NCO excess (see Fig. S1a) and b)). However, weak intensity of the peak at 2270 cm^{-1} in PU1.5/x:y suggests the reaction between NCO groups and urethanes, leading to formation of allophanates, resulted in the partial crosslinking.[1] On the other hand, samples with a 1.05-fold NCO excess are fully reacted, linear and chain-extended by urea formation before the phase inversion step.

After water addition,[2] as a result of the shifting band VI [29] in the PUD1.5/x:y series (Fig. 2c), an additional peak assigned to non-bonded carbonyl groups of PCD at 1705 cm^{-1} (band V) appeared [30], but it was not deconvoluted separately due to overlap with band IV. In samples containing a 1.5-fold NCO excess, water-crosslinking was also observed in this step by the formation of new band (III) at 1687–1694 cm^{-1}, attributed to H-bonded carbonate [31] and biuret [30]. Moreover, strongly (band I) and weakly (band II) urea-bonded peaks were observed at 1625 cm^{-1} and 1664 cm^{-1}, respectively. [28] The highest intensity of the band I for PUD1.5/2:1 suggests the highest amount of urea formation compared to other PUD/x:y. The lack of the NCO peak at 2270 cm^{-1} in PUD1.5/x:y (see Fig. S1d)) confirms the full isocyanate conversion to urea and biuret after water addition.

Crosslinked samples containing different PCD:DMPA molar ratios have also been compared (Fig. S2). No differences in peaks V, VI and VII were observed. However, band III, corresponding to H-bonded carbonate and biuret formation, was most visible for PUD1.5/1:2 (Fig. S2 a), suggesting the greatest crosslinking density for this sample. For comparison, in PUD1.5/2:1, band III is weak and overlapped with band II. This result may be explained by the lowest HDI wt% used in the reaction (see Table S1), which gives the smallest amount of possible biuret junction points. Moreover, since PUD1.5/2:1 is characterized by the strongest urea peak and the weakest biuret peak in PUD1.5/x:y series, it suggests domination of the chain extension by urea formation over the crosslinking via biuret formation, as a result of the lowest mobility of PU chains in the sample containing the highest amount of PCD. Thus, the main crosslinking of this sample occurs in acetone. Changes in peaks I and II were also observed. Band I represents "ordered" urea, where one urea C═O is H-bonded with both N—H groups of a nearby urea (urethane), whereas band II, corresponding to a "disordered" fashion, is assigned to urea C═O groups bonded to only one N—H of urethane or urea. [28] An increase in the ratio of the absorbances of peaks I and II was observed when the PCD amount increases, most visibly for PUD1.5/2:1 (Fig. S2 b). This result may suggest that the most hard-soft segment separation[28] exists for this sample.

3.2. Dynamic mechanical thermal analysis (DMTA)

Monitoring of the crosslink formation in the two reaction steps was carried out by DMTA analysis for samples with a 1.5 NCO excess. For this purpose, pre-polymer suspensions in acetone (PU1.5/x:y) and water dispersions (PUD1.5/x:y) were dried to obtain films measurable by DMTA.

The crosslinking density, ν, was determined from the storage modulus, G', at a temperature well above T_g, using Eq. (1), according to the theory of rubber elasticity:

$$\nu = G'/RT \quad (1)$$

where ν is the crosslinking density, G' is the shear storage modulus above the glass transition temperature, $R = 8.314\ J\ K^{-1}\ mol^{-1}$ is the gas constant, and T is the temperature at which G' was determined [32]. The obtained data are presented in Table 2.

Table 2
The crosslinking density of samples with a 1.5 NCO excess before (PU) and after water addition (PUD).

Sample	G', MPa, $T = 50\,^{\circ}C$	Crosslink density, ν, mol dm^{-3}
PU1.5/2:1	24.3	9.0
PU1.5/1:1	14.6	5.4
PU1.5/1:2	4.2	1.6
PUD1.5/2:1	23.2	8.6
PUD1.5/1:1	21.0	7.8
PUD1.5/1:2	31.8	11.8

Table 3
Parameters obtained from the light scattering analysis of PU particles dissolved/dispersed in acetone.

Sample	$\langle S^2\rangle_z^{1/2}$, nm[a]	$\langle R_H^{-1}\rangle_z^{-1}$, nm[b]	ρ[c]	M_w, g/mol
PU1.05/2:1	240	120	2.0	4.9×10^6
PU1.05/1:1	N/A	3	N/A	15×10^3
PU1.05/1:2	N/A	7	N/A	53×10^3
PU1.5/2:1	180	210	0.86	25×10^6
PU1.5/1:1	290	430	0.67	121×10^6
PU1.5/1:2	280	750	0.4	64×10^6

[a] gyration radius.
[b] hydrodynamic radius.
[c] ratio of gyration radius to the hydrodynamic radius.

Before water addition, the highest crosslinking density was found for the sample with the highest PCD content (PU1.5/2:1). This result may be explained by the largest amount of long chains and hydrogen bonds being created between urethane groups of the pre-polymer and the carbonyl groups of the PCD. Thus, in this case the particles are close enough to each other to create the polymer network easily. In contrast, the short chains of PU1.5/1:2 are more separated, which prevents their junction.

In the step of water addition, the crosslinking reaction as well as the phase inversion occurs, after which the hydrophobic core created by PCD is surrounded by the hydrophilic shell of DMPA [20]. From the comparison of the sample with the highest PCD amount before (PU1.5/2:1) and after dispersion (PUD1.5/2:1), no difference after the two steps was observed. This result may be caused by the weak water penetration of the PU nanoparticles due to the formation of the most hydrophilic PUD. This finding also suggests that the phase inversion is faster than water crosslinking.

In contrast, a significant increase in the crosslinking density for the sample containing the highest DMPA content (PUD1.5/1:2) was observed. This result may be explained by the creation of a high number of short NCO-terminated pre-polymer chains in acetone by PU1.5/1:2 and the highest HDI wt% used in the reaction. In the dispersion step, water can easily penetrate through the particles due to the high amount of hydrophilic DMPA to react with isocyanate groups to create biuret crosslinks (see Fig. 1).

3.3. Light scattering measurements of PU nanoparticles in acetone

To investigate PU nanoparticle self-assemblies in acetone and water, the solutions were studied by static and dynamic light scattering, SLS and DLS. SLS measurements were evaluated by the Berry method, while DLS measurements of apparent diffusion coefficients were treated as dynamic Zimm plots. The representative Berry and dynamic Zimm plots for the PU1.5/1:1 sample are shown in Fig. 3. The parameters obtained by fitting the SLS and DLS data of all studied samples are summarized in Table 3.

[1] It follows from the kinetics of model reactions Ref. [41], that the formation of allophanate is less significant and slower than biuret.
[2] To avoid negative peaks from H_2O, PUDs were dried before FTIR analysis.

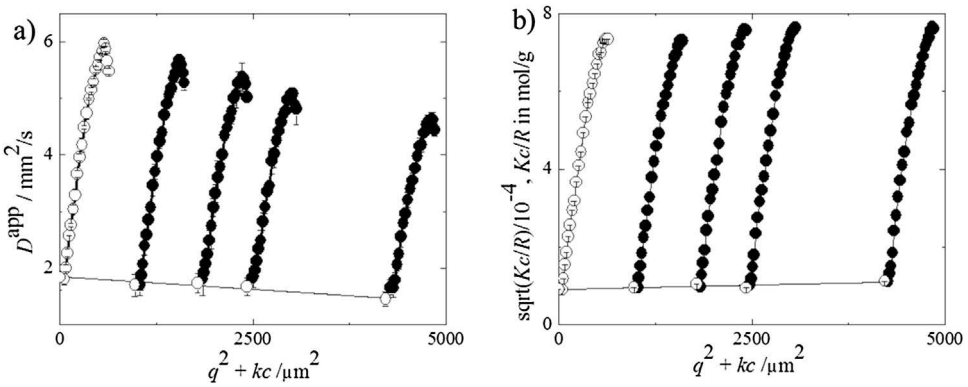

Fig. 3. Comparison of a) dynamic Zimm plot and b) Berry plot of PU1.5/1:1 in acetone solutions.

While the low molar masses of PU1.05/1:1 and PU1.05/1:2 correspond to molecularly solubilized polymers with a low degree of crosslinking, the molar masses of the other polymers indicate the formation of more compact nanoparticles with a large degree of crosslinking. It is noteworthy that the molar mass (see Table 3) scales with the hydrodynamic radius as $M_w \sim R_H$[1,7], which means that the mass fractal dimension of the formed particles is close to that of aggregates formed by diffusion-limited cluster aggregation. The ratio of the gyration radius to the hydrodynamic radius, ρ, has been used as an indicator of the PU nanoparticle shape in acetone dispersions. In the case of PU1.05/2:1, the ρ parameter of approximately 2 suggests a rod-like morphology of the particles. This observation is confirmed by the presence of a q^2-independent relaxation mode in DLS corresponding to rotational diffusion of cylindrical particles. On the other hand, PU1.5/2:1, PU1.5/1:1 and PU1.5/1:2 exhibit ρ values below 1, which are typical for compact spherical objects. ρ values lower than 0.6 (observed for sample PU1.5/1:2) were reported for microgel particles in which loose peripheral chains strongly affect their hydrodynamic behavior and thus the value of R_H, but the chains contribute only negligibly to the mass distribution of the particle and thus to the value of R_g [33,34].

Moreover, PU1.5/1:2 was the most swellable in acetone, as indicated by the lowest observed density (obtained from M_w and R_H as $d = 3\,M_w/4\pi N_A R_H{}^3$), which confirms the lowest crosslinking density among the samples containing a 1.5-fold NCO excess. Increasing the PCD amount resulted in changes of PU chain architectures toward compact spheres. These changes may be caused by differences in PU chains lengths, which confirms the results obtained from DMTA analysis.

Samples with 1.5 isocyanate excess were further characterized by SALS. The comparison of the SALS experiment and fitted data are given in Supplementary results (Fig. S3).

3.4. Dynamic light scattering (DLS) analysis of particles dispersed in water

DLS measurements of aqueous dispersions were carried out for investigation of PU self-assemblies at a 173° (back angle) scattering angle after water addition and acetone removal. Since PUs are composed of hydrophilic and hydrophobic segments, addition of H_2O causes the phase inversion. As a result, the core-shell structure is formed, where PCD-based soft segments are surrounded by DMPA-based hard segments, providing hydrophilic ionic groups.

The DLS results are summarized in Table 4. The biggest particles in the PUD1.05/x:y series were observed for the sample containing the highest PCD amount (PUD1.05/2:1), due to the highest number of long PU chains. On the other hand, this sample had the lowest value of ζ because of having the lowest DMPA content and thereby the lowest number of COO^- groups. The narrowest size distribution

Table 4
DLS results of final PUDs.

Sample	$<R_H{}^{-1}>_z{}^{-1}$, nm	ζ-potential, mV	PDI[a]
PUD1.05/2:1	53.9 ± 0.1	−47.5 ± 2.9	0.05
PUD1.05/1:1	28.8 ± 0.1	−64.9 ± 0.6	0.05
PUD1.05/1:2	21.0 ± 0.3	−60.5 ± 1.6	0.22
PUD1.5/2:1	72.1 ± 0.2	−40.5 ± 1.8	0.09
PUD1.5/1:1	34.0 ± 0.3	−44.0 ± 3.1	0.14
PUD1.5/1:2	29 ± 0.5 and 147.5 ± 9.5	−44.6 ± 2.3	0.48

[a] size-dispersity index.

(PDI) of PU nanoparticles in water was calculated for PUD1.05/2:1 and PUD1.05/1:1, indicating the most homogenous samples. The highest PDI value was calculated for PUD1.05/1:2, which suggests that short-chained PUs can easily create aggregates.

When a 1.5-fold NCO excess is used, the situation becomes more complex. Phase inversion and water-crosslinking occur simultaneously. In all cases of crosslinked PUs, higher values of R_H and PDI and lower values of ζ in comparison to linear samples were observed. Thus, formation of polymer networks contributes to the expansion of PU nanoparticles.

The similarity in ζ values for PUD1.05/2:1 and PUD1.5/2:1 suggests that in both samples, the ionic groups of DMPA are not trapped in the PU network; rather, they surround the polymer core, providing stability in water. This result is an explanation for the low crosslinking density of PUD1.5/2:1, calculated from G' (see DMPA section). The comparison of PUD1.05/1:1 with PUD1.5/1:1 and PUD1.05/1:2 with PUD1.5/1:2 revealed a significant increase in ζ. These differences may indicate that COO^- groups are trapped in the polymer network, which confirms the high crosslinking density of PUD1.5/1:1 and PUD1.5/1:2 obtained from DMTA measurements. Particles containing a high amount of PCD were the largest in both the crosslinked and linear forms due to possessing the highest amount of PCD long chains. An inhomogeneity of nanoparticles containing the highest content of DMPA was observed for the 1.5 NCO excess (PUD1.5/1:2). In this case, two domains of particles, 30% with R_H = 29 nm and 70% with R_H = 147.5 nm, were evident. This observation confirmed the tendency to form agglomerates when short PU chains are present in high quantities.

3.5. Model of PU chain lengths and evolution of nanoparticle microstructures

Information about PU chain lengths and the results obtained from FTIR, DMPA, SLS and DLS allow us to propose a structural model of the self-assembly of the PU nanoparticles. The Avogadro software was used for estimation of the chain lengths including consideration of the bond angles between the molecules.

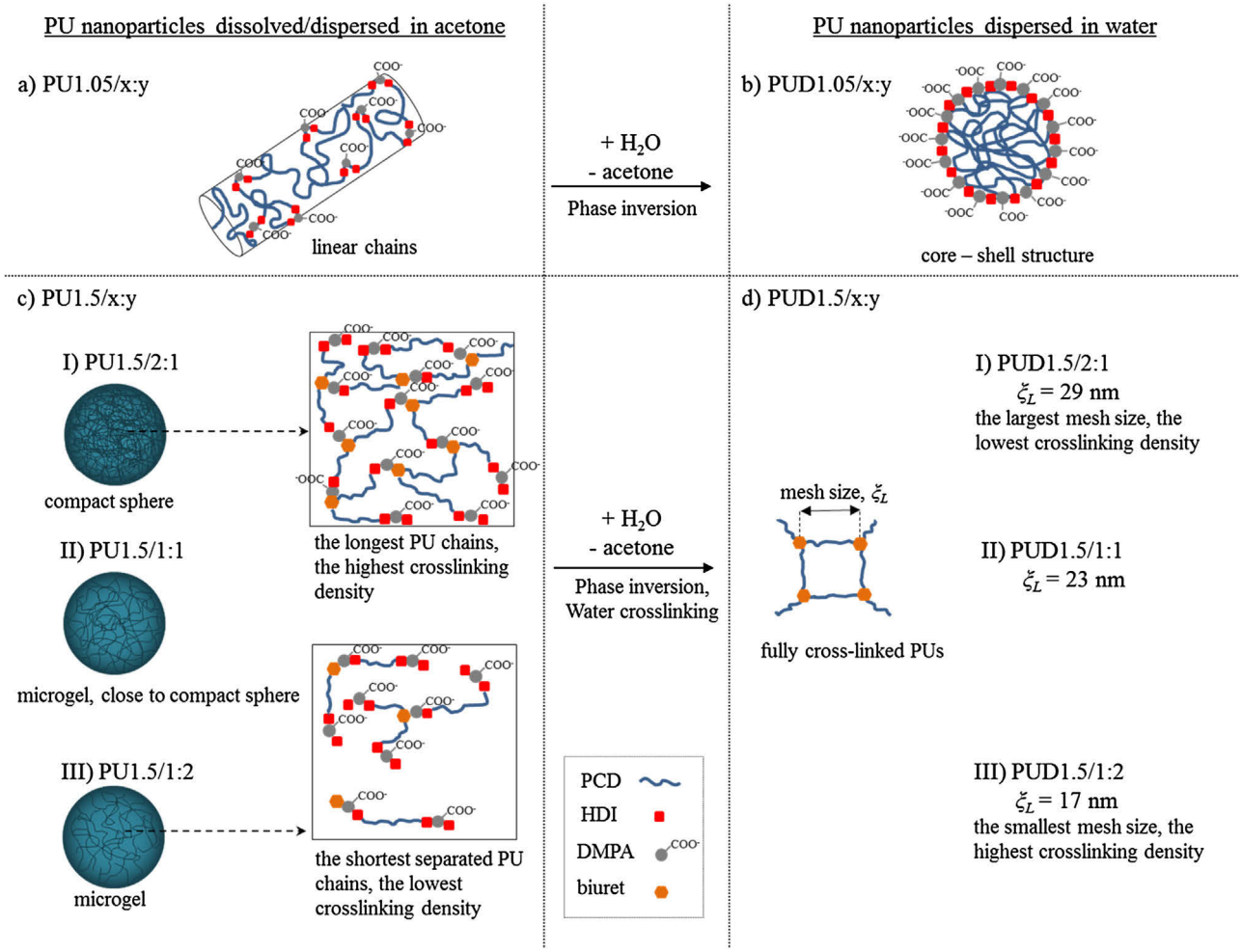

Fig. 4. Model of the PU nanoparticle self-assemblies.

The main components used for synthesis of the PUDs were DMPA, HDI and PCD. Since the structural formulas of DMPA and HDI are well known, the chain lengths were estimated by the Avogadro software as 7 Å for DMPA and 15 Å for HDI. The PCD used for preparation of PUDs was commercial T4672. The first two numbers refer to methylene units in the copolymer (C4 and C6); the third number is the amount of C_4 units. Thus, the name T4672 refers to 70 mol% C_4 units and thereby a molar ratio C4:C6 = 7:3. The last number describes the molecular weight of the PCD [26]. Since the M_W of T4672 has been detected by GPC as 2770 g mol^{-1} (see experimental section), the number of methylene units was calculated as 14 C4:6 C6. Based on this information, the chain length of PCD T4672 was estimated as 194 Å. To confirm the results obtained from Avogadro, the chain lengths of all components were calculated from bond lengths given in the literature [35,36] to be 15 Å for HDI, 8 Å for DMPA and 205 Å for PCD T4672. The similarity of the obtained values allowed us to use the estimations given by Avogadro for further analyses.

As mentioned in the experimental section, the prepared PUDs contained different NCO excesses and the following PCD:DMPA:HDI molar ratios: 1:1:2, 1:2:3 and 2:1:3. When considering a linear system with an equal molar ratio of PCD and DMPA, we can accept that one repeating unit is composed of one molecule of PCD, one molecule of DMPA and 2 molecules of HDI, with the NCO excess neglected in this assumption. Taking this into account, the chain length of PUD1.05/1:1 was estimated as 231 Å. The two remaining samples containing the 1.05 NCO excess were characterized in the same fashion. The chain length of PUD1.05/1:2 was calculated to be 169 Å and that of PUD1.05/2:1 to be 293 Å. These estimations are in a good agreement with the previous sections, where samples with the highest PCD amount have the longest PU chains.

Based on the obtained results, we can propose a model of the self-assembly of linear and crosslinked PU nanoparticles in acetone and water. The model of PU evolution during the reaction is shown in Fig. 4. All samples containing a 1.05-fold NCO excess in the form of pre-polymer are well dissolved in acetone. The reason for this behavior is that the organic solvent easily penetrates the PU chains due to the possibility of the dissolution of both hydrophilic and hydrophobic PU parts. Thus, hard and soft segments are randomly located while dissolved in acetone (Fig. 4a). When water is added, the phase inversion occurs. As a result, PU nanoparticles self-assemble into a core-shell structure, where hydrophobic soft segments are surrounded by hydrophilic hard segments (Fig. 4b). This structure provides the aqueous stability of PU nanoparticles.

The presence of water in the used components and the ingress or admission of moisture to the reaction mixture during synthesis needs to be considered to use the proper amount of HDI. Thus, the 1.05-fold NCO excess resulted in linear PUs. In these samples, the hydroxyl groups of DMPA and PCD were fully converted to polyurethane groups, while a small amount of urea was a product of the reaction between moisture and the rest of the NCO groups (see FTIR section). Therefore, the PU1.05/x:y samples were fully reacted

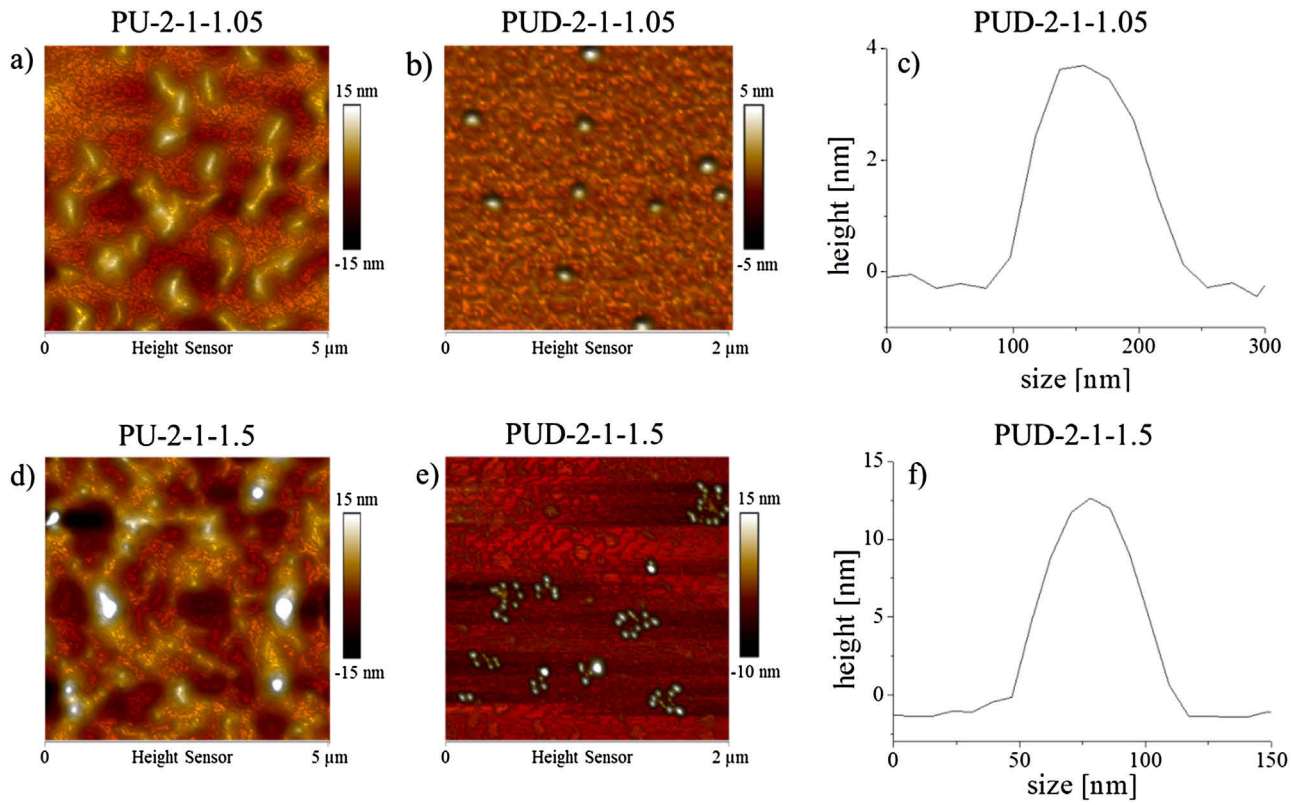

Fig. 5. Height AFM micrographs of polyurethane nanoparticles deposited on mica surfaces prepared from acetone solutions/dispersions: a) PU1.05/2:1, d) PU1.5/2:1 (5 µm × 5 µm) and water dispersions: b) PUD1.05/2:1, e) PUD1.5/2:1 (2 µm × 2 µm) and surface profiles of c) PUD1.05/2:1, f) PUD1.5/2:1.

while in acetone, and no free NCO groups were present before water addition.

When a 1.5-fold NCO excess is used (PU1.5/x:y), the PU nanoparticles are initially crosslinked in acetone. In these cases, the pre-polymer chains are NCO-terminated, and free NCO groups are present in acetone as well. The differences in these samples (Fig. 4c) depending on the component molar ratios are evident. PU1.5/2:1, containing the highest amount of PCD and thereby long chains, turned out to form a compact sphere. This result may be explained by a sufficiently short distance between the long PU chains while dispersed in acetone, which results in the facile creation of the polymer network. Decreasing the PCD:DMPA molar ratio causes the formation of shorter PU chains and increases their mutual distance. Thus, in the PU1.5/x:y series, PU1.5/1:2 contains the shortest PU chains, which are the most separated from each other in the organic solvent. As a result, the pre-polymer with the lowest crosslinking density forms as a swollen microgel in acetone.

The water addition to samples containing a 1.5-fold NCO excess causes both the phase inversion and crosslinking. Thus, the nanoparticle self-assembly into core-shell structures and the final crosslinking occur simultaneously. Since water reacts with NCO groups present at the ends of the pre-polymer chains to give biuret junction points, the chain lengths of specific PUs play a key role in the crosslinking density. From the calculated chain lengths of linear PUs, we can estimate the mesh sizes of crosslinked PUs. Based on these calculations, we can assume that PUD1.5/2:1 has the largest mesh sizes (Fig. 4 d) in the PUD1.5/x:y group and therefore the lowest crosslinking density. Moreover, this sample contains the highest amount of hydrophobic PCD, which blocks water penetration and crosslinking. As a result, no changes in crosslinking density between the pre-polymer PU1.5/2:1 and dispersion PUD1.5/2:1 were present, which suggests that the final crosslinking occurs in acetone. Increasing the DMPA content causes easier water penetration and crosslinking due to increasing the hydrophilic segment fraction. Moreover, because the pre-polymer chains of PU1.5/1:1 and PU1.5/1:2 are shorter than those of PU1.5/2:1, they form a higher number of terminal NCO groups and therefore a higher number of biuret junction points after water addition. Thus, the sample containing the most DMPA (PUD1.5/1:2) has the smallest mesh sizes and the highest crosslinking density.

3.6. Atomic force microscopy (AFM)

The self-assembly of PU nanoparticles was observed by AFM through visualization of the separated molecules. Samples containing the highest PCD amount were chosen for these analyses due to possessing the highest particle sizes and therefore the best conditions for measurements. Highly diluted ($\sim 2\,g\,L^{-1}$) acetone (PUx/2:1) and water dispersions (PUDx/2:1) were deposited on freshly cleaved mica by the droplet-evaporation method.

Fig. 5 shows height images of the particles, both linear and crosslinked, and typical surface profiles of the nanoparticles obtained from water dispersions. It was observed that particles obtained from the PU1.05/2:1 solution (Fig. 5a) were elongated and disc-shaped, while drying the PU1.5/2:1 yielded more spherical but less separated particles (Fig. 5d). This result may be explained by the linear character of PU1.05/2:1, because of which PU chains are well dissolved in acetone. After evaporation of the organic solvent, the nanoparticles collapse, giving elongated structures. In comparison, PU1.5/2:1 self-assembles into more compact but aggregated structures. This behavior is a result of the crosslinked character of these nanoparticles.

All particles formed after water evaporation are spherical (Fig. 5b, e) due to the phase inversion resulting in the core-shell structure. The particles from each sample were manually selected. They first flattened, and then their width and height were detected

Table 5
Average sizes of the PU nanoparticles containing the highest PCD amount, detected from AFM images.

Sample	Height, nm	Diameter, nm	Diameter/Height ratio
PU1.05/2:1	6.9	345.0	50.0
PU1.5/2:1	10.3	268.2	26.0
PUD1.05/2:1	4.0	126.2	31.5
PUD1.5/2:1	13.4	57.4	4.3

by the automatic particle analysis option of the NanoScope Analysis software. The average values and diameter/height ratios are summarized in Table 5. These results are in good agreement with values obtained from previous analyses. The differences between particle sizes detected by light scattering and AFM could be explained by the fact that DLS measurements were performed on acetone/water dispersions, while AFM samples were dried before the analyses. Other reasons for possible inaccuracy in the AFM measurements are the tip-broadening effect, giving overestimated dimensions, and pancake deformation caused by attractive interactions between the PU particles and mica surface [37,38]. However, the softness/hardness of the nanoparticles seems to be the main parameter influencing their size and shape as measured by this method. Calculation of the diameter/height ratio gives the possibility to estimate both these features. Since height reduction of nanoparticles measured by AFM is a result of the soft matter compression caused by the tip [39], hard particles should be unlikely to be deformed.[3]

It is well known that the diameter/height ratio <4 for solid nanostructures [40]. Based on this information, we can conclude that all measured nanoparticles except PUD1.5/2:1 are soft. Examination of the particles dried from acetone dispersions revealed that the sample containing 1.5 NCO excess (PU1.5/2:1) had harder particles than the linear one (PU1.05/2:1) due to higher crosslinking density. An obvious decrease in the diameter/height ratio and therefore an increase in the nanoparticle hardness were observed after water addition. This observation can be explained by creation of the specific structure where soft segments form the core of the particles surrounded by shell composed of hard segments. This core-shell structure not only provides dispersity in water but also significantly increases the hardness of nanoparticles. Moreover, from the comparison of PU1.5/2:1 and PUD1.5/2:1, which have the same crosslinking density (see DMTA section), we can conclude that the hardness of the nanoparticles depends more on the core-shell structure than on the density of crosslinking.

4. Conclusions

Stable PUDs containing 1:1, 2:1 and 1:2 PCD:DMPA molar ratios were prepared without any chain extender via modified acetone method. The PU nanoparticles are starting form for PU coatings. It was found that using a 1.05-fold NCO excess compared to OH_{total} groups gives linear PUs, while a 1.5-fold NCO excess leads to water-crosslinked nanoparticles. Self-assembly of the PU nanoparticles was investigated in acetone before the water addition (step I) and after water dispersion (step II). It was concluded that linear PUs are well dissolved rod-like particles in acetone, and after water addition they create spherical core-shell structures due to phase inversion. In the cases of samples with a 1.5-fold NCO excess, the initial crosslinking occurs in step I, where PU particles are in the form of a microgel or a compact sphere. However, in step II, the simultaneous phase inversion and final water-crosslinking leads to formation of spherical particles with different mesh sizes and crosslinking densities. All prepared PUDs can be potentially used as mechanically strong coatings/films in biomedicine or as packaging materials.

[3] Comparison of the nanoparticle hardness/softness is possible while using the same measurement parameters and type of AFM tip.

Acknowledgments

This work was supported by the Grant Agency of the Czech Republic (Czech Science Foundation) [grant number 13-06700S]. The authors would like to thank Mrs. I. Vlasáková for DMTA measurements. Moreover, Magdalena Serkis would like to thank the Charles University, Faculty of Science for the opportunity to pursue her PhD study.

Appendix A. Supplementary data

Supplementary data associated with this article can be found, in the online version, at http://dx.doi.org/10.1016/j.porgcoat.2017.03.003.

References

[1] V. García-Pacios, V. Costa, M. Colera, J.M. Martín-Martínez, Affect of polydispersity on the properties of waterborne polyurethane dispersions based on polycarbonate polyol, Int. J. Adhes. Adhes. 30 (2010) 456–465.
[2] V. García-Pacios, Y. Iwata, M. Colera, J.M. Martín-Martínez, Influence of the solids content on the properties of waterborne polyurethane dispersions obtained with polycarbonate of hexanediol, Int. J. Adhes. Adhes. 31 (2011) 787–794.
[3] S.M. Cakić, M. Špírková, I.S. Ristić, J.K. B-Simendić, M. M-Cincović, R. Poręba, The waterborne polyurethane dispersions based on polycarbonate diol: effect of ionic groups content, Mater. Chem. Phys. 138 (2013) 277–285.
[4] H.-D. Hwang, H.-J. Kim, UV-curable low surface energy fluorinated polycarbonate-based polyurethane dispersion, J. Colloid Interface Sci. 362 (2011) 274–284.
[5] V. García-Pacios, M. Colera, Y. Iwata, J.M. Martín-Martínez, Incidence of the polyol nature in waterborne polyurethane dispersions on their performance as coatings on stainless steel, Prog. Org. Coat. 76 (2013) 1726–1729.
[6] S.M. Cakić, I.S. Ristić, M. Marinović-Cinović, M. Špírková, The effects of the structure and molecular weight of the macrodiol on the properties polyurethane anionic adhesives, Int. J. Adhes. Adhes. 41 (2013) 132–139.
[7] V. García-Pacios, J.A. Jofre-Reche, V. Costa, M. Colera, J.M. Martín-Martínez, Coatings prepared from waterborne polyurethane dispersions obtained with polycarbonates of 1,6-hexanediol of different molecular weights, Prog. Org. Coat. 76 (2013) 1484–1493.
[8] A. Santamaria-Echart, I. Fernandes, A. Saralegi, M.R.P.F.N. Costa, F. Barreiro, M.A. Corcuera, A. Eceiza, Synthesis of waterborne polyurethane-urea dispersions with chain extension step in homogeneous and heterogeneous media, J. Colloid Interface Sci. 476 (2016) 184–192.
[9] N. Liu, Y. Zhao, M. Kang, J. Wang, X. Wang, Y. Feng, N. Yin, Q. Li, The effects of the molecular weight and structure of polycarbonatediols on the properties of waterborne polyurethanes, Prog. Org. Coat. 82 (2015) 46–56.
[10] D.-K. Lee, H.-B. Tsai, R.-S. Tsai, Effect of composition on aqueous polyurethane dispersions derived from polycarbonatediols, J. Appl. Polym. Sci. 102 (2006) 4419–4424.
[11] D.-K. Lee, H.-B. Tsai, Z.-D. Yang, R.-S. Tsai, Polyurethane dispersions derived from polycarbonatediols by a solvent-free process, J. Appl. Polym. Sci. 126 (2012) E275–E282.
[12] M. Serkis, R. Poręba, J. Hodan, J. Kredatusová, M. Špírková, Preparation and characterization of thermoplastic water-borne polycarbonate-based polyurethane dispersions and cast films, J. Apll. Polym. Sci. 132 (2015) 42672.
[13] M. Serkis, M. Špírková, J. Kredatusová, J. Hodan, R. Bureš, Organic-inorganic nanocomposite films made from polyurethane dispersions and colloidal silica particles, Compos. Interfaces 23 (2016) 157–173.
[14] M. Serkis, M. Špírková, J. Hodan, J. Kredatusová, Nanocomposites made form thermoplastic waterborne polyurethane and colloidal silica: the influence of nanoslica type and amount on the functional properties, Prog. Org. Coat. 101 (2016) 342–349.
[15] H. Fang, H. Wang, J. Sun, H. Wei, Y. Ding, Tailoring elastomeric properties of waterborne polyurethane by incorporation of polymethyl methacrylate with nanostructural heterogeneity, RSC Adv. 6 (2016) 13589–13599.
[16] R.D. Irwin, NTP Summary Report on the Metabolism, Disposition, and Toxicity of 1,4-Butanediol, Technical Report for United States Department of Health and Human Services, 1996 (May).
[17] S.-Y. Oh, M.-S. Kang, J.C. Knowles, M.-S. Gong, Synthesis of bio-based thermoplastic polyurethane elastomers containing isosorbide and polycarbonate diol and their biocompatible properties, J. Biomater. Appl. 30 (2015) 327–337.

[18] H. Wang, Y. Shen, G. Fei, X. Li, Y. Liang, Micromorphology and phase behavior of cationic polyurethane segmented copolymer modified with hydroxysilane, J. Colloid Interface Sci. 324 (2008) 36–41.
[19] M. Aurilia, F. Piscitelli, L. Sorrentino, M. Lavorgna, S. Iannace, Detailed analysis of dynamic mechanical properties of TPU nanocomposite: the role of the interfaces, Eur. Polym. J. 47 (2011) 925–936.
[20] A. Santamaria-Echart, A. Arbelaiz, A. Saralegi, B. Fernández-d'Arlas, A. Eceiza, M.A. Corcuera, Relationship between reagents molar ratio and dispersion stability and film properties on waterborne polyurethanes, Colloid Surf. A Physicochem. Eng. Asp. 482 (2015) 554–561.
[21] F. Li, R. Tuinier, I. Van Casteren, R. Tennebroek, A. Overbeek, F.A.M. Leermakers, Self-organization of polyurethane pre-polymers as studied by self-consistent field theory, Macromol. Theor. Simul. 25 (2016) 16–27.
[22] A. Dong, G. Hou, D. Sun, Properties of amphoteric polyurethane waterborne dispersions II: macromolecular self-assembly behavior, J. Colloid Interface Sci. 266 (2003) 276–281.
[23] D.B. Otts, L.A. Cueva-Parra, R.B. Pandey, M.W. Urban, Film formation from aqueous polyurethane dispersions of reactive hydrophobic and hydrophilic components; spectroscopic studies and Monte Carlo simulations, Langmuir 21 (2005) 4034–4042.
[24] F.M.B. Coutinho, M.C. Delpech, Degradation profile of films cast from aqueous polyurethane dispersions, Polym. Degrad. Stab. 70 (2000) 49–57.
[25] S. Jia, J. Qu, C. Wu, W. Liu, R. Chen, S. Zhai, Z. Huang, F. Chen, Novel dynamic elongational flow procedure for reinforcing strong, tough, thermally stable polypropylene/thermoplastic polyurethane blends, Langmuir 29 (2013) 13509–13517.
[26] M. Špírková, R. Poręba, J. Pavličević, L. Kobera, J. Baldrian, M. Pekárek, Aliphatic polycarbonate-based elastomers and nanocomposites: I. The influence of hard-segment content and macrodiol-constitution on bottom-up self-assembly, J. Appl. Polym. Sci. 126 (2012) 1016–1030.
[27] A.K. Mishra, D.K. Chattopadhyay, B. Sreedhar, K.V.S.N. Raju, FT-IR and XPS studies of polyurethane-urea-imide coatings, Prog. Org. Coat. 55 (2006) 231–243.
[28] J.T. Garrett, R. Xu, J. Cho, J. Runt, Phase separation of diamine chain-extended poly(urethane) copolymers: FTIR spectroscopy and phase transitions, Polymer 44 (2003) 2711–2719.
[29] T. Mondal, K. Dan, J. Deb, S.S. Jana, S. Ghosh, Hydrogen-bonding-induced chain folding and vesicular assembly of an amphiphilic polyurethane, Langmuir 29 (2013) 6746–6753.
[30] K.-H. Nitta, M. Kuriyagawa, Thermoplastic polyurethanes, in: O. Olabisi, K. Adewale (Eds.), Handbook of Thermoplastics, second edition, CRC Press, Boca Ratan, 2016, pp. 387–396.
[31] E.A. Murillo, P.P. Vallejo, L. Sierra, B.L. López, Characterization of hyprbranched polyol polyesters based on 2,2-bis (methylol propionic acid) and pentaerythriol, J. Appl. Polym. Sci. 112 (2009) 200–207.
[32] K. Rodzeń, A. Strachota, F. Ribot, L. Matějka, J. Kovářová, M. Trchová, M. Šlouf, Reactivity of the tin homolog of POSS, butylstannoxane dodecamer, in oxygen-inducted crosslinking reactions with an organic polymer matrix: study of long-time behavior, Polym. Degrad. Stab. 118 (2015) 147–166.
[33] S.K. Dhayal, Mesoscale Srtucture and Techno-functional Properties of Enzymatically Cross-Linked α-Lactalbumin Nanoparticles Ph.D. Thesis, Wageningen University, 2015 (May).
[34] J. Hotz, W. Meier, Vesicle-templated polymer hollow spheres, Langmuir 14 (1998) 1031–1036.
[35] J. Ludvík, J. Urban, J. Jirkovský, P. Zuman, Evidence of N–N single bond as a hindrance of electron delocalization in cyclic and acyclic azines, in: D.G. Peters, H.J. Schäfer, M.S. Workentin, J. Yoshida (Eds.), Reactive Intermediates in Organic and Biological Electrochemistry, The Electrochemical Society, Pennington, 2001, pp. 132–134.
[36] B. Song, S. Yang, L. Jin, P.S. Bhadury, Environment-Friendly Antiviral Agents for Plants, Springer, New York, 2010, pp. 64–71.
[37] J.H. Saavedra, S.M. Acuña, P.G. Toledo, P.M. Claesson, AFM forces between mica and polystyrene surfaces in aqueous electrolyte solutions with and without gas bubbles, J. Colloid Interface Sci. 410 (2013) 188–194.
[38] P. Matějíček, M. Štěpánek, M. Uchman, K. Procházka, M. Špírková, Atomic force microscopy and light scattering study of onion-type micelles formed by polystyrene-block-poly(2-vinylpyridyne) and poly(2-vinylpyridyne)-block-poly(ethylene oxide) copolymers in aqueous solutions, Collect. Czech. Chem. Commun. 71 (2006) 723–738.
[39] Y. Ebenstein, E. Nahum, U. Banin, Tapping mode atomic force microscopy for nanoparticle sizing: tip-sample interaction effects, Nano Lett. 2 (2002) 945–950.
[40] M.B. Fritzen-Garcia, B.G. Zanetti-Ramos, C.S. de Oliveira, V. Soldi, A.A. Pasa, T.B. Creczynski-Pasa, Atomic force microscopy imaging of polyurethane nanoparticles onto different solid substrates, Mater. Sci. Eng. C 29 (2009) 405–409.
[41] M. Špírková, M. Kubín, K. Dušek, Side reactions in the formation of polyurethanes: model reactions between phenylisocyanate and 1-butanol, J. Macromol. Sci. Chem. A 24 (10) (1987) 1151–1166.

Supplementary results:

The LS data were fitted to the equation:

$$\left[\frac{Kc_p}{\Delta R_\theta(q,c_p)}\right]^{1/2} = \frac{1}{M_W{}^{1/2}}\left(1 + \frac{1}{6} R_g{}^2 q^2 + \cdots\right)^{1/2}\left(1 + M_W A_2 c_p\right) \qquad \text{(S1)}$$

where K is the contrast factor given by $K = 4\pi^2 n_D{}^2 (dn/dc_p)^2/(\lambda^4 N_A)$ (dn/dc_p is the refractive index increment of the polymer with respect to the solvent and λ is the wavelength of the incident light), $\Delta R_\theta(q, c_p)$ is the corrected Rayleigh ratio depending on the polymer concentration c_p and the magnitude of the scattering vector $q = (4\pi n_0/\lambda)\sin(\theta/2)$ (θ is the scattering angle and n_0 is the refractive index of the solvent), M_W is the weight-averaged molar mass, $R_g{}^2$ is the z-averaged squared radius of gyration, and A_2 is the "light-scattering-averaged" osmotic second virial coefficient of the polymer in solution.

Table S1. Composition of the PU/PUD samples.

Sample	HDI, wt%	PCD, wt%	DMPA, wt%
PU1.05/2:1	11.4	85.8	1.6
PU1.05/1:1	14.1	80.6	5.3
PU1.05/1:2	18.9	71.6	9.5
PU1.5/2:1	15.4	81.9	2.7
PU1.5/1:1	19.0	76.0	5.0
PU1.5/1:2	24.0	66.3	8.7

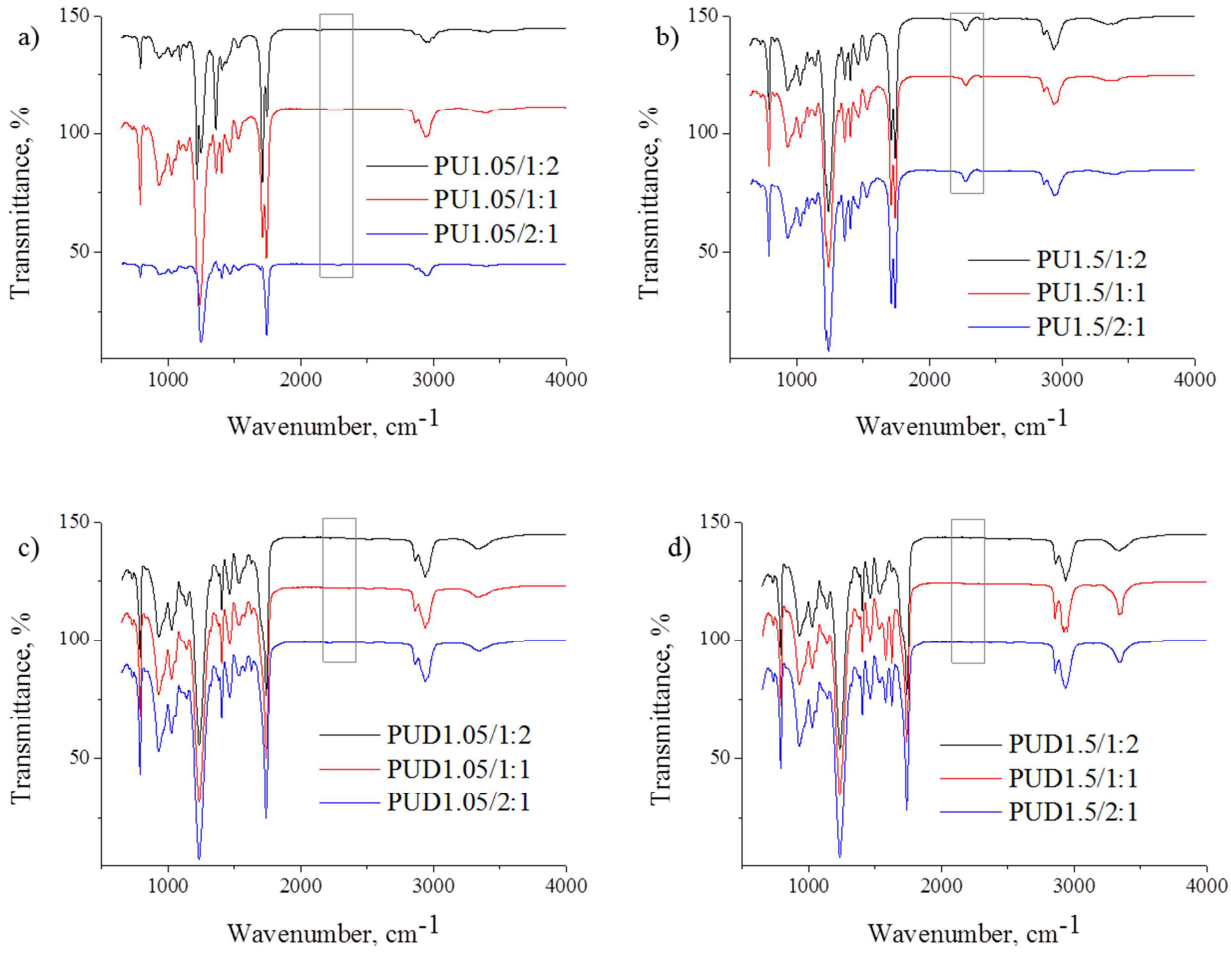

Figure S1. FTIR spectra of PU nanoparticles in acetone: a) PU1.05/x:y, b) PU1.5/x:y and dried PUDs: c) PUD1.05/x:y, d) PUD1.5/x:y. The marked region is attributed to the occurrence of isocyanate groups.

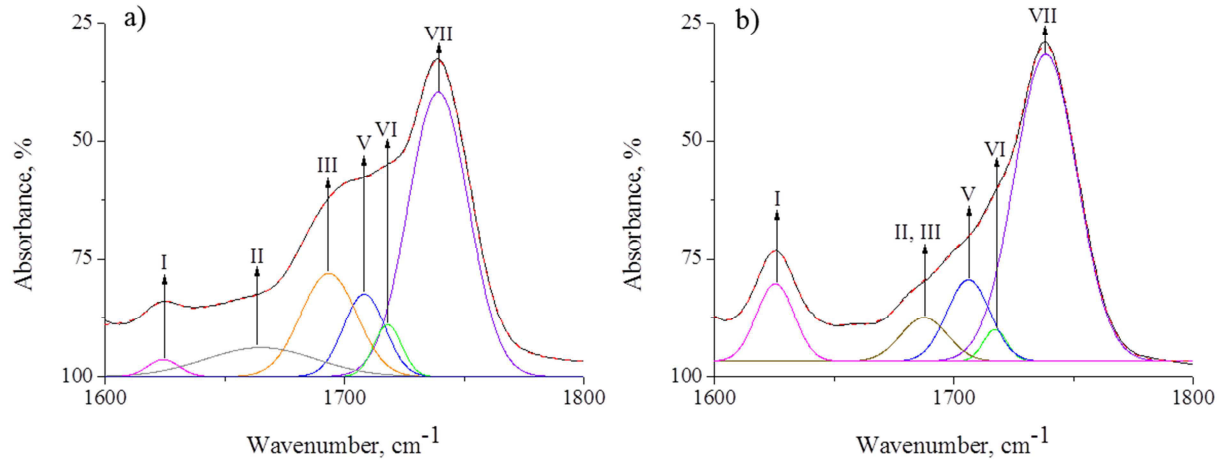

Figure S2. Deconvoluted carbonyl region of the FTIR spectra: a) PUD1.5/1:2, b) PUD1.5/2:1.

SALS measurements were performed to confirm the size and structure of the PU nanoparticles in acetone. Since this method is appropriate for the investigation of large length-scale structures, samples containing a 1.5 NCO excess were chosen for this purpose. To obtain information about the nanoparticle structures, model fitting of the experimental data was conducted. Due to the obtained rod-like shape of the dry particles deposited on mica after acetone evaporation during AFM analysis, we adopted a cylindrical shape model for the SALS analysis.

The representative scattering curve of PU1.5/1:1 (Fig. S3) confirmed that the intensity profile of this sample is consistent with a worm-like structure. A fit to a cylindrical model showed that the nanoparticles are thin rods.

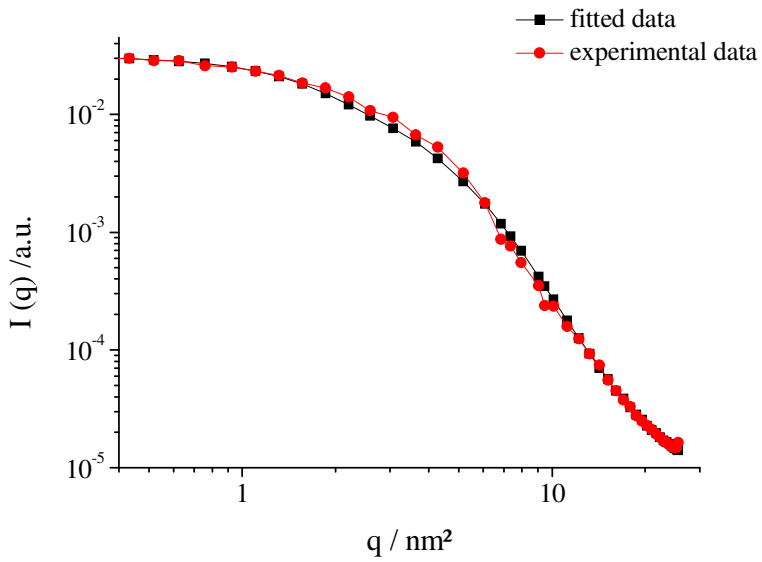

Figure S3. SALS scattering intensity data for PU1.5/1:1. The red line is a fit to a cylinder form factor.

Polymer Degradation and Stability 119 (2015) 23–34

Contents lists available at ScienceDirect

Polymer Degradation and Stability

journal homepage: www.elsevier.com/locate/polydegstab

Hydrolytic stability of polycarbonate-based polyurethane elastomers tested in physiologically simulated conditions

Magdalena Serkis, Milena Špírková*, Rafał Poręba, Jiří Hodan, Jana Kredatusová, Dana Kubies

Institute of Macromolecular Chemistry AS CR, v.v.i., Heyrovskeho nam. 2, 162 06 Prague 6, Czech Republic

ARTICLE INFO

Article history:
Received 26 February 2015
Received in revised form
21 April 2015
Accepted 28 April 2015
Available online 8 May 2015

Keywords:
Polyurethane
Elastomer
Hydrolytic stability
Surface analysis
Mechanical properties
Thermal properties

ABSTRACT

The hydrolytic stability of all-aliphatic polyurethane (PU) films made from polycarbonate-based aliphatic macrodiols (MD), diisocyanate-1,6-hexane and butane-1,4-diol (BD) were tested at 37 °C in phosphate buffer for a period up to 12 months. Two macrodiols, differing in composition and chain regularity and two MD-to-BD ratios were chosen for PU synthesis. The isocyanate-to-total hydroxyl ratio was kept constant and equal to 1.05. The functional properties of the original polyurethane films and films being immersed for 1, 3, 6 and 12 months in model physiological environment (37 °C at pH = 7.4) were studied on segmental up to macroscopic levels. The combination of SEM, AFM, FTIR, DSC, tensile and swelling analyses were used. It was found that prepared PU films are very good elastomeric materials with outstanding mechanical and suitable thermal properties keeping these properties practically unchanged for a period of up to 12 months. They can be practically used for example as strong and durable topcoats.

1. Introduction

Novel thermoplastic polyurethanes (TPUs) and their nanocomposites belong to a family of thermoplastic elastomers (TPEs) which have been synthesized and studied for a longer time with the goal of their practical applications, such as tissue engineering, implants, scaffolds, drug delivery [1–8], electronics [9–11] or as coatings and packaging materials [12–17]. The TPU popularity arises from the relatively easy targeting of desired end-use properties by optimizing the polymer composition and preparation procedure. PUEs are distinguished by their long-term dynamic performance, low dynamic stiffening, high wear, low abrasion, fat and oil resistance and suitable noise- and vibration-damping properties [18]. TPUs combine the mechanical properties of conventional thermoplastics (elasticity and flexibility) with the characteristics of chemically cross-linked elastomers (high strength and modulus). The relative simplicity and versatility of TPU manufacturing (e.g. casting, spraying, injection, extruding), the possibility of using bio-based or renewable resources [19–23] together with the possibility of their recycling or reuse, as contrary to chemically cross-linked thermosets, further increase their popularity and practical impact.

Polyurethanes have been used in medical applications for several decades. The first PUs were long-term biomaterials utilized for vascular implants and grafts, catheters and biomedical devices [1,24–27] although high demands for new materials require the more suitable biodegradable or bioresorbable products, i.e. the materials with short or limited live-time [7,28]. The use of novel materials for this purpose requires not only detailed description of mechanical, surface, thermal and other end-use properties but also information on their stability/degradability. The functional properties of PU elastomers depend on a number of factors, such as chemical nature of starting components (macrodiol, diisocyanate, chain extender), overall reaction conditions during PU preparation, the contents and lengths of the soft and hard segments, the degree of the phase separation/mixing, the strength of hydrogen bonds and dipole–dipole interactions, the mobility and orientation (packing) of building units within the hard segments, temperature profile, etc. Furthermore, if the material is designed to be subject to aggressive environment and its stability/degradation resistance has to be tested, various additional factors, such as temperature, time and conditions of the exposure have to be taken into account.

* Corresponding author.
E-mail address: spirkova@imc.cas.cz (M. Špírková).

http://dx.doi.org/10.1016/j.polymdegradstab.2015.04.030
0141-3910/

Because the causes of degradation processes differ depending on the intended application, it is impossible to propose general conditions or protocol for PU degradation/stability tests.

The degradation process must be meticulously studied especially in the case of potential medical, biomedical or food applications. Different reaction conditions for stability/degradation tests have been carefully specified and testing conditions have been thoroughly chosen with regard to the intended use. Short tests of thermal stability are the most common analyses of PU stabilities [19–22,29–33]. However, the material-stability tests must also be conducted in substantially different environments. Information on long-term mechanisms such as hydrolytic stability (testing the samples immersed either in chemical or oxidative environment [13,23,24,34–38] or in water or saline buffer [23,39,40]), flame- [29], bio- [2,37,41] or irradiation stabilities [42,43] are indispensable before the new material can be used in practice. Simultaneously, stability tests have to be conducted at several different temperatures (e.g. at 37 °C [2,32,36–40], 50 °C [34], 55 °C [39], 60 °C [13], 70 °C [35,39,44], 80 °C [23] and 85 °C [39] and for different time periods, measured in days or weeks [23,34,36,38], months [2,24,37,44] or years [40].

All-aliphatic polyurethanes based on polycarbonate macrodiols belong to a relatively novel class of PU elastomeric systems. Polycarbonate-based PUs were initially prepared from aromatic isocyanates [31,35,37,45]. The aliphatic [36,14–17,30] and cycloaliphatic isocyanates [43,44] were increasingly used later, especially for coatings and biomedical PU applications. The advantage of all-aliphatic polycarbonate-based PUEs is their higher stability to oxygen as compared to aromatic-based PUs. The other benefit is the fact that aliphatic compounds formed during the degradation process are less toxic than those from aromatic-based PUs [7,45]. While the first advantage is important for general coating applications, the second is significant in medical or biomedical PU applications. Even though the good hydrolytic stability of polycarbonate-based macrodiols is relatively well known, e.g., from the producer leaflets, systematic detailed studies devoted to the preparation and testing the stability of all-aliphatic polycarbonate-based PUs (which would disseminate the pieces of information for a broad community of polymer scientists) are relatively scarce [36].

A series of aliphatic PUs prepared from polycarbonate-based macrodiols (MD), hexamethylene-1,6-diisocyanate and butane-1,4-diol (BD) with relatively broad hard-to-soft segment ratio [14,15,46] was characterized by a set of analytical methods. Best utility properties were found for PU systems having $[OH]_{MD}/[OH]_{BD}$ ratio equal to 1 or 2. Conditions of preparation and multi-scale characteristics of the complex four-component PU films (containing also a degradable D,L-lactide-based linker in the PU backbone) were recently published [16,17]. Though the end-use properties of three- and four-component PUs were studied in detail on segmental to macroscopic levels, no degradation tests under physiologically simulated conditions were performed on these systems. This paper is the continuation and extension of the three-component polycarbonate-based PU study [14,15,30] and it describes a part of our purely academic long-term research. The ultimate goal is the preparation of controllably degradable materials which can find potential use in biomedical applications. All aliphatic PUs were used because the products of their hydrolysis are relatively low toxic compounds. The first step of the long-term research is the topic of this manuscript and it consists in the study of suitable materials (without biodegradable units) with appropriate properties that are stable enough and can be destabilized by incorporation of units with hydrolytically cleavable bonds. The system can also be used as a reference material for determination of the efficiency of the D,L-lactide based linker on the hydrolytic degradation process of more complex four-component PUs or the influence of controlled elongation on the hydroltytic stability of three- and four-component PUs.[1]

2. Experimental

2.1. Materials

Two commercially available polycarbonate-based macrodiols, T4672 (marked as "T4", number-average molar mass M_n = 2770 g mol^{-1}, dispersity $Đ_M$ = 3.20) and T5652 (marked as "T5",number-average molar mass M_n = 2874 g mol^{-1}, dispersity $Đ_M$ = 3.23), kindly provided by Asahi Casei Co., Japan; butane-1,4-diol (BD), dubutyltin dilaurate (DBTDL) and 1,6-diisocyanatohexane (HDI, all Fluka) were used. The idealized schematic representation of structures of polycarbonate-based diols T4 and T5 is shown in Fig. 1.

T4672 polycarbonate-based macrodiol is characterized by higher regularity and higher rigidity (only **even** methylene $-CH_2-$ units), T5652 higher irregularity and higher flexibility (**even** and **odd** methylene $-CH_2-$ units at **equal** molar ratio) [15]. However, both macrodiols contain on average 23 carbonate groups per one macrodiol chain.

2.1.1. Preparation procedure

Prior to the reaction, all components were thoroughly mixed in a dried acetone in order to obtain the homogenous solutions. After the solvent evaporation at the room temperature, the reaction mixtures were poured into the Teflon molds and placed in an oven under the nitrogen atmosphere. The changes in composition were achieved by varying the molar ratios of hydroxyl group components, i.e., of polycarbonate macrodiol (either T4672, marked as "T4" or T5652, marked as "T5") and the chain extender. All the reactions proceeded in bulk at 90 °C for 24 h in the presence of organotin catalyst DBTDL (50 ppm mol^{-1} of urethane groups) at constant r ratio (r = $[NCO]/[OH]_{total}$ = 1.05; where $[OH]_{total} = [OH]_{MD} + [OH]_{BD}$), while $R = [OH]_{MD}/[OH]_{BD}$ was either 1 or 2. Individual sample codes and composition are summarized in Table 1, 1st and 2nd columns. The hard segment content (HSC, Table 1, 3rd column) was calculated as the weight percentage of BD and HDI components with respect to the total mass of all reagents used for the particular sample preparation. The final thickness of films was 250 ± 25 μm.

For example, the code T5-2/6 means PU sample prepared from macrodiol T5652 at $(OH)_{T5652}/(OH)_{BD}$ ratio equal to 2, immersed to PBS buffer at 37 °C for 6 months.

The properties of prepared PU films were measured by a combination of several analytical methods ("raw" samples). Major parts of films were cut into diverse shaped pieces and placed into glass degradation flask. The degradation process proceeded in phosphate-buffered saline solution (PBS)[2] with additional 0.02 wt% of sodium azide NaN_3, at 37 °C for 1, 3, 6 and 12 months, respectively. While the buffer environment and temperature were the same, the specimen shape differed according to the method of analysis: (a) dumbbell-shaped samples for tensile properties were cut from the PU film and fixed to the PE frames, prepared for this purpose in IMC or (b) pieces of PU films were fixed on the inert thread. Both kinds of immersion enabled uniform and free access of

[1] Degradation studied of four-component PU systems and three- and four-component PUs hydrolyzed under given strain will be published in the forthcoming papers.

[2] PBS – Phosphate-Buffered Saline contain monobasic potassium phosphate, sodium chloride, and dibasic sodium phosphate.

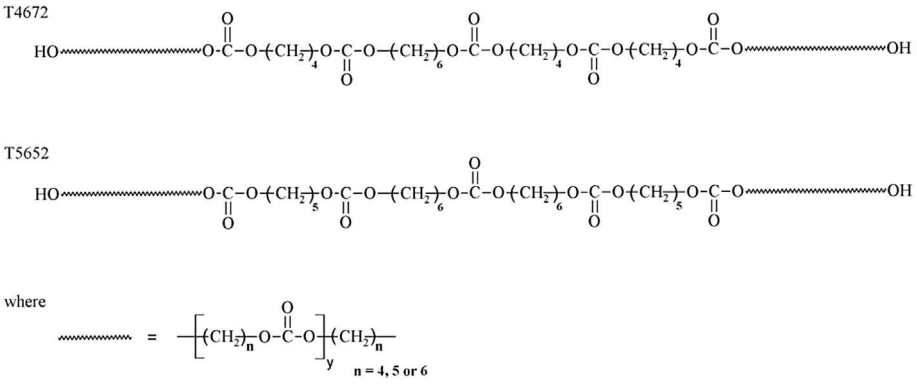

Fig. 1. Schematic representation of macrodiol chains of T4672 (T4, top) and T5652 T5, bottom).

PBS solution to the surface of the specimen being further measured. After the appropriate time (1, 3, 6 and 12 months), PU samples were pulled out from the buffer, washed, quickly dried and immediately measured by the set of experimental methods.

2.2. Methods of characterization

2.2.1. Scanning electron microscopy (SEM)

Surface microstructure of PU films was measured by Scanning Electron Microscope (SEM) on the instrument Vega Plus TS 5135 (Tescan, Czech Republic). Before SEM analysis, upper sides of the PU films (or their cross sections; after previous freeze-fracture at the temperature of liquid nitrogen) were sputtered with 4 nm Pt layer using vacuum sputter coater SCD 050 (Balzers, Czech Republic).

2.2.2. Atomic force microscopy (AFM)

The investigation of the topography and heterogeneity relief from the nano-to micrometer levels was done by AFM. PU films were measured either on the upper film side, “top images” or after previous freeze-fracture at the temperature of liquid nitrogen “cross-section images”. Atomic force microscope (Dimension Icon, Bruker), equipped with the SSS-NCL probe, Super Sharp SiliconTM - SPM-Sensor (NanoSensors™ Switzerland; spring constant 35 N m^{-1}, resonant frequency ≈ 170 kHz) was used for the analysis. Measurements were performed under ambient conditions using the tapping mode AFM technique. AFM scans covered the areas from 500 × 500 nm^2 to 50 × 50 μm^2.

2.2.3. Differential scanning calorimetry (DSC)

Differential scanning calorimetry (DSC) analyses were carried out on a Perkin Elmer DSC 8500 calorimeter with nitrogen purge gas (20 cm^3 min^{-1}). The instrument was calibrated for temperature and heat flow using indium as a standard. Samples of about 10 mg were encapsulated into hermetic aluminum pans. The analyses were performed in cycle heating – cooling – heating from −80 °C to 200 °C at 10 C min^{-1}. Two-minute isothermal plateaux were inserted before and between the ramps.

All presented results were recorded on the first heating cycle which assesses the material's properties in the as-prepared condition. Glass transition temperature (T_g) was defined as a midpoint between the glassy and rubbery branches of the DSC trace. Melting temperature of soft segments ($(T_m)_s$) and hard segments ($(T_m)_h$) and temperature of relaxation (T_r) as maxima of the endotherm peaks were evaluated. For all endotherm peaks corresponding transitions enthalpies (ΔH_x, i.e. ΔH_r, ($\Delta H_{m)s}$, ($\Delta H_{m1)h}$ and ($\Delta H_{m2)h}$) in jouls per gram were also evaluated The difference between the T_g of pure macrodiol and PU film (ΔT_g) was used for the estimation of the degree of the hard/soft phase separation in PU systems.

Table 1
Code, composition and hard-segment content of PU films.

Code[a]	Molar ratio $(OH)_{MD}$: $(OH)_{BD}$		HSC[b] (wt%)
T4-1/X	1	1	18.5
T4-2/X	2	1	14.1
T5-1/X	1	1	18.1
T5-2/X	2	1	13.5

X = 0, 1, 3, 6 or 12 (time in months of the sample immersion in PBS at 37 °C).
[a] T4: macrodiol T4672; T5: macrodiol T5652.
[b] HSC = $(m_{BD} + m_{HDI})/(m_{MD} + m_{BD} + m_{HDI})$.

2.2.4. Tensile characterization

Static mechanical properties were measured on an Instron model 6025/5800R (Instron Limited, UK) equipped with a 100 N load cell, according to test method ISO 527 at room temperature with a cross-head speed of 10 mm min^{-1}. Dumbbell shaped specimens corresponded to the ISO 527-2/5B type: total specimen length 35 mm, length and width of the narrowed part: 12 and 2 mm, thickness 0.25 mm. Selected tensile characteristics were determined: Young's modulus E (modulus of elasticity, given in MPa), tensile strength σ_b (maximum stress before braking the material, given in MPa), elongation-at-break ε_b (percentage increase in length before the sample break) and toughness (energy to break the sample per volume unit, given in mJ mm^{-3}). Reported values were the averages of at least five measurements. Presented tensile curves were taken from the measurements closest to each calculated average value.

2.2.5. Swelling experiments and mass loss determination

Each swelling and mass loss experiment consisted of 5 different measurements of 30–50 mg pieces of the given PU film. The percentage of swelling was determined as the mass increase after the swelling experiment and percentage mass loss is given as the mass decrease of the fully dried sample after swelling experiment, both compared to the sample mass before experiment. Resulting swelling and mass loss values are the mean values of five experiments made on different pieces of given PU film.

2.2.6. FTIR spectroscopy

The FT-IR spectra were recorded on a Perkin–Elmer Paragon 1000 PC FT-IR spectrometer using the reflective ATR (Attenuated total reflection) technique Specac MKII Golden Gate Single Reflection ATR System with a diamond crystal with the angle of incidence 45°. The samples were directly put on the diamond crystal and measured. All spectra were measured at wavenumber range

4400–450 cm^{-1} with resolution 4 cm^{-1} and with 16 scans. Software Spectrum v2.00 was used for processing the spectra.

3. Results and discussion

The composition of the films prepared and further analyzed in the stability tests is based on the knowledge of previously tested PU elastomers made from MD, HDI and BD. They were characterized mainly on thicker sheets (thickness 2 mm) or films (thickness 500 μm) [14,15,46]. The detailed multidisciplinary analysis of functional properties of all films was performed. The set of analytical methods covers the scales spanning from segmental levels (NMR and FTIR spectroscopy), through nanometer-to-micrometer-scale characteristics (SAXS, WAXD, AFM, TEM, SEM) up to macroscopic-scale characteristics (DMTA, DSC, TGA, tensile and gas transport property measurements). Very good end-use (especially mechanical) properties were achieved if $[OH]_{MD}/[OH]_{BD}$ was 1 or 2 [15]. No long-term degradation/stability tests on these systems were realized so far, however. The hydrolytic stabilities in the model physiological environment were preliminary tested by most of abovementioned multiscale characteristic. In the stability/degradation tests, the fixed thickness (250 ± 25 μm) was set. After the evaluation of all results, the set of surface, mechanical, swelling and thermal analyses in the period up to 12 months was chosen as the representative output.

The hydrolytic stability of PU systems has been studied from several aspects. In this paper, we concentrated mainly on the changes of functional properties with time. As the stability tests were realized at 37 °C, which corresponds to the human body temperature (i.e., at the temperature higher by ca 15 °C than is the storage temperature), the samples are in fact exposed not only to the PBS environment, but also to the long-time thermal conditioning. This fact will be discussed in relevant chapters, mainly in Chapter SEM and DSC.

3.1. Surface morphology

Surface characteristics are very important pieces of information on material properties, especially for coating and film applications. So that, all PU samples were studied by SEM and AFM analyses into details. While SEM detected surface morphology on micrometer-to-millimeter scales, AFM evaluated nanometer-to micrometer surface features, heterogeneity and roughness mapping included.

3.1.1. Scanning electron microscopy – SEM

Surface morphology changes for raw PU samples and PU samples subjected to hydrolytic testing were analyzed by SEM first. Surface morphology differences are visible at all magnifications (from 200 to 7000), but are more pronounced at higher magnifications. In this paper, the magnification 1500 was chosen for visualization of the surface relief and surface changes (if any) in detail.

Microscopy analysis of PU films revealed that PUs before the immersion to PBS (raw PUs) mutually differ, as visible in Fig. 2, left. The T4-based PUs have more regular surface compared to T5-based analogs. Films prepared at ratio $R = 1$ (T4-1/0 and T5-1/0) contain numerous surface heterogeneities: needle-like formations on T5-1/0 and scaly formations on T4-1/0. The PUs prepared at ratio $R = 2$ (T4-2/0 and T5-2/0) are distinguish by spherical formations of diameter ca 10 μm, being more pronounced on T5-1/0. Detailed analysis of sample surface T4-1/0 will be given in the part AFM.

SEM analysis of PU films after 12 month-stability tests revealed that the surface reliefs undergo some changes on the surface, but no substantial destruction of the surface was found. The softer sample T5-2/12 further features irregular surface cracking,

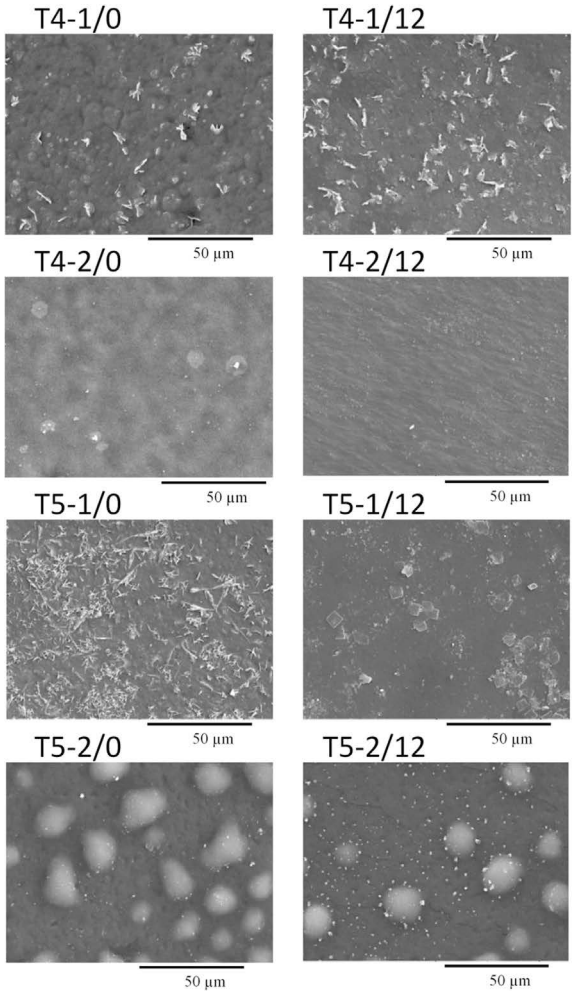

Fig. 2. Surface reliefs of PU samples T4-1/0, T4-2/0, T5-1/0 and T5-2/0 before (left) and after 12 month-stability tests (T4-1/12, T4-2/12, T5-1/12 and T5-2/12; right). Magnification 1500×.

however. Needle-like structures of T5-1/0 were re-organized into cubic formations on the sample T5-1/12. Spherical formations are more regular and 'scaly' formations are more frequent on T5-1/12 compared to T5-1/0. Sample T4-1/X was chosen as the representative sample of detailed surface analysis by SEM (followed by AFM analysis for the comparison and completion of SEM results).

Detailed SEM analysis of T4-1/X: After the immersion to PBS, film surface relief becomes more heterogeneous and rougher, especially after 1 month of the immersion (Fig. 3, left). This effect is probably caused by the long-time conditioning at 37 °C leading to the re-organization and re-packing of flexible linear chains forming PU film (this effect will be discussed in the part DSC). No substantial changes on cross sections are visible; just the fracture area is smoother in T4-1/1 and especially T4-1/6 compared to T4-1/0. No visible destructions of the film surface, the area close to the surface and the inside were found, which gives evidence about very good hydrolytic stability and reliability of materials prepared.

3.1.2. Atomic force microscopy

Atomic force microscopy was used for the visualization of surface morphology and mainly heterogeneity changes on the nano-to-micrometer scale. AFM analyzes were realized either on upper PU film side ("top") or on the surface of freeze-fractured samples ("cross-section"). As the height images did not show substantial and significant topography differences on the nano- and

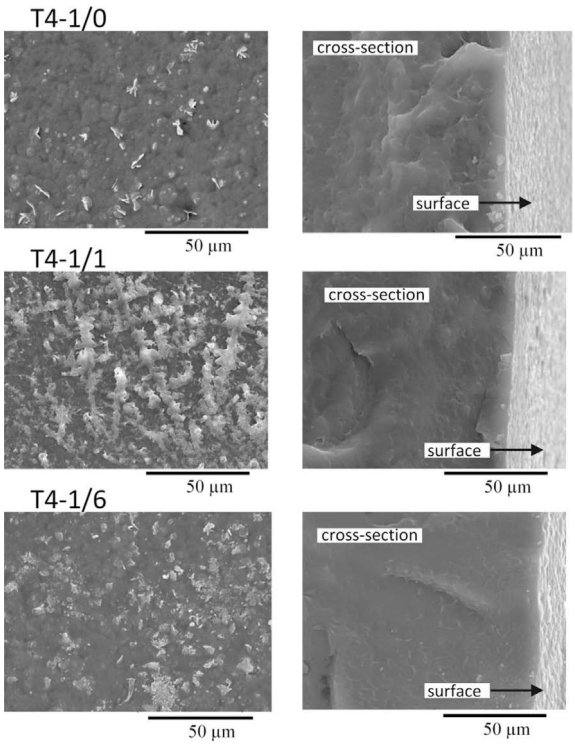

Fig. 3. The comparison of the surface (left) and cross section-surface (right) reliefs of T4-1/0 (top), T4-1/1 (middle) and T4-1/6 (bottom). Magnification 1500×.

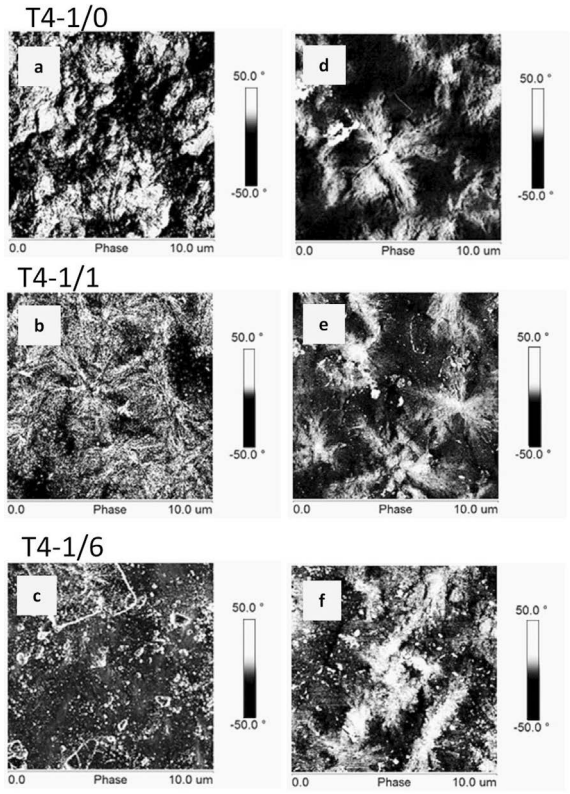

Fig. 5. Phase images of sample T4/1-0 (a, d, top), T4-1/1 (b,e, middle) and T4-1/6 (c,f, bottom). Surface images (a–c, left) and cross-section images (d–e, right).

micrometer levels, we put the main attention on phase images, illustrating changes in tip–sample interactions, and thence in material heterogeneity.

Selected AFM images are given in Figs. 4–6. Fig. 4 shows the topography and heterogeneity relief on area 50 × 50 um^2 comparable with areas detectable by SEM at higher magnificence. Comparing Fig. 3 (top, left) with Fig. 4 (left), no substantial topography differences of PU film analyzed by SEM and AFM were detected.

Fig. 5 summarizes phase images of top and cross sections of T4-1/0, T4-1/1 and T4-1/6, i.e. of the same samples shown in Fig. 3 (SEM analysis). Area 10 × 10 um^2 enables to visualize nm-to μm-size heterogeneity reliefs.

Similar to SEM results, (Fig. 3), AFM images of top and cross-sections of individual films differ for given sample (T4-1/X). All (top and cross section) surfaces feature the heterogeneous character on the nano-to-micrometer scales. The heterogeneous character of PU films can be explained by the segmental character of each PU chain, being formed by soft segments (macrodiol) and hard segments (HDI + BD product). So that, softer (soft-segment rich) and more rigid (hard-segment rich) localities can be found not only inside but also on the PU surface. Cross-section images of samples T4-1/0, T4-1/1 and T4-1/6 detected μm-size spherulite structures indicating the high level of self-organization of the hard segments into regular supramolecular structures. However, spherulite formations in T4-1/6 sample are already not so regular compared to T4-1/0 and T4-1/1. Top images of selected PU films differ, depending on time of immersion. Heterogeneities of top samples T4-1/0 and T4/1-6 are more or less randomly distributed on the surface without any significant ordering. On the other hand, highly assembled spherulite structures were found on the surface of T4-1/1. Bigger ordered structures (size 10°–10^2 μm) were on this sample also detected by SEM (Fig. 3, left, middle).

AFM was also used to detect the origin of the spherical formations found on the top of T5-2/0 sample. The height and phase images of the sample are given in Fig. 6. It is evident, that these spherical structures are of the same constitution as the surrounding, unlike nano-to-micrometer “scaly” formation. They are different (harder) than the rest of the PU material. Two regions

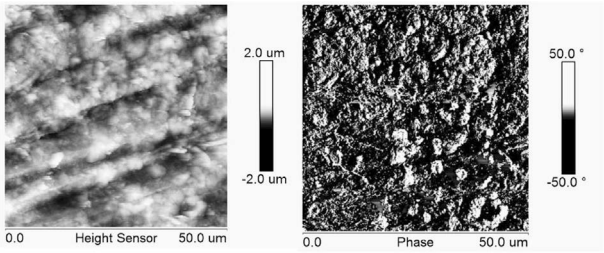

Fig. 4. Height (left) and phase (right) images of the T4-1/0 surface.

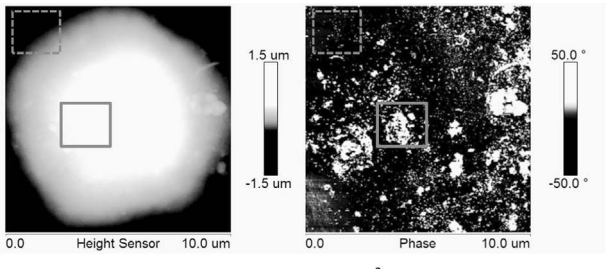

Fig. 6. Height (left) and phase (right) 10 × 10 μm^2 images of the spherical formation of sample T5-2/0. (Homogeneous area of different morphology and heterogeneous area of identical height are highlighted by broken and full rectangles, respectively).

confirming this statement are highlighted in Fig. 6: homogeneous material of different height (broken rectangle) and heterogeneous material of identical height (full rectangle).

The spherical formations on the sample T5-2/X and relatively rough and heterogeneous surface character of all raw films are probably the consequence of the removal of the last traces of the solvent from the film surface before finalizing PU formation. If analyzed roughness of scans 50 × 50 um^2, all R_a values are 10^2 nm order and R_{max} are of 10° μm order in the maximum. It means: though the surface relief is different and dependent on the sample composition and on time of immersion, all surfaces of PU films can be considered as regular and relatively smooth on the macroscopic level.

As the changes in surface morphologies are assigned to the re-organization and re-packing of polyurethane changes, this phenomena will be further discussed with thermal and mechanical properties in the subsequent chapters.

3.1.3. *Differential scanning calorimetry – DSC*

DSC was used to follow and characterize thermal transitions occurring during progressive heating of raw PU as well as PUs subjected to the hydrolytic degradation process. Recorded DSC curves are complex and contain multiple endothermic events in the region between 45 and 180 °C, in addition to glass transition of the amorphous parts of the material found at around −35 °C. Due to the presence of multiple peaks, all DSC curves presented in this chapter were divided into three temperature regions marked I, II and III as seen in Fig. 7, left top.

The low temperature region I shows transitions associated with glass transition of the amorphous part of the soft segments. Determined T_g values were found to be somehow lower for T5-based series (- 39 to - 41 °C) as compared to T4-based one (−34 to −36 °C). Lower T_g in the T5 series can be explained by higher irregularity and flexibility of the polycarbonate chains in T5 macrodiol [15].

From the difference between the T_g of pure macrodiol and each one of the prepared PU films (ΔT_g), the degree of phase separation of soft and hard segments was assessed. As the ΔT_g was found to be virtually constant (12–13 °C for all raw samples) the separation degree can be said to be independent on both the composition (R value) and the type/regularity of the macrodiol used. Moreover, the ΔT_g values remain substantially unchanged even during the degradation tests (ΔT_g values for the treated films differed by max ± 2 °C; with very slight tendency to higher values indicating increasing phase mixing with longer time of immersion); see Table 2. The relevant DSC curves of all samples including the raw and the treated PU films are given in Fig. 7 and relevant DCS data can be found in Table 2.

The second endothermic region (II) shows temperatures between 45 and 100 °C and reflects thermal behavior of PU soft segments, while the third region (III), covering temperatures over 120 °C, is connected to thermal transitions of the hard segments. The relaxation enthalpy values in region II increases with increasing soft-segment content in the given macrodiol, i.e. with higher R value it applies that $(\Delta H_r)_{T4\text{-}2/0} > (\Delta H_r)_{T4\text{-}1/0}$ and $(\Delta H_r)_{T5\text{-}2/0} > (\Delta H_r)_{T5\text{-}1/0}$. On the other hand, melting enthalpies in region III were found to decrease with increasing R value; $(\Delta H_{m1})_{T4\text{-}2/0} < (\Delta H_{m1})_{T4\text{-}1/0}$ and $(\Delta H_{m1})_{T5\text{-}2/0} < (\Delta H_{m1})_{T5\text{-}1/0}$.

In the endothermic region II all raw PUs show a single peak between 52 and 60 °C, marked in Fig. 7 by dashed line. However, for the immersed samples this peak splits in two: minor peak at about 50 °C and major peak at around 70 °C. In order to find the origin of this peak splitting and to exclude the influence of PBS solution, two samples (T4-1/0 and T5-1/0) were annealed at 37 °C in inert gas

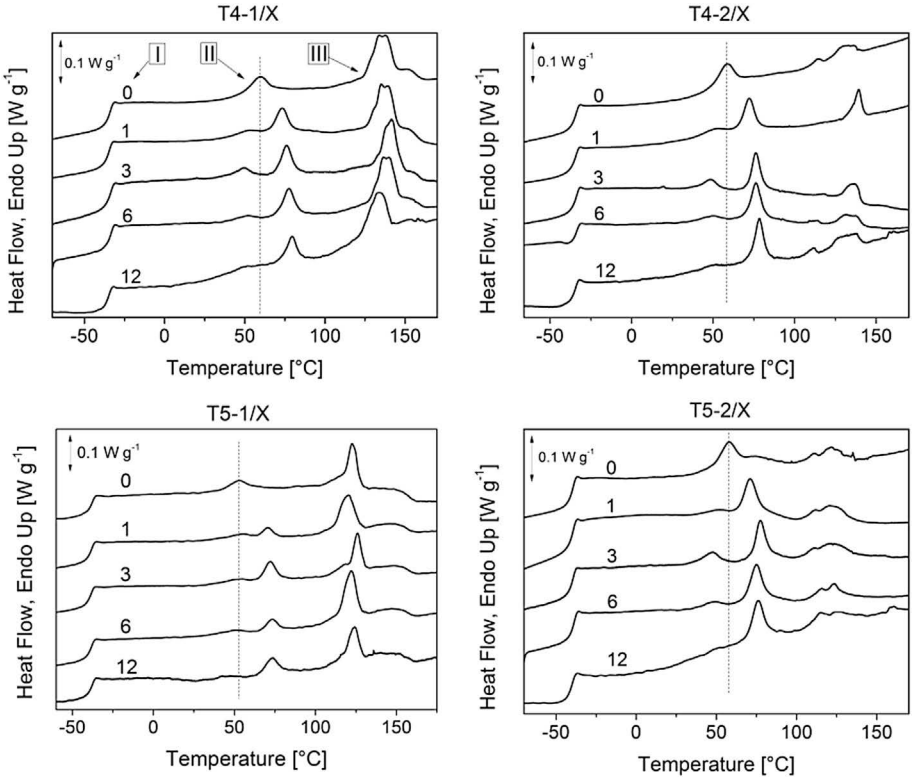

Fig. 7. The DSC curves of PU series T4-1/X (top left), T4-2/X (top right), T5-1/X (bottom left) and T5-2/X (bottom right). Months of PBS immersion X (=0, 1, 3, 6 and 12) mark individual DSC curves. Temperature regions I, II and III are given in sample T4-1/X. (Temperatures of peak position of all raw PUs in the endothermic region I are drawn by broken lines).

Table 2
Thermal properties of raw and treated PU films: T4-1/X (a), T4-2/X (b), T5-1/X (c), T5-2/X (d).

(a) T4-1/X

Sample	T_g (°C)	T_r (°C)	ΔH_r (J g^{-1})	$(T_m)_s$ (°C)	$(\Delta H_m)_s$ (J g^{-1})	$(T_{m1})_h$ (°C)	$(\Delta H_{m1})_h$ (J g^{-1})	$(T_{m2})_h$ (°C)	$(\Delta H_{m2})_h$ (J g^{-1})
T4-1/0	−35	60	4	–	–	134	7	153	0.2
T4-1/1	−35	*	*	73	* 5	135	8	153	0.3
T4-1/3	−34	49	1	76	3	142	8	156	0.2
T4-1/6	−34	52	1	78	3	135	7	154	0.2
T4-1/12	−34	*	*	80	* 3	133	7	158	0.3

(b) T4-2/X

Sample	T_g (°C)	T_r (°C)	ΔH_r (J g^{-1})	$(T_m)_s$ (°C)	$(\Delta H_m)_s$ (J g^{-1})	$(T_{m1})_h$ (°C)	$(\Delta H_{m1})_h$ (J g^{-1})
T4-2/0	−35	58	4	–	–	130	3
T4-2/1	−35	*	*	72	* 7	139	2
T4-2/3	−35	48	2	76	4	137	3
T4-2/6	−34	49	1	76	5	132	3
T4-2/12	−36	*	*	776	* 5	130	3

(c) T5-1/X

Sample	T_g (°C)	T_r (°C)	ΔH_r (J g^{-1})	$(T_m)_s$ (°C)	$(\Delta H_m)_s$ (J g^{-1})	$(T_{m1})_h$ (°C)	$(\Delta H_{m1})_h$ (J g^{-1})	$(T_{m2})_h$ (°C)	$(\Delta H_{m2})_h$ (J g^{-1})
T5-1/0	−39	53	3	–	–	123	7	149	2
T5-1/1	−39	*	*	72	* 3	120	7	149	2
T5-1/3	−39	50	*	72	* 4	126	5	150	2
T5-1/6	−39	50	1	73	2	122	7	147	2
T5-1/12	−39	*	*	73	* 3	125	5	140	2

(d) T5-2/X

Sample	T_g (°C)	T_r (°C)	ΔH_r (J g^{-1})	$(T_m)_s$ (°C)	$(\Delta H_m)_s$ (J g^{-1})	$(T_{m1})_h$ (°C)	$(\Delta H_{m1})_h$ (J g^{-1})
T5-2/0	−40	58	7	–	–	122	3
T5-2/1	−40	*	*	71	* 8	121	4
T5-2/3	−40	48	2	77	5	121	4
T5-2/6	−40	48	1	75	5	124	3
T5-2/12	−41	*	*	76	*5	123	3

*: Peak positions or (ΔH_x) values could not be separated quantitatively.

(N_2) for one month. Subsequently, DSC curves were recorded and compared to results of the original samples T4-1/0 and T5-1/0 (Fig. 8).

As can be seen from Fig. 8 a slight shift of the peak maxima of endotherm II toward higher temperatures (about 10 °C) is detected for both systems. Moreover, small peaks at temperature around 50 °C can also be found (marked in each figure by an arrow). It is assumed that this splitting of the original peak is the result of temperature-induced reorganization of the soft-segment domains into more organized and stable crystalline forms of ordered polycarbonate sequences. The increase of the relevant ΔH values in this region $(\Delta H_m)_s$ as compared to the values of the raw samples (ΔH_r) indicates a co-crystallization of the amorphous part of the soft segment occurring on annealing at 37 °C (Table 2). Similarly, PU samples containing higher soft-segment fraction i.e. T4/2-X and T5/2-X also showed distinct changes in the DSC curves in this region (see Fig 7 right.).

From Fig. 7 follows that the low temperature endothermic event in region II was present for both the raw and treated films regardless of their particular compositions (sometimes not measurable quantitatively). The origin of this peak is most probably associated with relaxation processes, mostly of the amorphous parts of soft segments occurring at the soft-hard segment interphase, but also partially of the crystalline soft–soft segments [15].

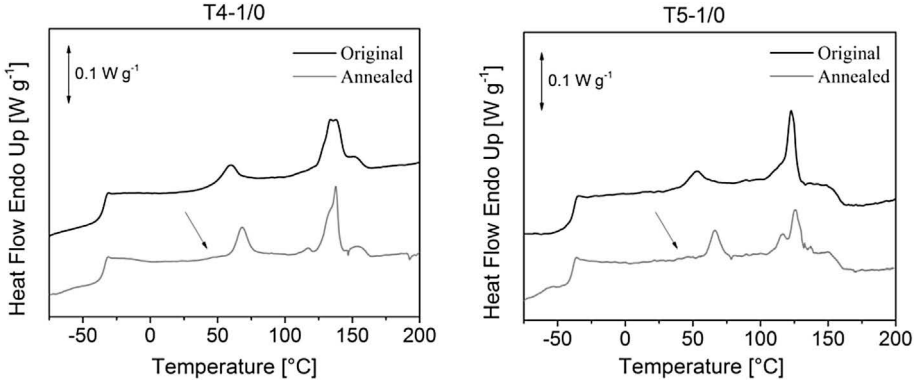

Fig. 8. DSC analysis confirming the reorganization and rearrangement processes caused by temperature influence on material conditioning in nitrogen; samples T4-1/0 (left) and T5-1/0 (right).

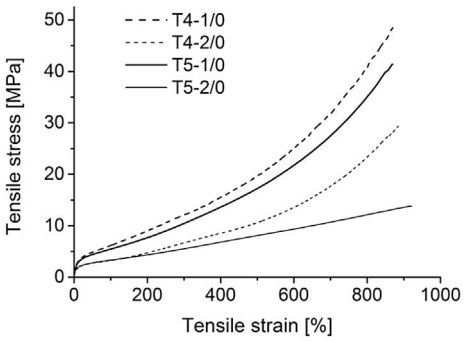

Fig. 9. The tensile curves of raw PU samples prepared from different macrodiols and at different hard-segment content (ratio *R*).

The multiple endothermic processes in the region III (over 100 °C) are related to gradual melting of crystalline (highly organized) hard-segment domains of different size distribution and ordering.

Observation of the changes occurring in the relevant part of the DSC curves (above 100 °C) in Figs. 7 and 8 confirms that the hard-segments also, to some extent, undergo re-ordering and re-distribution processes during the conducted stability tests. Nevertheless, relevant melting ΔH values in this region (ΔH_{m1} and in the case of $R = 1$ also ΔH_{m2}) do not substantially change and are more-or-less constant (see Table 2).

All temperature transitions of both T5-1/X and T5-2/X series including the T_g values of soft segments, relaxation processes in region II corresponding to soft-segment melting and relaxation temperatures as well as the hard-segment melting temperature in region III have systematically lower values than those of T4-1/X and T4-2/X series. The cause of these behavioral differences can be related to the more irregular structure of T5 macrodiol as compared to the more rigid and regular character of T4.

The soft segment T_g values and the relaxation temperatures in region II were both found to be about 5 °C lower for films in T5-as compared to material in the T4-series. This shift in the temperature values is dependent on the type of the macrodiol used for the preparation of the films and can be regarded as another evidence that relaxation enthalpy is related to structure of polycarbonate-based soft-segment chains.

On the other hand, the melting temperatures in region III (120–140 °C) were found to be between 10 and 12 °C higher for the T4-based as compared to T5-based systems. The hard-segment domains to which these melting points correspond are identical in composition (BD + HDI product) and very similar in percentages in both the T4 and T5 series for the given *R* value (see Table 1) and should therefore exhibit similar values. Clearly, the behavior of the more regular T4 soft-segment macrodiol regions contributes to better arrangement and packing of the hard segments in the PU films resulting in higher melting points (see Table 2).

3.1.4. Tensile properties

Tensile tests were performed for all samples, both raw PUs and PU films after 1, 3, 6 and 12 months of immersion in PBS. The influence of the macrodiol regularity and MD-to-BD ratio on tensile dependences was determined for untreated samples T4-1/0, T4-2/0, T5-1/0 and T5-2/0 as given in Fig. 9.

Fig. 9 shows that tensile properties are substantially influenced by both the chain regularity of the polycarbonate macrodiol (T4 versus T5) and the *R* ratio (the hard-segment content). While the tensile strength (σ_b) values were relatively high and varied, from 15.4 to 50.1 MPa, all the samples showed similar and high values of the elongation at break (ε_b between 841 and 918%). Higher σ_b is found in samples prepared either from more regular macrodiol T4 (macrodiol type influence) and/or at ratio $R = 1$ (hard-segment content influence). If comparing PU samples TY-1/0 and TY-2/0 (Y = 4 or 5), higher $\Delta\sigma_b$ difference was found for the more irregular T5 macrodiol. S-shape of the tensile curves caused by the strain-induced crystallization (SIC) is visible for all PU films with the exception of T5-2/0. Such stress-induced crystallization arises as a result of chain alignment, leading to better chain fitting and in consequence to sample reinforcement. While in the T5 series the SIC is present merely in the sample with sufficiently high HS content (i.e. $R = 1$), it is observed for both samples of the T4 series. Such independence on the HS content for the T4-based series implies that both the hard segment domains (samples with lower *R* values) and the soft segments originating from the macrodiol are involved in the SIC process. The lack of SIC in T5-2/0 stems from its lower chain regularity of the polycarbonate chain and thus lower ability to arrange in a proper manner for the crystallization to occur. On the other hand, this particular sample (T5-2/0) also showed the highest elongation at break. The tensile tests confirmed that mechanical properties (especially tensile strength and toughness) can be easily tuned, simply by changing the PU composition (i.e. by macrodiol regularity and ratio *R*). In this way the tensile strength can be modified by the factor of 3 and toughness by the factor of 2 (see Table 3 for details).

In order to examine the influence of the PBS solution on the mechanical properties of the investigated materials, tensile tests were further performed on samples after different immersion times (1–12 months). The comparison of tensile properties of the raw and treated PU films are presented in Figs. 10–12: Young's modulus values in Fig. 10, elongation-at-break in Fig. 11, and strength and toughness in Fig. 12.

It was found that tensile strength, elongation-at-break and toughness (see Figs. 10–12) decreased very slightly with increasing immersion time with more distinct decrease of the tensile properties was observed in both T5 series as compared to the T4 analogs. As an exception, substantial increase of both tensile strength and toughness was observed for the T4-2/X series in the period of up to 6 months. Individual tensile characteristics for this sample are given in Table 4.

From Fig. 10 it can be found that at the early stages of the immersion experiment (up to 3 months) Young's modulus mostly increases as compared to the raw PU films. This increase stems from the samples being conditioned at 37 °C which leads to re-organization and co-crystallization processes of the soft segment polycarbonate chains (see also the DSC section). This trend is uniform for lower hard-segment contents ($R = 2$), unlike opposite

Table 3
Selected tensile properties of raw PU films.

Sample code	Young's modulus *E* (MPa)	Tensile strength σ_b (MPa)	Elongation-at-break ε_b (%)	Energy-to-break (mJmm^{-3})
T4-1/0	57.8 ± 2.8	50.1 ± 4.7	863 ± 23	177.5 ± 11.9
T4-2/0	30.1 ± 2.6	28.4 ± 4.8	863 ± 52	96.7 ± 14.3
T5-1/0	45.8 ± 2.6	41.4 ± 4.0	841 ± 30	147 ± 14.3
T5-2/0	38.6 ± 2.2	15.4 ± 2.2	918 ± 48	79.4 ± 10.5

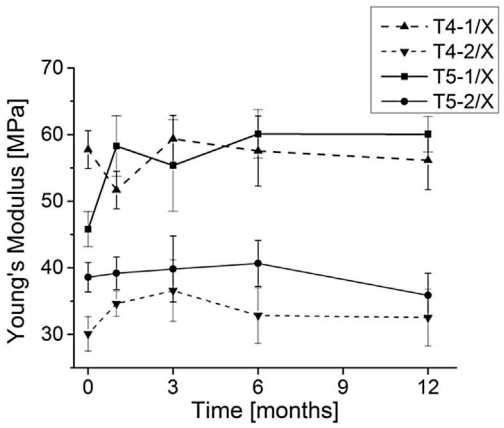

Fig. 10. Influence of the immersion time on Young's modulus values for T4-and T5-series.

dependence of films prepared at higher hard-segment content ($R = 1$). The dissimilar behavior of T4-1/1 compared to softer T5-1/1, T4-2/1 and T5-2/1 analogs signs the complexity process of the re-organization and re-packing of PU chains especially for the short time of the immersion. Increase of Young's modulus (and tensile strength after 3 months of the immersion, see also Fig. 12 left) can be the result of either an increased number of crystalline (or highly organized) domains or their better organization both resulting in slight reinforcement of the material. After 12 months of immersion, E values are similar to E of raw PU films; the only exception is Young's modulus of T5-1/12 higher by ca. 10 MPa compared to value E of T5-1/0.

The influence of the immersion time, macrodiol regularity (T4 vs T5) and R on the ultimate elongation is presented on Fig. 11. All ε_b values slightly decrease with increasing time of immersion, with the exception of slight ε_b increase of T4-1/6 and T5-1/6. Whereas the values of elongation at break for both T4 and T5-1/X series do not differ significantly regardless of time, the values of T5-2/12 is seen to decrease significantly. This pronounced reduction is possibly due to hydrolysis of the PU material proceeding at the surface of the material (cf. Fig. 2, bottom left). This behavior can be caused by the composition of the PU sample having low hard-segment content and at the same time containing macrodiol with relatively irregular chain structure.

Tensile strengths values map the process of PU chain re-organization with changes detectable mainly for short time of immersion (up to 3 months), and very slight tendency to the degradation after 12 months, see Fig. 12 left. Toughness, expressed as the energy to break of a given volume unit of the sample, can be considered a quality criterion of a material. All toughness values for the treated samples more or less oscillated around the reference values of relevant raw PU samples (see Fig. 12 right); for samples T4-2/1, T4-2/3 and T4-2/6 the toughness values were higher and for T4-1/12, T4-2/12 and T5-2/12 they were lower than the relevant

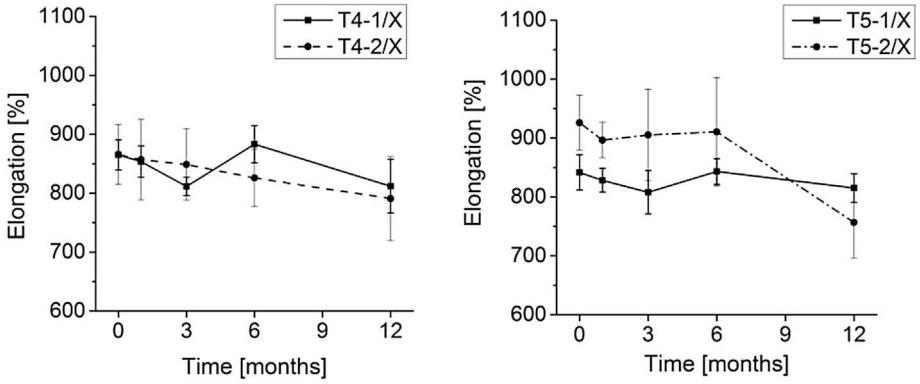

Fig. 11. The impact of immersion time on elongation-at-break (T4-series, left and T5 series, right).

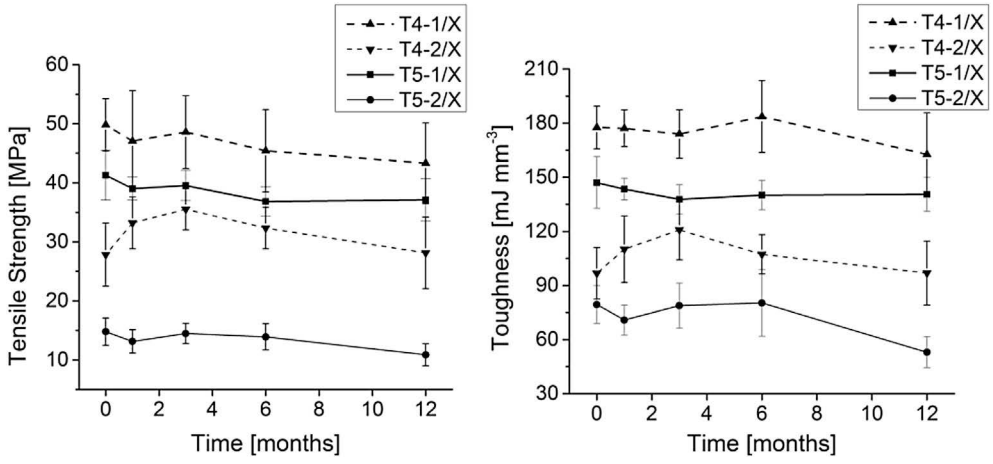

Fig. 12. The impact of immersion time on tensile strength, σ_b (left) and toughness (right) for T4 and T5-based series at different R values.

Table 4
Selected tensile properties of T4-2/X series.

Sample code	Young's modulus E (MPa)	Tensile strength σ_b (MPa)	Elongation-at-break ε_b (%)	Energy-to-break (mJmm^{-3})
T4-2/0	30.1 ± 2.6	27.8 ± 5.3	866 ± 51	96.7 ± 14.3
T4-2/1	34.6 ± 1.9	33.2 ± 4.4	857 ± 69	110.1 ± 18.4
T4-2/3	36.6 ± 4.6	35.5 ± 3.5	849 ± 61	120.8 ± 16.7
T4-2/6	32.8 ± 4.2	32.3 ± 3.5	826 ± 48	107.3 ± 10.9
T4-2/12	32.5 ± 4.3	28.1 ± 6.1	791 ± 71	96.8 ± 17.7

original values. Sample T5-1/X is clearly the least susceptible to toughness changes of all the PU materials. Moreover, PU films based on the more regular T4 macrodiol seem to be more resistant to the degradation process than the T5 based one. The slight deterioration of the mechanical tensile properties with immersion time indicates a very slow progress of the hydrolytic process. With the exception of the T5-2/12 sample, the PU films can be considered as being stable and resistant to hydrolytic degradation at 37 °C, for the period of 12 months.

Also, the observed behavior of sample T4-2/X is rather surprising (for details, see Table 4). During the immersion its tensile strength and toughness increased by 25% compared to values obtained for the raw T4-sample, probably caused by strong and efficient re-organization and time- and temperature-induced partial crystallization of the soft segments (also confirmed by the appearance of distinct DSC peak at around 70 °C). On the other hand, the sample T5-2/X is distinguished by the most distinct deterioration of tensile properties. Consequently, macrodiol chain regularity is the key factor influencing mechanical properties when the concentration of the hard segments is low (high R values). However, at higher contents of the hard segments, the impact of chain regularity on the resulting mechanical properties becomes increasingly less pronounced. The same trend was concluded for similar types of PU elastomers studied recently [14,15,46].

3.1.5. Swelling and mass loss experiments

Swelling as well as mass loss was almost negligible in all cases (the values did not exceed 1 wt%), with maximal value for swelling at 0.38 wt% and mass loss varying between 0.54 and 0.93 wt% (maximal value). With the values oscillating around zero, no systematic trend was possible to estimate, except for a slight tendency of higher swelling and higher mass loss for T4-series, with $R = 2$ and longer immersion times.

In accordance with results from other analytical techniques, all swelling and mass loss experiments confirmed very high hydrolytic stability for all PU films in model physiological.

3.1.6. FTIR

FT-IR analysis was used for investigation of the long-term impact of immersion on hydrolytic stability and thereby chemical structure of the PU films. Detailed spectrum analysis of the polycarbonate-based PU systems with the description of characteristic bands belonging to the specific functional groups can be found elsewhere [14].

In case of a hydrolysis occurring during the immersion, the reaction can in principle proceed either on the carbonate or urethane functional groups. In this case changes best visible at carbonyl C═O (from 1800 to 1600 cm^{-1}) and amide N–H (3500–3200 cm^{-1}) stretching regions would be present. Representative FT-IR spectra of the T5-2-X sample before and after immersion (12 months) are presented in Fig. 13 with no significant changes visible. Furthermore, hydrolysis of carbonate and urethane linkages proceeds with the formation of hydroxyl and primary amine groups accompanied by CO_2 liberation. The absence of any characteristic and distinctive O–H stretching vibration at around 3550–3200 cm^{-1} or C–O stretching vibration at around 1250–1000 cm^{-1} also suggests that the extent of hydrolysis is insignificant. This behavior was found for all compositions regardless of the type of polycarbonate or ratio R used for film preparation.

4. Conclusions

The durability of four highly elastomeric PU films was tested in model physiological conditions (37 °C at pH = 7.4) for a time period of up to 12 months by a set of analytical methods. Scanning electron and atomic force microscopies, DSC, FTIR, and tensile and swelling tests enabled a detailed multi-scale description of the processes occurring on the surface and in the bulk of the films during hydrolytic tests. The performed stability tests show that the degradation processes are complex continuous processes dependent on (i) the liquid medium, (ii) temperature and (iii) time of immersion.

FTIR analyses did not revealed any substantial changes in the constitution of the linear PU chains (forming PU films) caused by the stability tests. Also SEM images of the cross sections did not show any destruction of the surface, the area close to the surface or to the bulk of the films. These observations are in accordance with negligible changes of swelling and mass loss values found and shown to depend neither on sample composition nor the time of immersion. All these experiments signalize stability of the investigated properties from segmental up to macroscopic levels.

On the other hand, the analyses revealed that the samples undergo changes during the long time immersion in PBS and their properties change. The changes can be explained as follows: Because all samples contain only linear aliphatic PU chains with regularly distributed polar urethane and carbonate groups within each chain, they assemble into the hard- and soft-segmental domains of the micrometer size. However, the physical crosslinking centers (hydrogen bonds and other dipole–dipole interactions), which are the pre-requisites for the assembly, can be temporary

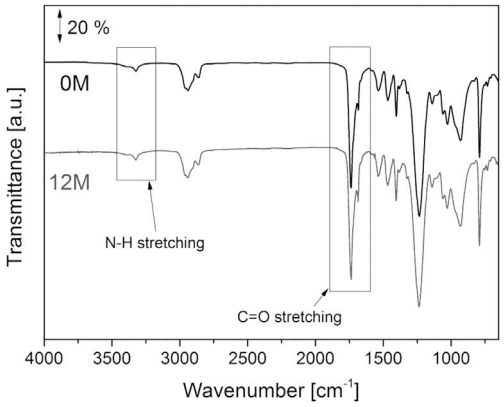

Fig. 13. FT-IR spectrum of raw T5-2 sample and after 12 months of immersing in PBS solution at 37 °C.

broken and re-built. This re-organization, re-packing and possible partial co-crystallization was detected by the SEM, AFM, DSC and indirectly by the tensile characterization technique. A substantial re-ordering caused by temperature conditioning was detected mainly in the soft-segment regions and on the soft-hard segment interphases, and to some extent also in the region of hard segments. The extent of re-ordering is pronounced at the beginning of the stability tests (1 month), as detected by DSC. Another slower and temporary process proceeding from 3 to 6 months is explained as partial temporary 'endorsed' crystallization of the polycarbonate part of the films possible through the restricted motion of the flexible polymer chains (though both pure polycarbonate macrodiols are otherwise fully amorphous). After 12 months of immersion, the film made from more irregular macrodiol and containing lower amount of hard-segments (marked as T5-2/12) feature a starting tendency to degradation detected by fine surface cracks and deterioration of the tensile properties. This process has to be predominantly of physical character, as no evidence of chemical processes was found (e.g. by FTIR).

When compared to the starting PU material, the macrodiol chain regularity and hard-segment contents of the PU samples prepared substantially influence the resulting tensile strength (from 15 to 50 MPa) and toughness (from 79 to 178 kJ mm^{-3}), while elongation at break is very similar and high for all samples (840–920%).

These experiments show that highly elastic films of various tensile strength and toughness according to the intended use can be obtained depending on the materials chosen. When comparing the overall results of the stability tests, the film marked as T4-1/X is the best candidate and T5-2/X the worst candidate for possible practical use as strong elastomeric film durable in model physiological conditions for a time period of up to 12 months.

Acknowledgment

The Authors wish to thank the financial support of the Grant Agency of the Czech Republic (Czech Science Foundation, project No. 13-06700S).

References

[1] Gunatillake PA, Martin DJ, Meijs GF, McCarthy SJ, Adhikari R. Designing biostable polyurethane elastomers for biomedical implants. Aust J Chem 2003;56(6):545–57.
[2] McBane JE, Sharifpoor S, Cai KH, Labow RS, Santerre JP. Biodegradation and in vivo biocompatibility of a degradable, polar/hydrophobic/ionic polyurethane for tissue engineering applications. Biomaterials 2011;32(26):6034–44.
[3] Khan F, Dahman Y. A novel approach for the utilization of biocellulose nanofibers in polyurethane nanocomposites for potential applications in bone tissue implants. Des Monomers Polym 2012;15(1):1–29.
[4] Mi HY, Jing X, Salick MR, Peng XF, Turng LS. A novel thermoplastic polyurethane scaffold fabrication method based on injection foaming with water and supercritical carbon dioxide as coblowing agents. Polym Eng Sci 2014;54(12):2947–57.
[5] Chen QZ, Liang SL, Thouas GA. Elastomeric biomaterials for tissue engineering. Prog Polym Sci 2013;38(3–4):584–671.
[6] Mi HY, Salick MR, Jing X, Jacques BR, Crone WC, Peng XF, et al. Characterization of thermoplastic polyurethane/polylactic acid (TPU/PLA) tissue engineering scaffolds fabricated by microcellular injection molding. Mater Sci Eng C-Mater 2013;33(8):4767–76.
[7] Baudis S, Ligon SC, Seidler K, Weigel G, Grasl C, Bergmeister H, et al. Hard-block degradable thermoplastic urethane-elastomers for electrospun vascular prostheses. J Polym Sci Pol Chem 2012;50(7):1272–80.
[8] Cherng JY, Hou TY, Shih MF, Talsma H, Hennink WE. Polyurethane-based drug delivery systems. Int J Pharm 2013;450(1–2):145–62.
[9] Špírková M, Duszová A, Poręba R, Kredatusová J, Bureš R, Fáberová M, et al. Thermoplastic polybutadiene-based polyurethane/carbon nanofiber composites. Compos Pt B–Eng 2014;67:434–40.
[10] Perez-Madrigal MM, Gianotti MI, Armelin E, Sanz F, Aleman C. Electronic, electric and electrochemical properties of bioactive nanomembranes made of polythiophene: thermoplastic polyurethane. Polym Chem 2014;5(4):1248–57.
[11] Sankar RM, Meera KS, Mandal AB, Jaisankar SN. Thermoplastic polyurethane/single-walled carbon nanotube composites with low electrical resistance surfaces. High Perform Polym 2013;25(2):135–46.
[12] Król P. Synthesis methods, chemical structures and phase structures of linear polyurethanes. Properties and applications of linear polyurethanes in polyurethane elastomers, copolymers and ionomers. Prog Mater Sci 2007;52(6):915–1015.
[13] Ramirez M, Miller KR, Soucek MD. Linking of oligoesters hydrolysis to polyurethane coatings. J Appl Polym Sci 2014;131(9):40198.
[14] Špírková M, Poręba R, Pavličević J, Kobera L, Baldrian J, Pekárek M. Aliphatic polycarbonate-based polyurethane elastomers and nanocomposites. I. The influence of hard-segment content and macrodiol-constitution on bottom-up self-assembly. J Appl Polym Sci 2012;126(3):1016–30.
[15] Poręba R, Špírková M, Brožová L, Lazić N, Pavličević J, Strachota A. Aliphatic polycarbonate-based polyurethane elastomers and nanocomposites. II. Mechanical, thermal, and gas transport properties. J Appl Polym Sci 2013;127(1):329–41.
[16] Špírková M, Machová L, Kobera L, Brus J, Poręba R, Serkis M, et al. Multiscale approach to the morphology, structure, and segmental dynamics of complex degradable aliphatic polyurethanes. J Appl Polym Sci 2015;132(10):41590.
[17] Poręba R, Kredatusová J, Hodan J, Serkis M, Špírková M. Thermal and mechanical properties of multiple-component aliphatic degradable polyurethanes. J Appl Polym Sci 2015;132:41872.
[18] Engels HW, Pirkl HG, Albers R, Albach RW, Krause J, Hoffmann A, et al. Polyurethanes: versatile materials and sustainable problem solvers for today's challenges. Angew Chem Int Ed 2013;52(36):9422–41.
[19] Javni I, Petrović ZS, Guo A, Fuller R. Thermal stability of polyurethanes based on vegetable oils. J Appl Polym Sci 2000;77(8):1723–34.
[20] Corcuera MA, Rueda L, d'Arlas BF, Arbelaiz A, Marieta C, Mondragon I, et al. Microstructure and properties of polyurethanes derived from castor oil. Polym Degrad Stab 2010;95(11):2175–84.
[21] Saralegi A, Rueda L, d'Arlas BF, Mondragon I, Eceiza A, Corcuera MA. Thermoplastic polyurethanes from renewable resources: effect of soft segment chemical structure and molecular weight on morphology and final properties. Polym Int 2013;62(1):106–15.
[22] More AS, Palaskar DV, Cloutet E, Gadenne B, Alfos C, Cramail H. Aliphatic polycarbonates and poly(ester carbonate)s from fatty acid derived monomers. Polym Chem 2011;2(12):2796–803.
[23] Kong XH, Liu GG, Curtis JM. Novel polyurethane produced from canola oil based poly(ether ester) polyols: synthesis, characterization and properties. Eur Polym J 2012;48(12):2097–106.
[24] Tanzi MC, Mantovani D, Petrini P, Guidoin R, Laroche G. Chemical stability of polyether urethanes versus polycarbonate urethanes. J Biomed Mater Res 1997;36(4):550–9.
[25] Golomb G, Wagner D. Development of a new invitro nodel for studying implantable polyurethane calcification. Biomaterials 1991;12(4):397–405.
[26] Lopezlopez G, Pascual A,Perea EJ. Effect of plastic catheter material on bacterial adherence and viability. J Med Microbiol 1991;34(6):349–53.
[27] Pinchuk L. A review of the biostability and carcinogenity of polyurethanes in medicine and the new-generation of biostable polyurethanes. J Biomat Sci–Polym E 1994;6(63):225–67.
[28] Zhou LJ, Liang D, He XL, Li JH, Tan H, Li JS, et al. The degradation and biocompatibility of pH-sensitive biodegradable polyurethanes for intracellular multifunctional antitumor drug delivery. Biomaterials 2012;33(9):2734–45.
[29] Chattopadhyay DK, Webster DC. Thermal stability and flame retardancy of polyurethanes. Prog Polym Sci 2009;34(10):1068–133.
[30] Poręba R, Špírková M, Pavličević J, Budinski-Simendić J, Szecsenyi KM, Hollo B. Aliphatic polycarbonate-based polyurethane nanostructured materials. The influence of the composition on thermal stability and degradation. Compos Pt B–Eng 2014;58:496–501.
[31] Ochiai B, Amemiya H, Yamazaki H, Endo T. Synthesis and properties of poly(carbonate-urethane) consisting of alternating carbonate and urethane moieties. J Polym Sci A Polym Chem 2006;44(9):2802–8.
[32] Król P, Król B, Chmielarz P, Wojturska J. Assessment of susceptibility to hydrolytic degradation of different types of polyurethanes in terms of their use as biomaterials. Polimery 2013;58(4):282–91.
[33] Sui HL, Ju X, Liu XY, Cheng KM, Luo YW, Zhong FC. Primary thermal degradation effects on the polyurethane film. Polym Degrad Stab 2014;101:109–13.
[34] Tanzi MC, Fare S, Petrini P. In vitro stability of polyether and polycarbonate urethanes. J Biomater Appl 2000;14(4):325–48.
[35] Sobczak M, Debek C, Oledzka E, Nalecz-Jawecki G, Kolodziejski WL, Rajkiewicz M. Segmented polyurethane elastomers derived from aliphatic polycarbonate and poly(ester-carbonate) soft segments for biomedical applications. J Polym Sci A-Polym Chem 2012;50(18):3904–13.
[36] Labow RS, Meek E, Santerre JP. Hydrolytic degradation of poly(carbonate)-urethanes by monocyte-derived macrophages. Biomaterials 2001;22(22):3025–33.
[37] Dempsey DK, Carranza C, Chawla CP, Gray P, Eoh JH, Cereceres S, et al. Comparative analysis of in vitro oxidative degradation of poly(carbonate urethanes) for biostability screening. J Biomed Mater Res A 2014;102(10):3649–65.
[38] Chan-Chan LH, Solis-Correa R, Vargas-Coronado RF, Cervantes-Uc JM, Cauich-Rodriguez JV, Quintana P, et al. Degradation studies on segmented

polyurethanes prepared with HMDI, PCL and different chain extenders. Acta Biomater 2010;6(6):2035–44.
[39] Chaffin KA, Chen XJ, McNamara L, Bates FS, Hillmayes MA. Polyether urethane hydrolytic stability after exposure to deoxygenated water. Macromolecules 2014;47(15):5220–6.
[40] Rueda L, d'Arlas BF, Corcuera MA, Eceiza A. Biostability of polyurethanes. Study from the viewpoint of microphase separated structure. Polym Degrad Stabil 2014;108:195–200.
[41] Christenson EM, Anderson JM, Hittner A. Biodegradation mechanisms of polyurethane elastomers. Corros Eng Sci Technol 2007;42(4):312–23.
[42] Murray KA, Kennedy JE, McEvoy B, Vrain O, Ryan D, Cowman R, et al. The influence of electron beam irradiation conducted in air on the thermal, chemical, structural and surface properties of medical grade polyurethane. Eur Polym J 2013;49(7):1782–95.
[43] Zhang C, Jiang XJ, Zhao ZY, Mao LX, Zhang LQ, Coates P. Effects of wide-range gamma-irradiation doses on the structures and properties of 4,4′-dicyclohexyl methane diisocyanate based poly(carbonate urethane)s. J Appl Polym Sci 2014;131(22):41049.
[44] Kozakiewicz J, Rokicki G, Przybylski J, Sylwestrzak K, Parzuchowski PG, Tomczyk KM. Studies of the hydrolytic stability of poly(urethane-urea) elastomers synthesized from oligocarbonate diols. Polym Degrad Stab 2010;95(12):2413–20.
[45] Tang YW, Labow RS, Santerre JP. Isolation of methylene dianiline and aqueous-soluble biodegradation products from polycarbonate-polyurethanes. Biomaterials 2003;24(17):2805–19.
[46] Špírková M, Pavličević J, Strachota A, Poręba R, Bera O, Kapráková L, et al. Novel polycarbonate-based polyurethane elastomers: composition-property relationship. Eur Polym J 2011;47(5):959–72.

Polymer Degradation and Stability 125 (2016) 115–128

Contents lists available at ScienceDirect

Polymer Degradation and Stability

journal homepage: www.elsevier.com/locate/polydegstab

Experimental study of the simulated process of degradation of polycarbonate- and D,L-lactide-based polyurethane elastomers under conditions mimicking the physiological environment

Milena Špírková*, Magdalena Serkis, Rafał Poręba, Lud'ka Machová, Jiří Hodan, Jana Kredatusová, Dana Kubies, Alexander Zhigunov

Institute of Macromolecular Chemistry AS CR (IMC), Heyrovsky Sq.2, 16206, Prague 6, Czech Republic

ARTICLE INFO

Article history:
Received 16 November 2015
Received in revised form
7 January 2016
Accepted 8 January 2016
Available online 11 January 2016

Keywords:
Polyurethane
Elastomer
Hydrolytic degradation
Mechanical properties
Thermal properties
Surface analysis

ABSTRACT

The extent of the hydrolytic degradation of aliphatic polyurethane (PU) films made from polycarbonate-based aliphatic macrodiol (MD), diisocyanate-1,6-hexane, butane-1,4-diol (BD) and D,L-lactide-based oligomeric diol (DLL) was tested in phosphate-buffered saline (PBS) for a period of up to 12 months. Two macrodiols of equal molecular weight (~2000 Da), differing in chain composition and regularity, and equal MD-to-BD-to-DLL molar ratios were chosen for the PU synthesis. The isocyanate-to-total hydroxyl group ratio was kept constant at 1.05. The functional properties of raw four-component polyurethane films and samples immersed for 1, 3, 6, 9 and 12 months in a model physiological environment (37 °C, pH = 7.4) were studied from the segmental up to the macroscopic level. Tensile testing and water uptake experiments, as well as DSC, SEM, AFM, FTIR and WAXD analyses, were used for the comprehensive characterization of the raw and PBS-treated films. The study shows that the untreated four-component PU films are highly elastomeric materials with very high tensile strength and suitable thermal properties for potential medical coating/film applications. The DLL oligomeric diol turned out to be a very efficiently degradable unit, leading to substantial mechanical property deterioration. The products of more regular macrodiol have higher tendency to the degradation process; 89% or 94% of the original toughness value is lost in just 12 months of immersion. The studied type of PU can be practically used either as fairly stable high-performance elastomers for short-term applications (up to 3 months) or as degradable materials, when the time of exposure to the physiology-mimicking conditions is sufficient.

1. Introduction

Polyurethanes have been used in medicine for several decades [1–8], but the purposes of their utilization have changed during this long period of time. The first PUs were applied as robust and long-term stable biomaterials for the fabrication of catheters, vascular grafts, biomedical devices and implants [2,3,5–7]. However, current demands require the development of efficient biodegradable or bioresorbable materials with short or limited lifetimes [8–14].

Thermoplastic polyurethanes (TPUs) represent a very popular and important part of polyurethane industrial products, even though they are not produced in such high quantities as PU foams. TPUs have two main advantages as follows: (i) targeted functional properties can be achieved relatively easily by modification of the polyurethane composition and preparation procedure, and (ii) various sizes and complicated shapes of TPU products can be obtained by casting, extrusion, injection or spraying techniques. TPUs exhibit excellent mechanical properties due to their advantageous combination of elasticity and flexibility together with high strength and Young's modulus. The simplicity of their recycling is a further positive criterion of their utility. Although PUs and their blends and nanocomposites have previously been employed in tissue engineering, as scaffolds, and in drug delivery [7,10,15–21], they are still amply studied from the point of view of further potential applications in medicine [13,22–24]. The safe use of biomaterials with required lifetimes in biomedicine requires not only detailed information on their end-use properties but also the knowledge of their stability/degradability.

The functional properties of TPUs depend, in addition to other

* Corresponding author.
E-mail address: spirkova@imc.cas.cz (M. Špírková).

http://dx.doi.org/10.1016/j.polymdegradstab.2016.01.003
0141-3910/

factors, on their content of hard and soft segments, length, and spatial arrangement (intermixing or phase separation), which can be tuned by the choice of starting compounds (isocyanate, macrodiol and chain extender), reaction mixture composition, preparation protocol, and thermal history [25]. Therefore, the relationship between the composition, structure and properties, which will provide comprehensive descriptions of the mechanical, surface, thermal, swelling and other properties, has to be studied for each new PU system in detail.

In general, stability tests can be conducted from substantially different viewpoints (i.e., under different conditions, such as temperature, and exposure to different chemical and physical stimuli), with the aim of investigating different properties (e.g., thermal, oxidative, chemical, irradiation, flame, and hydrolysis) and on very different time scales. The conditions for the practical hydrolytic degradation/stability tests of various polymeric and composite materials are chosen individually according to the intended use, and they substantially differ in the temperature, time and environment of their sample exposures [5,8,14,15,26–38]. Long-term experiments under physiologically simulated conditions are essential for the assessment of the hydrolytic stability of new biomaterials to be used in medical applications [26,28,29,31,36,37,39].

Polycarbonate-based PUs belong to a relatively new class of PU elastomeric systems. The first PUs prepared from commercially available macrodiols were based solely on aromatic diisocyanates [33,34,40,41]. The use of aliphatic or cycloaliphatic diisocyanates in PU formulations [8,42–50] has become more popular for two main reasons, better stability during exposure to oxygen and UV radiation and lower degradation product toxicity than the use of aromatic-based diisocyanates [10,13,29,41].

In the present contribution, the preparation of TPU elastomeric films with a controlled lifetime in simulated physiological conditions is described. This study is a part of our long-term research, with the ultimate goal of the synthesis of controllably degradable materials that could find use in biomedical applications. Recently, we have examined the hydrolytic stability of PUs made from polycarbonate-based macrodiol, diisocyanate-1,6-hexane and butane1,4-diol under model physiological conditions. The study confirmed the high hydrolytic stability of the three-component PUs with the preservation of their excellent mechanical properties for up to one year [50]. The use of this reaction mixture for the preparation of degradable PUs seems to be counterproductive for the first view. However, the idea of incorporating small amounts of short degradable units into the PU backbone [51] was the stimulus and motivation for the present study. As the lactide-based derivatives are efficient degradable materials [39,51,52,53], we prepared an oligomeric D,L-lactide-based diol (DLL) containing, on average, two lactide units in the chain [45]. The conditions of the preparation and multi-scale characterization of the four-component PU films (containing, in addition to macrodiol, diisocyanate, chain extender and oligomeric DLL diol in the PU backbone) have been recently published [45,46].

The role of the polycarbonate-based diol is the formation of elastomeric TPU with excellent mechanical properties, whereas DLL is a hydrolytically degradable component built-up into the polyurethane backbone. Degradable ester units are thus regularly distributed in each PU chain and, hence, in the PU film. We believe that this setting could be more efficient for the hydrolytic degradation process compared with the currently popular mixing or blending of degradable lactide-based material into the polyurethane matrix [1,12,19,22,24,26].

The end-use properties of three- and four-component aliphatic TPUs were recently studied in detail on the segmental to macroscopic levels [42–47]. However, no degradation tests under physiologically simulated conditions have been performed thus far on PU systems containing DLL units. This paper is the continuation and extension of the degradation studies investigating the efficiency of DLL in the hydrolytic degradation process of four-component PUs [50].

2. Experimental

2.1. Materials

Two commercially available polycarbonate-based macrodiols, T4672 (marked as "T4", number-average molar mass $<M_n> = 2770$ g mol^{-1}, dispersity $Đ_M = 3.20$) and T5652 (marked as "T5", number-average molar mass $<M_n> = 2874$ g mol^{-1}, dispersity $Đ_M = 3.23$), which were kindly provided by Asahi Casei Co., Japan, as well as butane-1,4-diol (BD), dibutyltin dilaurate (DBTDL) and 1,6-diisocyanatohexane (HDI, all from Fluka), were used. The synthesis and detailed characterization of oligomeric D,L-lactide-based diol (DL-L) are described elsewhere [45]. A schematic representation of the structures forming the PU chain is shown in Fig. 1.

As the T4672 polycarbonate-based macrodiol contains only *even* methylene $-CH_2-$ units, it exhibits higher regularity and higher rigidity. On the other hand, T5652 contains *even* and *odd* methylene $-CH_2-$ units at an *equal* molar ratio and is therefore characterized by a higher irregularity and higher flexibility compared with T4672, as shown previously [44]. Both macrodiols contain, on average, approximately 23 ± 4 carbonate groups per chain. DLL contains, on average, 4 degradable ester units, distributed relatively regularly in the oligomeric diol (See Fig. 1).

2.1.1. Preparation procedure

All PU films were prepared by a one-step procedure. Prior to the reaction, all components were thoroughly mixed in dried acetone to obtain a homogenous solution that was subsequently poured into the Teflon forms. After solvent evaporation at room temperature, the Teflon moulds were placed in an oven in a nitrogen atmosphere. The equimolar ratios of the hydroxyl groups of macrodiol (MD = T4672 or T5652), BD and DLL used for PU film preparation were chosen on the basis of our previous studies [45,46]. All reactions proceeded in bulk at 90 °C for 24 h in the presence of the organotin catalyst DBTDL at very low concentration (50 ppm/mol of urethane groups) at constant r and R ratios ($r = [NCO]/[OH]_{total} = 1.05$, where $[OH]_{total} = [OH]_{MD} + [OH]_{BD} + [OH]_{DLL}$), and $R = [OH]_{MD} = [OH]_{BD} = [OH]_{DLL} = 1$. The final thickness of the films was 250 ± 25 μm. Individual sample codes and compositions are summarized in Table 1, 1st and 2nd columns. As the previous study revealed that the oligomeric DLL diol belongs to the soft-segment component [46], the hard-segment content (HSC, Table 1, 3rd column) was calculated as the weight percentage of BD and HDI with respect to the total mass of all reagents used.

The PU films were subsequently either measured by the set of analytical methods (raw samples) or cut into individual pieces and placed in a glass degradation flask. Degradation proceeded in the phosphate-buffered saline solution (PBS)[1] with an additional 0.02 wt% of sodium azide NaN_3 at 37 °C for 1, 3, 6, 9 and 12 months. Whereas the buffer environment and temperature were the same, the specimen shape differed according to the method of analysis as follows: (a) dumbbell-shaped samples for tensile properties and rectangular samples for the microscopy analyses were cut from the PU film and fixed to custom-built PE frames prepared for this purpose in IMC, and (b) pieces of PU films for water uptake and DSC analyses were fixed on an inert thread. Both types of immersion

[1] PBS – Phosphate-Buffered Saline contains monobasic potassium phosphate, sodium chloride, and dibasic sodium phosphate.

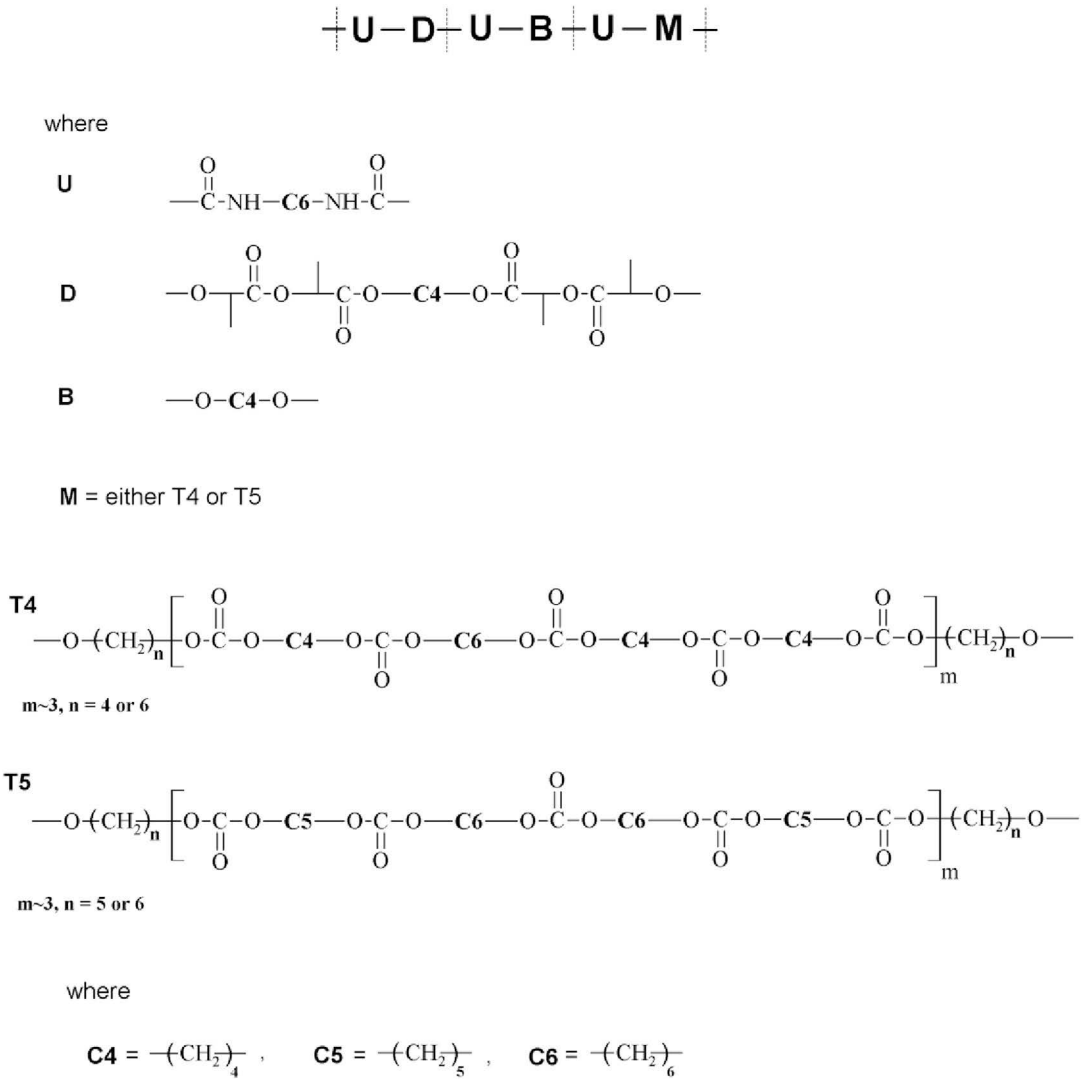

Fig. 1. Schematic representation of the PU chain structure made from HDI (sequence U), DLL (sequence D), BD (sequence B) and macrodiol T4 or T5 (sequence M).

Table 1
Code, composition and hard-segment content of PU films.

Code[a]	Molar ratio $(OH)_{MD}$: $(OH)_{BD}$: $(OH)_{DLL}$	HSC[b] (wt%)	DLL[c] (wt%)
T4-X	1.00: 1.01: 1.01	21.6	8.8
T5-X	1.00: 0.99: 1.00	21.9	8.8

X = 0, 1, 3, 6, 9 or 12 (time in months of the sample immersion in PBS at 37 °C).
[a] T4: macrodiol T4672; T5: macrodiol T5652.
[b] HSC = $(m_{BD} + m_{HDI})/(m_{MD} + m_{DLL} + m_{BD} + m_{HDI})$.
[c] DLL = $m_{DLL}/(m_{MD} + m_{DLL} + m_{BD} + m_{HDI})$.

enabled uniform and free access of the PBS solution to the surface of the specimen for further analysis. After a pre-set time (1, 3, 6, 9 and 12 months), the PU samples were pulled out from the buffer, washed, quickly dried and immediately measured by the set of experimental methods.

As the molar ratios *r* and *R* are constant, the sample codes in the paper correspond to the macrodiol type used for the preparation and the time of the PU film immersion in PBS. For example, the code T4-6 means the PU sample prepared from macrodiol T4672, which was immersed in PBS buffer at 37 °C for 6 months. Codes T4-0 and T5-0 are raw, untreated PU films.

2.2. Methods of characterization

2.2.1. Tensile characterization

The static mechanical properties were measured on an Instron model 6025/5800R (Instron Limited, UK) at room temperature with a cross-head speed of 10 mm min^{-1}. Dumbbell-shaped specimens correspond to the ISO 527-2/5B type; the total specimen length was 35 mm; the length and width of the narrowed part were 12 and 2 mm, respectively; and the thickness was 0.25 mm. The toughness was expressed as the energy necessary to break the sample per volume unit. The reported values were the averages of at least five measurements. The presented stress-strain curves were taken from the measurements closest to each calculated average value.

2.2.2. Water uptake and mass loss determination

Each water uptake and mass loss experiment consisted of 5 different measurements of 30–50 mg pieces of the given PU film. The percent water uptake was determined as the mass increase after the swelling experiment compared with the mass of dry sample after the experiment, and the percent mass loss is given as the mass decrease of the fully dried sample after the swelling experiment compared with the original sample mass. The resulting

water uptake and mass loss values are the mean values of five experiments made on different pieces of a given PU film.

2.2.3. FTIR spectroscopy

The FT-IR spectra were recorded on a Perkin–Elmer Paragon 1000 PC FT-IR spectrometer using the reflective ATR (attenuated total reflection) technique on a Specac MKII Golden Gate Single Reflection ATR System with a diamond crystal with an angle of incidence of 45°. The samples were put directly on the diamond crystal and measured. All spectra were measured at a wavenumber range of 4400–450 cm $^{-1}$ with a resolution of 4 cm^{-1} and 16 scans. Spectrum v2.00 software was used for processing the spectra.

2.2.4. Size-exclusion chromatography (SEC)

Size-exclusion chromatography of the polymer chains leached from the bulk material, before and after 12 months of immersion in PBS, was performed at 25 °C with two PLgel MIXED-C columns (300 × 7.5 mm, SDV gel with particle size 5 μm; Polymer Laboratories, USA) and with UV (UVD 250; Watrex, Czech Republic) and RI (RI-101; Shodex, Japan) detectors. Tetrahydrofuran was used as the leaching solvent and as a mobile phase at a flow rate of 1 mL/min. The molecular weight values were calculated using Clarity software (Dataapex, Czech Republic). Calibration was performed with polystyrene standards (PSS, Germany).

2.2.5. Scanning electron microscopy (SEM)

The surface microstructure of the PU films was measured by scanning electron microscopy (SEM) on a Vega Plus TS 5135 instrument (Tescan, Czech Republic). Before SEM analysis, the upper sides of the PU films (or their cross-sections, after freeze-fracturing at the temperature of liquid nitrogen) were sputtered with a 4 nm Pt layer using a SCD 050 vacuum sputter coater (Balzers, Czech Republic).

2.2.6. Atomic force microscopy (AFM)

The investigation of the topography and heterogeneity relief from the nano-to micrometre levels was conducted by AFM. PU films were measured either on the upper film side, “top images”, or after freeze-fracturing at the temperature of liquid nitrogen, “cross-sectional images”. An atomic force microscope (Dimension Icon, Bruker), equipped with an SSS-NCL probe, the Super Sharp SiliconTM - SPM-Sensor (NanoSensorsTM Switzerland; spring constant 35 N m^{-1}, resonant frequency ≈ 170 kHz) was used for the analysis. Measurements were performed under ambient conditions using the tapping mode AFM technique. AFM scans covered areas from 500 × 500 nm^2 to 50 × 50 μm^2.

2.2.7. Differential scanning calorimetry (DSC)

Differential scanning calorimetry (DSC) analyses were carried out on a Perkin Elmer DSC 8500 calorimeter with nitrogen as a purge gas (20 cm^3 min^{-1}). The instrument was calibrated for temperature and heat flow using indium as a standard. Samples of approximately 10 mg were encapsulated in hermetic aluminium pans. The analyses were performed in a cycle of heating – cooling – heating from −80 °C to 200 °C at 10 °C min^{-1}. Two-minute isothermal plateaux were inserted before and between the ramps.

The glass transition temperature was defined as the midpoint between the glassy and rubbery branches of the DSC trace, and the melting temperatures, as the maxima of the corresponding endotherm peaks. The recorded endotherm curves were evaluated as heats of melting in joules per gram.

2.2.8. Wide-angle X-ray diffraction (WAXD)

Diffraction patterns were obtained using a powder diffractometer HZG/4A (Seifert GmbH, Germany) in reflection mode. CuKα radiation (wavelength λ = 1.54 Å, 40 kV, 45 mA) monochromatized with a Ni foil (β filter) was used. The measurement was conducted in the range of 2θ = 1.4–40° with a 0.1° step, where 2θ is the scattering angle. The exposure time at each step was 10 s.

3. Results and discussion

At the very beginning of the discussion, the following facts concerning the structure of the studied PUs and some observations from our earlier studies should be noted. The studied segmented thermoplastic PUs contain in the PU backbone structural units derived from three different diols (differing substantially in structure and length). The two dihydroxyl components contribute to the soft segments (macrodiol, either T4 or T5, and oligomeric DLL), and two components are considered to be hard segments (BD and HDI) [45]. It follows that the four-component PUs are intrinsically complex systems due to the different properties of the two soft-segment (macrodiol and DLL) compounds, as was revealed by solid-state NMR spectroscopy in our recent studies [45,46]. However, the PILGRIM NMR spectra revealed that the behaviour of HDI itself (the hard-segment component) is far from simple [45]. It was also found that it can form either rigid or fairly flexible parts of the PU chain, depending on the type of hydroxyl component connected to it. Finally, the behaviour of BD depends on its environment, particularly on the nature of its covalently bound units. Whereas the BD unit incorporated into the DLL unit contributes solely to the flexible part of PU, the reaction product of BD with HDI exclusively forms the rigid domains. However, for the sake of clarity, the “classical” calculation of the hard- and soft-segment contents was used (for details, see Fig. 1 and Table 1).

The composition design of the four-component films prepared for testing the hydrolytic stability is based on the previous study of complex PU elastomers made from T5 macrodiol, BD, DLL and HDI [45,46]. Several compositions were previously tested, but only an equimolar ratio of all hydroxyl components (MD, DLL and BD) led to suitable mechanical properties that were comparable with those of the three-component system prepared without DLL. In this way, two series of four-component PU films containing an equimolar ratio of hydroxyl components were prepared for hydrolytic stability tests. The schematic PU structure is shown in Fig. 1: PU chains are formed by altering the MD, DLL and BD units mutually connected by HDI units.

Previous studies of simpler three-component PUs (without DLL) revealed that the overall hydrolytic stability of these systems (expressed as changes of surface, mechanical, swelling and thermal properties in the period up to 12 months) is very high [50]. In other words, the carbonate and urethane groups are sufficiently stable over the period of 12 months at the given experimental conditions (immersion to PBS at 37 °C). This paper is focused on the hydrolytic stability tests of four-component systems containing a certain fraction of a short oligo-diol based on racemic D,L-lactic acid (marked as DLL) as its derivatives are known to be easily hydrolysed under relatively mild conditions [39,51,52].

The hydrolytic stability is studied in this paper in the same manner as previously described [50]. Because the stability tests were conducted at 37 °C, i.e., the temperature corresponding to human body temperature, the PU samples were, in fact, exposed not only to the liquid PBS environment but also to long-term thermal conditioning.

3.1. Tensile properties

Previous studies revealed that all tensile characteristics, including the tensile strength, elongation at break and Young's modulus, depend strongly on the composition of the PUs and on

internal arrangement of domains at the microscopic level [42,44,46]. Tests of the hydrolytic stability of three-component PU films accompanied by thorough structural analyses reveal that the tensile properties sensitively reflect the re-organization and re-packing of PU chains [50]. Therefore, the tensile properties of the four-component PU samples before and after hydrolytic tests were measured first.

Tensile tests were performed on raw PUs and PU films after 1, 3, 6, 9 and 12 months of immersion in PBS. Selected tensile stress-strain dependences of raw films and those immersed in PBS for different pre-set times (3, 6 and 12 months) are given in Fig. 2. The Young's modulus, E; tensile strength, σ_b; elongation-at-break, ε_b; and toughness (expressed as the energy necessary to break the sample per volume unit, $mJ{\cdot}mm^{-3}$) for all samples are given in Table 2.

Fig. 2 and Table 2 show that the tensile properties of the raw four-component PU materials are almost unaffected by the type (and regularity) of the macrodiol chain, which is in contrast to the simpler three-component PU films studied previously [50]. The ultimate tensile strength values of the four-component PUs are almost identical (44.2 MPa for T4-0 and 47.9 MPa for T5-0), as are the elongations-at-break (740% for T4-0 vs. 739% for T5-0). Although the toughnesses of the raw PUs are similar (113.9 mJ mm^{-3} for T4-0 and 115.6 mJ mm^{-3} for T5-0), they are somewhat lower than those found for the three-component PUs, prepared at equimolar ratios of all components (177.5 mJ mm^{-3} for T4-and 147 mJ mm^{-3} for T5-based PU) [50]. The *S*-shape of the tensile curves appearing as the result of strain-induced crystallization is visible for both the raw PU films T4-0 and T5-0, which is similar to the three-component systems described previously [50]. Stress-induced crystallization arises due to chain alignment during uniaxial deformation, leading to a better arrangement of neighbour chains and, finally, to their crystallization, which results in appreciable sample reinforcement [42]. The tensile tests confirm that it is possible to prepare strong elastomeric materials containing D,L-lactide units in the polymer backbone.

From the comparison of the tensile properties of the raw four-component PU systems (containing DLL) with those of the simpler three-component PUs (without DLL) studied previously [50], the following conclusions can be reached:

(1) In contrast to those of the three-component PUs, the tensile characteristics of the more complex four-component PU systems are not influenced by the macrodiol chain regularity [50]. This fact can be explained by the high structural variability of the chains, which enables the formation of higher numbers of different types of reversible bonds (hydrogen bonds and dipole–dipole interactions) in four-component PUs compared with in three-component systems (for details, see, e.g., Fig. 2 in Ref. 45). DLL thus acts as a compatibilising agent, 'effacing' significant features of macrodiol regularity and rigidity in the resulting PU material.

(2) The presence of DLL slightly decreases the elongation-at-break values compared with that in the three-component PU films [50].

(3) The tensile properties of PU made from DLL, HDI and BD, i.e., without any polycarbonate macrodiol, are relatively poor (elongation-at-break ca. 400%, tensile strength ca. 5 MPa, and toughness ca. 13 MPa [46]). That is why the tensile parameters (e.g., toughness) of four-component PUs are generally lower than those of three-component PUs prepared at an equimolar ratio of functional groups (samples T4-1/0 and T5-1/0 in Ref. 50).

However, thanks to the optimization of the composition and the conditions of the preparation procedure, mechanically strong PU materials marked as T4-0 and T5-0 were prepared.

The influence of the PBS immersion time on changes in the tensile properties (see Fig. 2 and Table 2) is very similar in both series, especially for the time scale up to 3 months. Some stress-induced crystallization is detectable only in films immersed up to 3 months for both the T4 and T5 series. However, after 6 months of immersion, the S-shape of the tensile curves disappears. This is most likely caused by structural changes (*e.g.*, by the breaking of long PU chains) due to the hydrolytic processes, as detected by FTIR and DSC (see Chapters 3.3. and 3.5.).

All tensile properties measured are somewhat worse for the T4-12 sample than for the T5-12 sample. Whereas, for example, the toughness of T4-12 represents only 6% of the value of the untreated sample, T4-0, for T5-12, it is 10.5% that of T5-0. The lower toughness may indicate the higher susceptibility of T4-based PU to hydrolysis compared with the T5-based analogue. On the other hand, the toughness values observed in the three-component PUs after 12 months of immersion in PBS were either unchanged (T4-based PU) or decreased merely to 90% of the initial value (T5-based PU) [50].

From the tensile tests, it is clear that DLL is an efficient component prone to hydrolysis that is responsible for the deterioration of the mechanical properties.

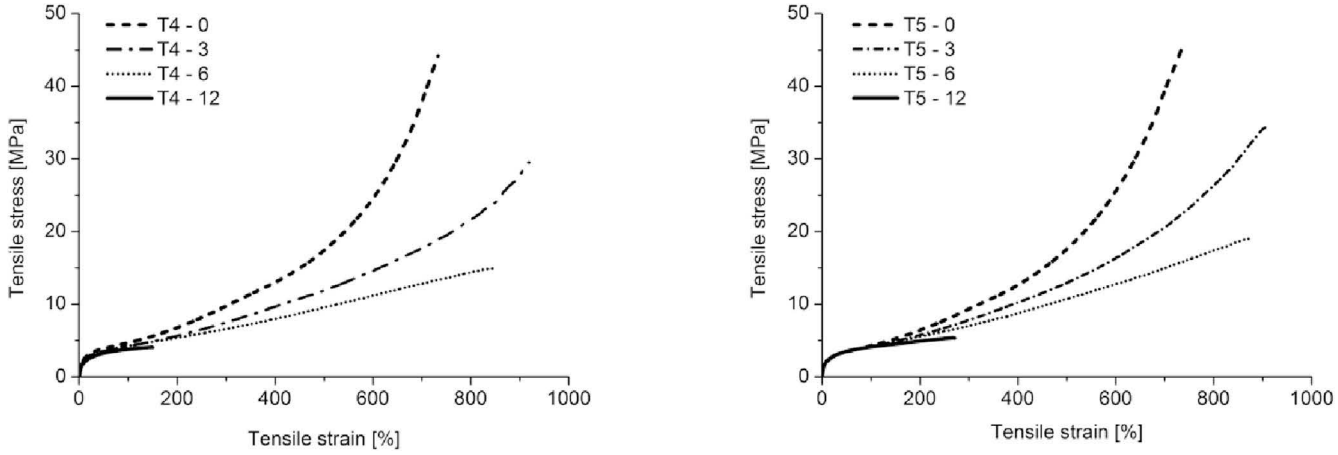

Fig. 2. Stress-strain dependences of the T4-X (left) and T5-X (right) series after 0, 3, 6 and 12 months of immersion in PBS.

Table 2
Selected tensile properties of raw PU films and PU films hydrolytically treated up to 12 months. (a) T4 series, (b) T5 series.

Code	Young's modulus (MPa)	Tensile strength σ_b (MPa)	Elongation-at-break ε_b, (%)	Energy-to-break (toughness) (mJmm^{-3})
(a) T4 series				
T4-0	42.5 ± 7.2	44.2 ± 3.2	740 ± 19	113.9 ± 7.0
T4-1	39.8 ± 5.6	37.0 ± 2.1	799 ± 23	112.3 ± 2.9
T4-3	41.2 ± 6.1	26.3 ± 5.3	868 ± 56	106.2 ± 14.8
T4-6	44.7 ± 3.1	13.9 ± 1.6	823 ± 43	68.5 ± 7.9
T4-9	40.4 ± 2.9	7.2 ± 0.6	509 ± 45	28.7 ± 3.5
T4-12	42.2 ± 3.2	3.9 ± 0.4	184 ± 0.4	7.0 ± 1.7
(b) T5 series				
T5-0	43.6 ± 4.8	47.9 ± 6.3	739 ± 26	115.6 ± 10.8
T5-1	40.8 ± 4.4	48.6 ± 3.0	775 ± 17	125.8 ± 7.2
T5-3	36.5 ± 3.9	36.5 ± 3.9	907 ± 29	128.8 ± 11.1
T5-6	45.5 ± 4.7	18.0 ± 1.5	874 ± 57	87.6 ± 10.9
T5-9	37.9 ± 4.6	8.2 ± 0.7	594 ± 17	35.1 ± 2.8
T5-12	46.3 ± 6.6	5.0 ± 0.4	274 ± 0.4	12.2 ± 1.8

3.2. Water uptake and mass loss experiments

In both series of studied samples, the values of the mass loss and water uptake increase with the time of sample immersion in PBS, which confirms the gradual hydrolytic degradation process of four-component PU films in model physiological conditions (Fig. 3 and Table 3). For 12 months of degradation time, the T5-based samples reach slightly higher water uptake and mass loss values compared with the T4-analogues (Table 3). The maximum values were 1.77 wt % for water uptake and 4.64 wt% for mass loss, both found for the T5-12 sample. As the maximum values of the analogous three-component PUs were 0.38 wt% for water uptake and 0.93 wt% for the mass loss, it is evident that the DLL located regularly in the PU backbone accelerates the hydrolytic process.

3.3. FT-IR spectroscopy and SEC

FTIR analysis was used to elucidate the origin of the gradual deterioration of the mechanical properties proceeding with the increasing immersion time in PBS. This technique was employed because it enables the monitoring of chemical changes occurring at the atomic level caused by temperature, chemical exposure to chemicals (ambient or artificial atmosphere/environment), and radiation [13,14,24,27,29,31,33–35,37]. A detailed analysis of the FTIR spectra of similar three-component polycarbonate (PC)-based PUs with respect to their structural analysis or to the extent of their H-bonding was published previously [42,43].

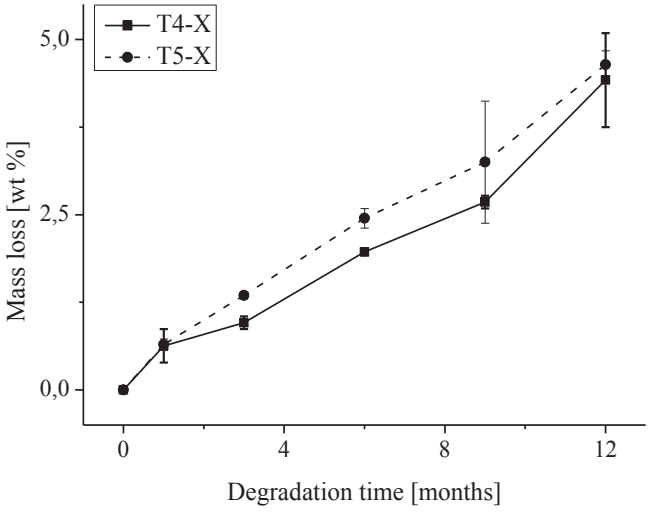

Fig. 3. Dependences of the mass loss on the time of PBS immersion.

In this work, we focus on the chemical and structural changes induced by physiologically simulated conditions. Because both the three- and four-component PUs had been immersed in PBS at 37 °C, they were subjected to the long-term annealing and hydrolysis at the same time. As has been shown previously [50], the three-component systems are hydrolytically stable, without significant mass loss or mechanical property deterioration, after 12 months of immersion in PBS.

In contrast to the three-component systems, the four-component systems were consciously designed to be moderately susceptible to hydrolysis (see Chapter 3.2.). Although the mechanical properties changed significantly with the increasing immersion time in PBS, the FTIR spectra remained nearly identical over the whole period (up to 12 months), as seen in Fig. 4.

Because the condensation reaction is reversible, it was expected that the hydrolysis of the ester groups in the DLL units would lead to the formation of the same significant amounts of carboxyl and hydroxyl groups.

It turns out, however, that no detectable specific stretching vibrations belonging to either hydroxyl OH (approximately 3300 cm^{-1}) or carbonyl C=O (1600-1800 cm^{-1}) were found. The only small, but significant change that occurred was found at approximately 1830 cm^{-1}. To exclude any influence of the PBS solution on the presence of the 1830 cm^{-1} peak in the FTIR spectrum, additional degradation tests in pure water were performed. To accelerate the hydrolysis and induce more pronounced changes in the chemical structure of the PU material (and thus intensify FTIR peaks), the hydrolysis was performed at 90 °C for up to 14 days. The

Table 3
Water uptake and mass loss values of the T4-series (a) and T5-series (b).

Code	Water uptake	Mass loss	Crystallinity
	wt %	wt %	%
(a)			
T4-0	0	0	27
T4-1	0.49 ± 0.15	0.63 ± 0.24	29
T4-3	0.01 ± 0.13	0.96 ± 0.09	35
T4-6	0.42 ± 0.22	1.97 ± 0.05	28
T4-9	0.84 ± 0.55	2.68 ± 0.09	26
T4-12	1.70 ± 0.88	4.42 ± 0.67	27
(b)			
T5-0	0	0	27
T5-1	0.44 ± 0.16	0.65 ± 0.08	30
T5-3	−0.02 ± 0.13	1.35 ± 0.05	36
T5-6	0.51 ± 0.31	2.45 ± 0.14	26
T5-9	1.52 ± 0.96	3.25 ± 0.87	32
T5-12	1.77 ± 0.63	4.64 ± 0.20	27

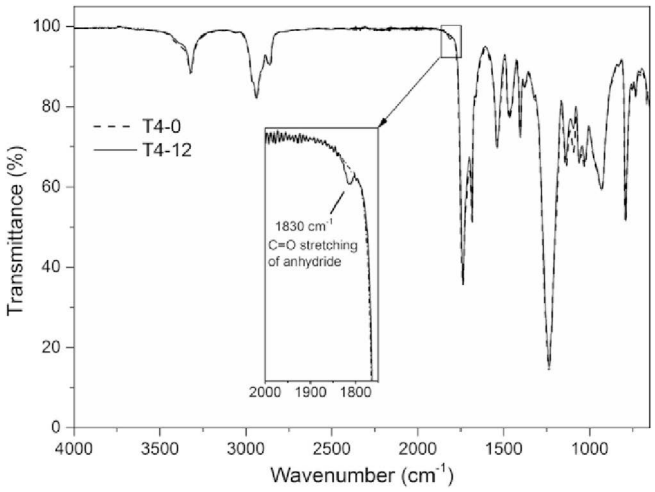

Fig. 4. FTIR spectra of the untreated sample before (T4-0, dashed line) and after 12 months of PBS immersion (T4-12, continuous line).

FTIR spectrum of the T4-0 sample subjected to 14 days hydrolysis in water at 90 °C is presented in Fig. 5.

From Fig. 5, it appears that the presence of the weak band at 1830 cm^{-1} is related more to the structural changes than to the presence of the PBS itself. Because the band in the region between 1810 and 1830 cm^{-1} corresponds to the stretching vibrations of the carbonyl C═O groups in anhydrides, it was concluded that one of the possible degradation paths runs through the formation of carboxylic groups with their subsequent recombination into anhydride groups. The other possible way (presumably the main degradation path) proceeds by the reversible cross-condensation of −OH and −COOH formed by the hydrolysis of ester groups from the DLL units in vicinal chains, as schematically shown in Fig. 6.

From these results, it follows that hydrolytic degradation is a dynamic process in which several recombination processes arising from ester group hydrolysis occur. Because PC-based PUs are highly hydrophobic materials [55], the hydrolysis should begin at the film surface and proceed inwards. This mechanism assumes significant structural changes in the surface and subsurface layers, and subsequently, it can lead to the leaching of polymer chains not involved in chain entanglements from the surface. This behaviour is in

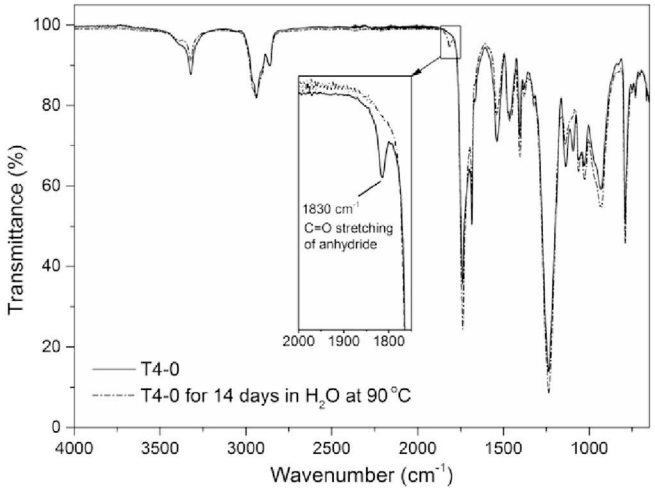

Fig. 5. FTIR spectra of the T4-0 sample before (dashed line) and after accelerated hydrolysis proceeding at 90 °C for 14 days (continuous line).

accordance with the significant mass loss of up to 5 wt % (see Fig. 3), which is not observed in three-component systems prepared without DLL units [50].

The proposed degradation mechanism was additionally supported by the results of the SEC experiments. As can be found in Table 4, no significant changes, either increases or decreases, in the number- and weight-average molar masses of the T4 and T5 series, before and after 12 months of PBS immersion, occurred. This indicates that the average length of the polymer chains leached from the bulk samples remained nearly constant over the entire period of time, and it was time- and environment-independent.

However, the dramatic decrease of the mechanical characteristics is unambiguous (see Chapter 3.1.) Such a deterioration of the mechanical properties is most likely the result of the aforementioned gradual leaching of polymer chains from the material surface (Chapter 3.3.), forming cavities and pores (Chapter 3.4.) and leading to the gradual material thickening and structure deformation. The overall material resistance and toughness are thus significantly reduced.

3.4. Surface morphology

The surface properties significantly influence the serviceability of coatings and films, and they are therefore very important material characteristics. As time- and temperature-dependent surface-morphology changes provide important information on coating/film durability and hence applicability, SEM and AFM analyses of raw PU samples and PU samples subjected to hydrolytic testing were performed in detail.

SEM enables detection of the surface relief on the micrometre-to-millimetre scale, whereas AFM is suitable for the evaluation of nanometre-to-micrometre surface features, including heterogeneity and roughness mapping included.

SEM images have been obtained at magnifications from 200 to 7000×. To visualize representative top and cross-section surface reliefs, a magnification of 750× was chosen for the SEM images, as summarized in Figs. 7 and 8. On the other hand, the SEM images in Fig. 9 showing random imperfections on some PU samples have been obtained with a magnification of 5000×, which makes it possible to compare surface reliefs detectable by AFM. AFM analyses were performed on areas ranging from 1 × 1 μm^2 to 50 × 50 μm^2, but only 10 × 10 μm^2 images are shown in this paper.

Both the SEM and AFM analyses of PU films reveal that the surfaces of raw, untreated PUs have relatively smooth and regular surfaces, although a somewhat 'laced' surface relief is visible, especially for the T4-0 sample. Nano-to micrometre-sized formations adhered on the T5-0 surface, and on almost all T4-X and T5-X films (X ≠ 0) they can be found. These formations are more frequent on the T5-X surfaces compared with their T4-X analogues. Although the reliefs after PBS immersion are more heterogeneous than for the raw PUs, no significant cracking on the surface was observed; the only exception was the T5-9 sample (Fig. 7). This observation supports the hypothesis of the gradual leaching of polymer chains from the film surface caused by hydrolysis, without a significant impact on the morphology changes.

It is necessary to emphasize that after 6 months of PBS immersion, all samples became opaque. However, within several hours after being pulled out from the PBS, they became transparent again. This confirms the high hydrophobicity of PC-based materials after the hydrolytic tests [55] and provides indirect proof of the proposed hydrolytic-recombination mechanism that does not produce significant amounts of hydrophilic groups (such as−OH) in samples submitted to hydrolysis in PBS. Because SEM and AFM imaging was performed on dried samples, insignificant surface differences between the swollen and dry samples cannot be

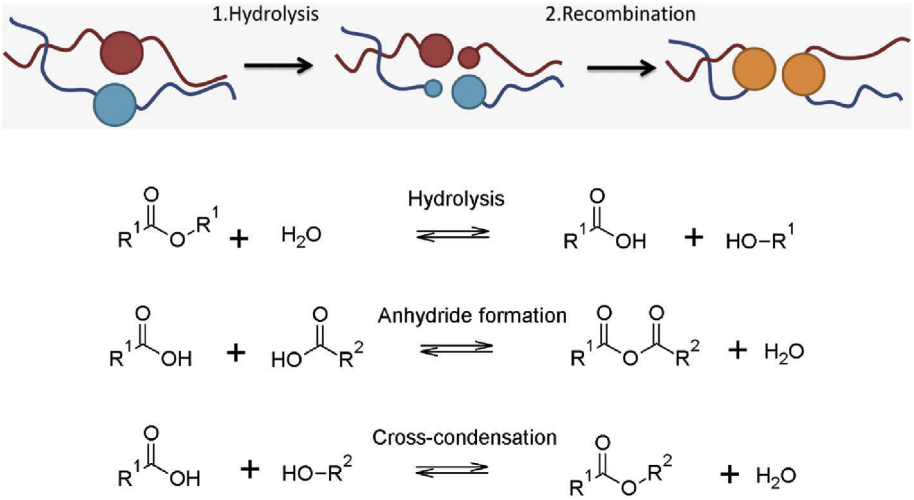

Fig. 6. Outline of possible reversible hydrolysis and recombination of PU chains during the hydrolytic process.

Table 4
Number- (<M_n>) and weight-average (<M_w>) molar masses and dispersity $Đ_M$.

Sample code	$M_n \times 10^4$ g mol^{-1}	$M_w \times 10^4$ g mol^{-1}	$Đ_M$
T4-0	10.0	17.7	1.78
T4-12	10.7	22.7	2.11
T5-0	20.7	24.6	1.19
T5-12	13.5	23.6	1.74

entirely excluded.

When the top and cross-section surface views were analysed (Fig. 8), no significant cracks or material destruction were observed either by SEM or by AFM. All samples are heterogeneous on the nano-to micrometre scale, as detected by AFM phase images in Fig. 8, top-right insets. The heterogeneous character of the PU samples originates from their complex composition (cf. with Figs. 11 and 12 in Ref. [45]). Some organized rod-shaped and radial formations of micrometre-size were detected on the cross-sections of all PUs analysed; the only exception is sample T5-6, which contains numerous nano-to micrometre-sized globular shapes, see Fig. 8, middle. Similar reliefs were also detected on the cross-section surfaces of the three-component PUs studied recently [50]. The organized structures in three- and four-component PU films were assigned to the self-organization of hard-segment domains made from HDI and BD into micrometre-size spherulite formations. The AFM phase views of the three- (Fig. 5 in Ref. 50) and four-component systems (Fig. 8 in this paper) look very similar, although their trends in tensile characteristics after hydrolytic treatment are significantly different. This implies that the hydrolytic process proceeds predominantly in the amorphous soft-segment region, without any significant changes in the highly organized part of the PU material.

Even though a relatively undestroyed surface relief was detected by SEM and AFM, imperfections randomly occur on the film surface, as well as on the cross-section surface, as a result of the dynamic hydrolytic process (in Fig. 9 a and c). Similar formations are detectable via AFM, Fig. 9 b and d.

3.5. Differential scanning calorimetry - DSC

In this research, DSC was used for the characterization of the thermal transitions occurring during the progressive heating of raw PUs, as well as PUs subjected to the hydrolytic degradation process. Our earlier studies indicate that the identification and assignment of observed heat effects to individual components in PUs composed of two different PC and DLL soft segments is extremely difficult – and in a number of cases, almost impossible [46]. The interpretation of the DSC results becomes even more complicated when the PU samples have been subjected to degradation in PBS at 37 °C. This paper exploits the experience gained in our earlier DSC studies of model two-, three- and four-component PU systems [42,44,46]. Thanks to our knowledge of the thermal behaviour of simpler three-component PUs prepared without DLL, we can exploit the DSC results on degradable samples for a deeper understanding of the role of key factors that control the hydrolytic stability [50].

All measured DSC curves are complex and are composed of multiple endothermic peaks in the region between 40 and 150 °C. The glass transition temperature T_g of the amorphous parts of the material occur at around −29 °C in the T4-series and −33 °C in the T5-series. The DSC curves of all samples including the raw and PBS-treated PU films are given in Fig. 10, and the relevant DSC data can be found in Table 5. Due to the presence of multiple peaks, all DSC curves are divided into three temperature regions, which were labelled I, II and III (see Fig. 10).

Low-temperature region I is ascribed to the glass transition of the amorphous part of the soft segments, being either of macrodiol or DLL origin. The second endothermic region (II) shows temperatures between 40 and 100 °C and reflects the thermal behaviour of the PU soft segments, and the third one (III), covering temperatures of approximately 130 °C, is connected with thermal events related to hard BD-HDI segments.

Endothermic region I: The T_g values were found to be somehow lower for the T5-based series (- 32 to - 36 °C) compared with the T4-based series (- 29 to - 32 °C). For the given PU compositions (see Table 1), the difference in the ΔT_g values of the PU films is directly related to the difference in T_g of pure T4 or T5 macrodiols[2] [44]. This indicates a similar extent of phase separation in both (T4 and T5) series. The shift of T_g to a higher temperature (by ca 5 °C) in the four-component PU systems (both T4-and T5-based) compared with the three-component systems studied previously [50] can be attributed a greater extent of phase mixing in the four-component system due to the presence of the D,L-lactide-based diol [46].

[2] T_g values of starting diols are −49 °C for T 4672, -53 °C for T 5652 and -37 °C for DLL.

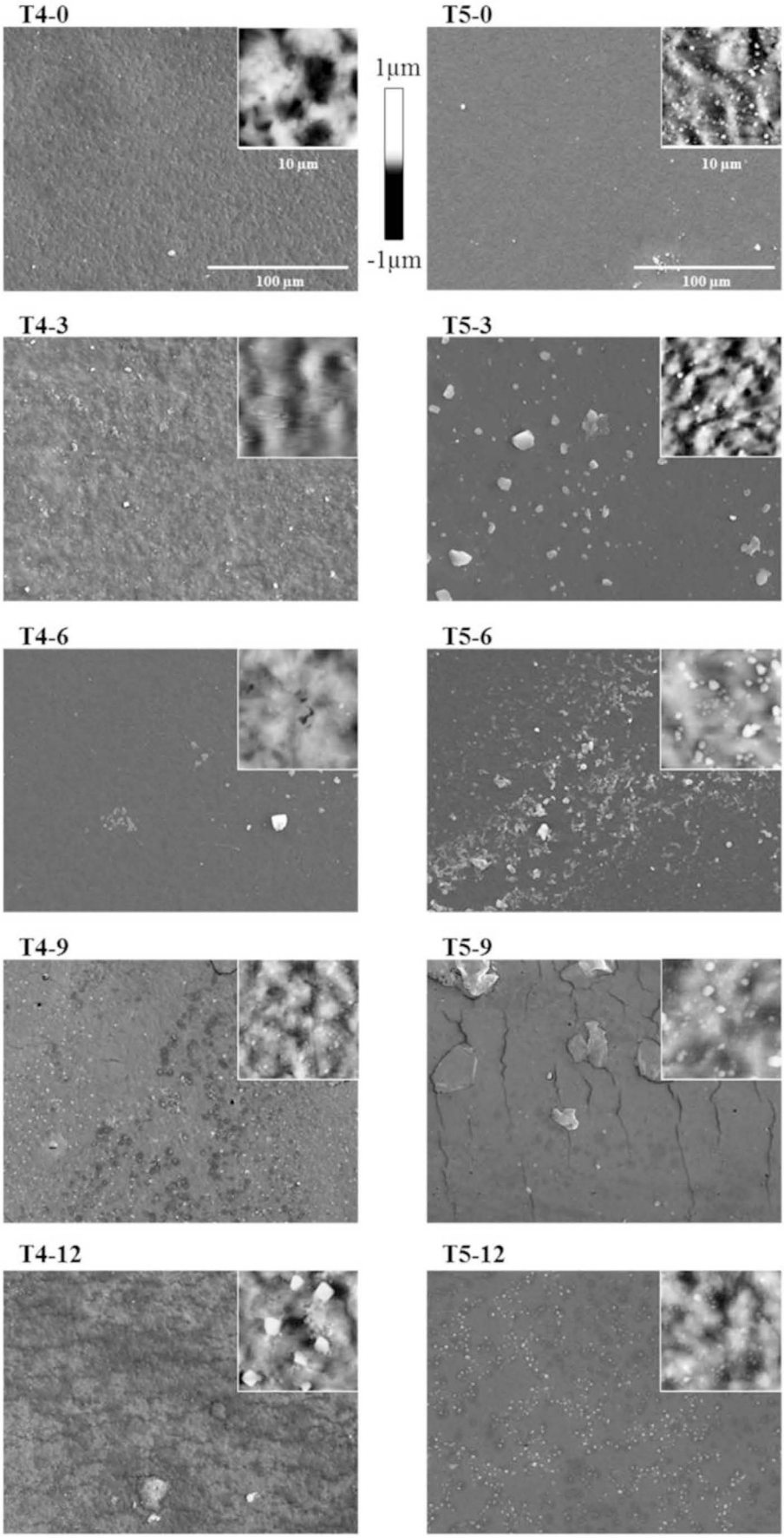

Fig. 7. SEM micrographs of top-side of PU raw T4-0 (top, left) and T5-0 (top, right), and PU films after 3, 6, 9 and 12 month-stability tests (T4-X series: left, T5-series: right). Magnification 750×. Corresponding AFM 2D-height reliefs (10 × 10 μm^2 areas) are given as the right-top insets of each SEM image. A black-and-white scale bar for all height AFM views is placed between the T4-0 and T5-0 SEM images.

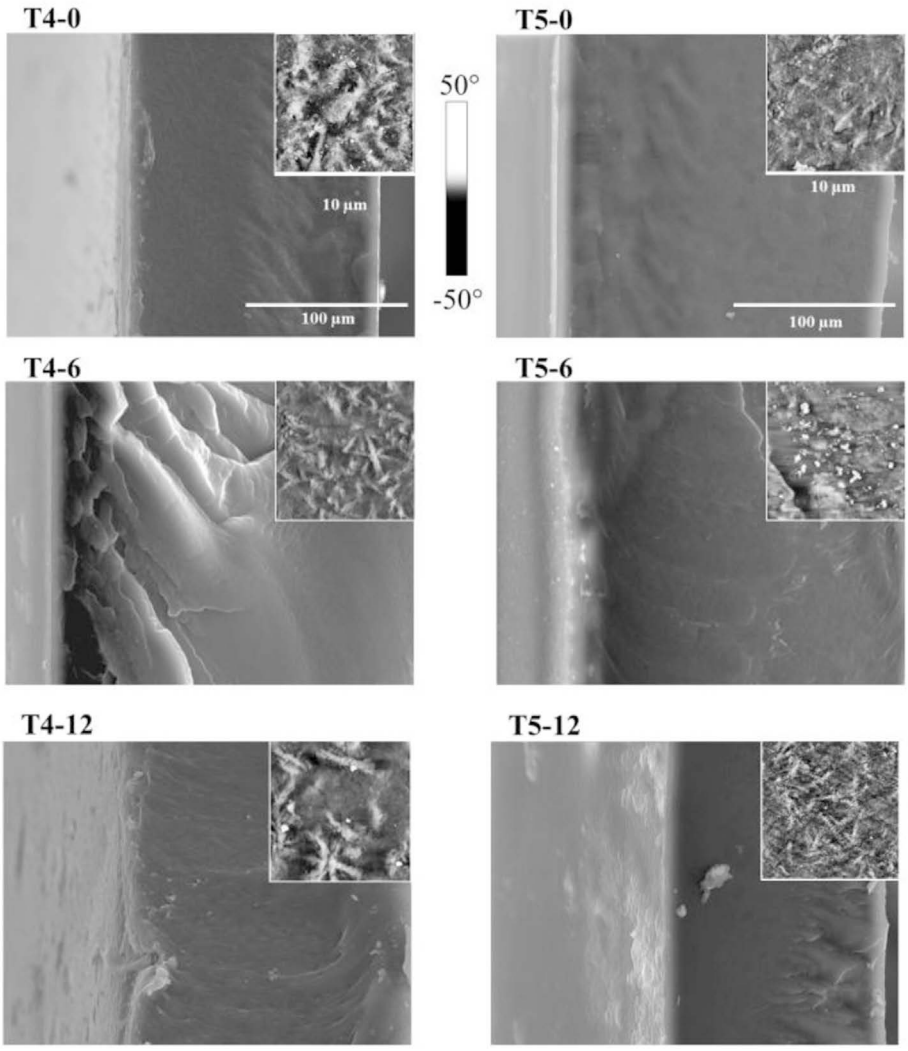

Fig. 8. SEM micrographs of surface reliefs (lighter left part), together with the cross-section surface (darker right part), magnification 750×. Local cross-section heterogeneity views (AFM phase images of area 10 × 10 μm^2) for relevant samples are given in the right-top inset of each SEM image. A black-and-white scale for all AFM phase images is placed between the T4-0 and T5-0 SEM images.

The phase mixing/separation of the soft and hard segments can be assessed from the difference between the T_g of the pure macrodiol and the T_g of the final PU films (ΔT_g) [50]; the higher the ΔT_g, the higher the extent of phase mixing. As the soft segments are composed of ca 20 wt% of DLL and ca 80 wt% of T4 or T5 macrodiol of different T_g values (see footnote ii), the ΔT_g technique for the estimation of the extent of phase mixing/separation is, in the case of complex PU systems, very approximate (for details, see, e.g., Ref. 46). It can be concluded that the T5-based PUs have a slightly higher tendency for phase mixing than their T4-analogues and that the phase mixing slightly decreases with a longer time of PBS immersion due to their slightly higher ΔT_g values in both cases. This observation opposes that of the three-component PUs [50], which were characterized by a very slight tendency to increase the phase mixing with a longer time of PBS immersion.

In the endothermic region II, both raw PUs show a single peak slightly above 50 °C, which is marked in Fig. 10 by a dashed line. The peak maximum is reached at the same temperature (53 °C in T4-0 sample and 54 °C in T5-0 one), which is somewhat lower than that found in the three-component PUs, being ca 58 °C [50].

For the treated PU samples, two peaks are detectable. One peak is at approximately 55 °C, a minor one for shorter times of immersion (1, 3 and 6 months) and the exclusive one for samples T4-9, T4-12 and T5-12. The peak at ca 80 °C, which is not present in the untreated samples, is of temporary character that is detectable only for samples after 1, 3 and 6 months of immersion and for the T5-9 sample.

Based on our previous study of the simpler three-component systems, we assume that the peak at a temperature of approximately 55 °C is associated with the relaxation of the amorphous parts of the soft segments located at the soft-hard segment interphase [44]. The splitting of the original peak and the appearance of a new peak at ca 80 °C is the result of the temperature-induced reorganization of the soft-segment domains and the formation of more organized partially crystalline forms of ordered polycarbonate sequences. Time-dependent measurements show that these crystalline soft-segment domains have a temporary character because the corresponding peaks either diminish (T5-9) or disappear (T4-12 and T5-12) with a longer time of PBS immersion. This phenomenon is related to the presence of DLL because in three-component PU systems, these peaks change negligibly over a period of 12 months (we have recently found that this melting endotherm does not depend on either the PU composition or the type of macrodiol used) [50].

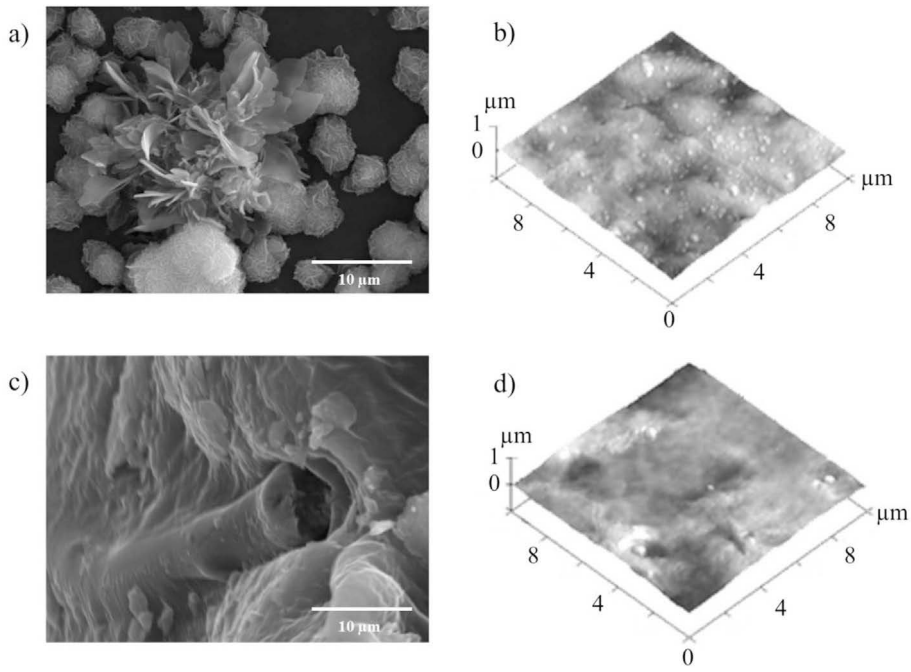

Fig. 9. Examples of surface imperfections detected on T4-9 sample top surface (a) and on T4-12 cross-section surface (c), magnification 5000×. 3D height AFM T4-9 top sample relief (b) and T4-12 cross-section surface relief (d) are shown for comparison.

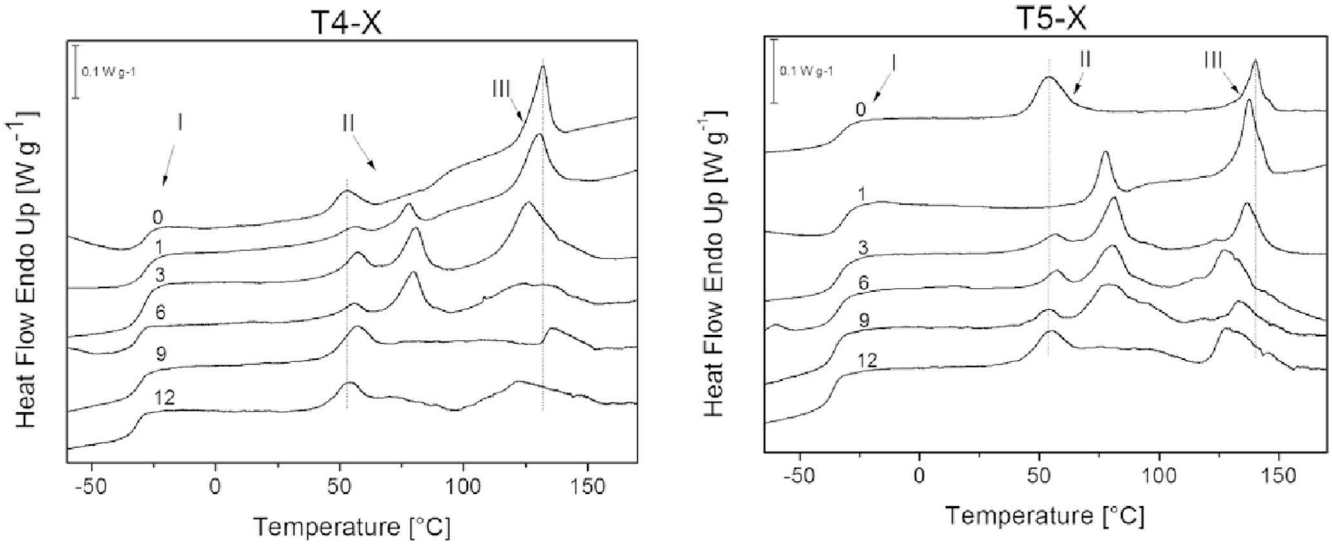

Fig. 10. DSC curves of the T4-X (left) and T5-X (right) series after different times of PBS immersion, where X = 0, 1, 3, 6, 9 and 12. Temperature regions I, II and III are highlighted in figures. (Temperatures of the peak position of both raw PUs in endothermic regions II and III are drawn by broken lines.)

The disappearance of the endotherms at approximately 80 °C can be rationalized by the results obtained from tensile testing and FTIR analysis (see chapter 3. 1 and 3.3.). As already mentioned and confirmed by FTIR, ester groups originating from D,L-lactide diol hydrolyse and subsequently can form anhydride groups. Because DLL units are present in both the hard and soft segment domains, such reorganization leads to structural changes in both the amorphous and crystalline regions of the polycarbonate soft segments together with ordered/crystalline hard segment domains.

The multiple endothermic processes in region III (over 100 °C) are related to the gradual melting of different crystalline hard-segment domains of different size distributions and orderings, or they can be associated with the mixing transition of the soft and hard segments [54]. Raw samples T4-0 and T5-0 and also T5-1 are distinguished by sharp peaks with maxima at 130 °C (T4-based series) and approximately 140 °C (T5-based series). The presence of a sharp melting endotherm indicates the relatively narrow size and length distributions of the hard segment crystals.

Distinctive changes in the peak shapes are related to the re-organization of the polymer structure caused by the hydrolysis of the ester groups in DLL units. The structural changes are not, however, reflected by the overall change in the degree of crystallinity. Therefore, the loss of mechanical properties is more a result of the structure modification than the hydrolysis itself. Changes in the endotherm peak appearance may indicate that hydrolysis, and thus bond scission and re-organization, proceeds to some extent in

Table 5
Thermal properties of raw and treated PU films: T4-X (a) and T5-X (b).

Sample	T_g (°C)	T_r (°C)	ΔH_r (J g^{-1})	$(T_m)_s$ (°C)	$(\Delta H_m)_s$ (J g^{-1})	$(T_m)_h$ (°C)	$(\Delta H_m)_h$ (J g^{-1})
(a) T4-X							
T4-0	−30	53	2	–	–	132	7
T4-1	−29	55	*	78	3	131	8
T4-3	−29	58	1	80	4	126	(8)*
T4-6	−32	56	1	80	5	125	(7)*
T4-9	−30	56	4	–	–	136	(4)*
T4-12	−32	54	3	–	–	122	(9)*
(b) T5-X							
T5-0	−33	54	8	–	–	140	5
T5-1	−32	–	–	78	3	138	7
T5-3	−33	56	(1)*	81	4	133	6
T5-6	−34	57	(1)*	80	5	127	(5)*
T5-9	−35	53	(1)*	79	*	133	(5)*
T5-12	−36	54	4	–	–	128	(6)*

* (−) ΔH_x values could not be determined quantitatively *or precisely (−)*

the hard segment domains, as well.

Previous experiments on-three component PUs [50] revealed that in the temperature transitions of T5-based PUs, i.e., T_g values of soft segments, relaxation processes in region II corresponding to soft-segment melting and relaxation temperatures, as well as the hard-segment melting temperature in region III, had systematically lower values than those of the T4-series. The cause of these behavioural differences was explained by the more irregular structure of the T5 macrodiol compared with the more rigid and regular character of T4 [50]. Unfortunately, the present study on four-component PUs did not confirm the observations described previously. For example, the T_{peak} values in regions II and III are very similar in the T4-and T5-series. DLL thus partially acts as a compatibilising agent, and the temperature differences in the properties of T4-and T5-based systems diminish. Moreover, four-component T4-based PU films are even more susceptible to hydrolysis compared with their T5 analogues.

Relatively surprising is the behaviour of PU samples at the melting temperatures in the III region (from 100 to 140 °C) when the three- and four-component PU systems are compared. The melting temperatures in region III are attributed to the disruption of the highly organized crystalline domains, being the same in composition (BDI + HDI products) and very similar in percentages. They should therefore exhibit similar values.

In general, the melting temperatures were found to be higher by ca 11 °C for all T4-based three-component systems compared with T5-based three-component systems [50]. On the other hand, four-component T4-and T5-based PUs have very similar melting temperatures, with even a slight tendency for T5-based PUs to have higher melting temperatures. Clearly, the behaviour of the more regular T4 soft-segment macrodiol regions contributes to a better arrangement and packing of the hard segments in three-component PU systems [50]. In four-component systems, on the other hand, the packing of the hard-segments is independent of the macrodiol used.

Highly organized (crystalline) soft, soft/hard and hard structures in regions II and III start to decompose after 6 months of PBS immersion, more significantly in the T4-series, to some extent. However, the WAXD experiments (Chapter 3.6.) did not confirm significant changes in the overall crystallinity caused by the hydrolytic treatment. This phenomenon can be explained by the fact that the hydrolytic treatment predominantly affects the amorphous soft-segment region, whereas the more organized/crystalline domains of the soft and preferably hard segments undergo changes only in the degree of ordering. This results in a decrease in $(T_m)_h$ and a broadening of the corresponding peaks for a longer immersion time, but the total $(\Delta H_m)_h$ values remain relatively constant for all samples, as is evident from Table 5.

3.6. WAXD

WAXD experiments have been performed as a complementary method to DSC analysis. WAXD profiles of the T4-X samples are shown in Fig. 11. After peak decomposition, which was made by Fityk fitting software [56], the degree of crystallinity was calculated as a ratio of the area under the crystalline peaks to total area under the diffractogram. The percent crystallinity for the T4-X and T5-X series is given in Table 3, 4th column. The results are very similar for the two series. From the sample composition (Table 1), and similar to previous experiments [46], it is obvious that the segments generally considered to be soft segments (i.e., PC and DL-L units) have to participate in crystalline domains and contribute to the overall degree of crystallinity measured by WAXD. It is clearly visible that neither the WAXD profiles or percentages of crystallinity are influenced by the hydrolytic treatment. The lack of significant changes in the WAXD results but substantial differences in the tensile properties and thermal (DSC) characteristics indicate that simultaneous overwhelming processes during the hydrolytic experiments proceed without any significant impact on the overall crystallinity degree. This means that the most important effects, which lead to the changes in the tensile properties, occur in the amorphous phase. The detection of highly organized spherulite formations even in samples featuring poor mechanical properties (T4-12 and T5-12 in Fig. 9) is the other information supporting our statement. The crystallinity slightly increases for a shorter time of hydrolysis (up to 3 months in both series) and then decreases and reaches similar values to those found in raw PU samples. The average size of all crystals in the PU samples was calculated using Scherrer's equation to be approximately 4 nm.

4. Conclusions

The degradability of two highly elastomeric four-component PU films immersed in model physiological conditions (37 °C, pH = 7.4) for time periods of up to 12 months was tested by a combination of several experimental methods. A detailed multi-scale description of the changes occurring on the surface and in the bulk of PU films during hydrolytic experiments was achieved using tensile tests, SEM, AFM, DSC, WAXD, SEC, FTIR and swelling tests. The behaviour

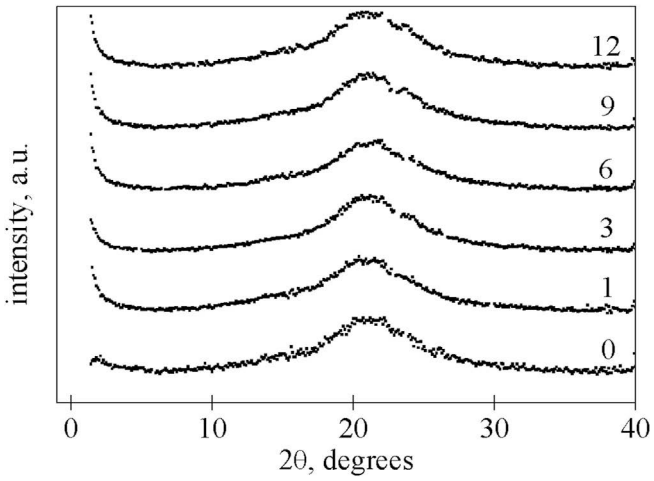

Fig. 11. WAXD profiles of the T4-X series. Time of sample immersion in months is given in the figure on the right side.

reflects a complex degradation process accompanied by structural changes depending on (i) the time of immersion in the liquid PBS medium and (ii) the temperature.

All PU samples have a segmental character. Both the hard and soft segments are composed of two components: the soft segments are either polycarbonate or D,L-lactide in origin, whereas the hard segments are products of diisocyanate-1,6-hexane and butane-1,4-diol. All PUs are formed by linear chains containing, in addition to non-polar (exclusively aliphatic) hydrocarbons, polar urethane, carbonate and ester groups. The building units self-assemble and form either permanent soft- and hard-segmental domains up to micrometre size or "stimuli-responding" domains that can be temporarily broken and re-built because they contain reversible crosslinking centres, such as hydrogen bonds and dipole–dipole interactions. This re-organization, re-packing and possible partial co-crystallization caused by long-term temperature conditioning (pronounced at the beginning of the stability tests, mainly in the soft-segment region and on the soft-hard segment interface, which has a strong impact on the tensile properties) was detected by a combination of characterization techniques – particularly by WAXD and DSC analyses.

The study shows that the chain regularity of the macrodiol has a negligible impact on the tensile properties of both the untreated PU films, which exhibit a high tensile strength (ca 45 MPa) and elongation-at break (ca 740%) and, hence, toughness (ca 115 mJ mm^{-3}). The tensile characteristics confirmed a very good and efficient DLL build-up into the PU chain. The gradual deterioration of the tensile properties starts after three months of PBS immersion, and it is more obvious in the PUs made from the more rigid and more regular T4 macrodiol compared with the T5 macrodiol. For example, the resulting toughness of the T4-based sample is approximately 6% of its original value, whereas the T5-analogue retains ca. 11% toughness, after 12 months of PBS immersion.

DSC measurements confirmed the changes in the thermal characteristics under conditions mimicking the physiological environment. Whereas the T_g of the soft segments were almost unchanged, differences were observed in the endotherm regions assigned to both the soft-segment and hard-segment thermal transitions. Whereas the sharp peaks in the endotherm region over 100 °C assigned to highly organized (crystalline) hard-segment domains became broader and shifted to lower temperatures, the endotherm region between 50 and 80 °C, which is ascribed to the thermal transitions of either soft segments or the mixing transition of soft and hard segments, has an even more complicated thermal history. All these characteristics confirmed the very complicated character of the PU films, reflecting the re-organization and re-packing of PU chains proceeding simultaneously with the hydrolytic process. As the WAXD experiments did not find any significant differences in the overall degree of crystallinity (ranking in all cases between 26 and 36%), the hydrolysis proceeds predominantly in the amorphous part of the material, i.e., in the soft-segment region.

Practically no changes in the IR spectra caused by hydrolysis were detected, with only the peak at ca. 1830 cm^{-1} pertaining to the stretching of carbonyl groups of anhydrides being aroused. This phenomenon is assigned to the proposed degradation paths running through the carboxylic group formation with subsequent recombination into anhydride groups. The other possible formation of anhydrides could proceed via the cross-coupling of –OH and –COOH formed by the hydrolysis of vicinal chains. The combination of spectroscopy results with the results of other techniques suggests that this hydrolytic process should cause gradual polymer chain leaching from the film after the recombination or cross-coupling reaction in the amorphous part of the PU film.

The hydrolytic process does not significantly influence the overall PU film morphology, either on the surface of the material or inside it, although rare channels or local imperfections are detectable, as proof of the hydrolytic efficiency. The very low water uptake (swelling) indicates the hydrophobic character of the materials. The mass loss gradually increases with time, and it reaches a maximum value of ca 5 wt% after 12 months of PBS immersion.

In complex PU systems, the DL-lactide based oligomer was found to be an efficient component for the hydrolytic process, even at a relatively low concentration (ca 9 wt %).

Acknowledgement

The authors wish to express their thanks for the financial support of the Grant Agency of the Czech Republic (Czech Science Foundation, project No. 13-06700S). Magdalena Serkis would like to thank the Charles University Faculty of Science for the opportunity to pursue her PhD studies.

References

[1] S. Gogolewski, A.J. Pennings, An artificial skin based on biodegradable mixtures of polylactides and polyurethanes for full-thickness skin wound covering, Macromol. Rapid. Commun. 10 (4) (1983) 675–680.
[2] G. Golomb, D. Wagner, Development of a new invitro model for studying implantable polyurethane calcification, Biomaterials 12 (4) (1991) 397–405.
[3] G. Lopezlopez, A. Pascual, E.J. Perea, Effect of plastic catheter material on bacterial adherence and viability, J. Med. Microbiol. 34 (6) (1991) 349–353.
[4] M. Pavlova, M. Draganova, Biocompatible and biodegradable polyurethane polymers, Biomaterials 14 (13) (1993) 1024–1029.
[5] M.C. Tanzi, D. Mantovani, P. Petrini, R. Guidoin, G. Laroche, Chemical stability of polyether urethanes versus polycarbonate urethanes, J. Biomed. Mater. Res. 36 (4) (1997) 550–559.
[6] L. Pinchuk, A review of the biostability and carcinogenity of polyurethanes in medicine and the new-generation of biostable polyurethanes, J. Biomat. Sci. Polym. E 6 (63) (1994) 225–267.
[7] P.A. Gunatillake, D.J. Martin, G.F. Meijs, S.J. McCarthy, R. Adhikari, Designing biostable polyurethane elastomers for biomedical implants, Aust. J. Chem. 56 (6) (2003) 545–557.
[8] R.S. Labow, E. Meek, J.P. Santerre, Hydrolytic degradation of poly(carbonate)-urethanes by monocyte-derived macrophages, Biomaterials 22 (22) (2001) 3025–3033.
[9] L.J. Zhou, D. Liang, X.L. He, J.H. Li, H. Tan, J.S. Li, Q. Fu, Q. Gu, The degradation and biocompatibility of pH-sensitive biodegradable polyurethanes for intracellular multifunctional antitumor drug delivery, Biomaterials 33 (9) (2012) 2734–2745.
[10] S. Baudis, S.C. Ligon, K. Seidler, G. Weigel, C. Grasl, H. Bergmeister, H. Schima, R. Liska, Hard-block degradable thermoplastic urethane-elastomers for electrospun vascular prostheses, J. Polym. Sci. Pol. Chem. 50 (7) (2012) 1272–1280.
[11] C.H. Tsou, H.T. Lee, M. De Guzman, H.A. Tsai, P.N. Wang, H.J. Cheng, M.C. Suen, Synthesis of biodegradable polycaprolactone/polyurethane by curing with H2O, Polym. Bull. 72 (7) (2015) 1545–1561.
[12] Q. Xing, R.B. Li, X. Dong, X.Q. Zhang, L.Y. Zhang, D.J. Wang, Phase morphology, crystallization behavior and mechanical properties of poly(L-lactide) toughened with biodegradable polyurethane: effect of composition and hard segment ratio Chinese, J. Polym. Sci. 33 (9) (2015) 1294–1304.
[13] B.R. Barrioni, S.M. de Carvalho, R.L. Orefice, A.A.R. de Oliveira, M.D. Pereira, Synthesis and characterization of biodegradable polyurethane films based on HDI with hydrolyzable crosslinked bonds and a homogeneous structure for biomedical applications, Mat. Sci. Eng. C Mater. 52 (2015) 22–30.
[14] A. Nakkabi, M. Sadiki, M. Fahim, N. Ittobane, S.I. Koraichi, H. Barkai, S. El Abed, Biodegradation of poly(ester urethane)s by Bacillus subtilis, Int. J. Environ. Res. 9 (1) (2015) 157–162.
[15] J.E. McBane, S. Sharifpoor, K.H. Cai, R.S. Labow, J.P. Santerre, Biodegradation and in vivo biocompatibility of a degradable, polar/hydrophobic/ionic polyurethane for tissue engineering applications, Biomaterials 32 (26) (2011) 6034–6044.
[16] F. Khan, Y. Dahman, A novel approach for the utilization of biocellulose nanofibers in polyurethane nanocomposites for potential applications in bone tissue implants, Des. Monomers Polym. 15 (1) (2012) 1–29.
[17] H.Y. Mi, X. Jing, M.R. Salick, X.F. Peng, L.S. Turng, A novel thermoplastic polyurethane scaffold fabrication method based on injection foaming with water and supercritical carbon dioxide as coblowing agents, Polym. Eng. Sci. 54 (12) (2014) 2947–2957.
[18] Q.Z. Chen, S.L. Liang, G.A. Thouas, Elastomeric biomaterials for tissue engineering, Prog. Polym. Sci. 38 (3–4) (2013) 584–671.
[19] H.Y. Mi, M.R. Salick, X. Jing, B.R. Jacques, W.C. Crone, X.F. Peng, L.S. Turng, Characterization of thermoplastic polyurethane/polylactic acid (TPU/PLA) tissue engineering scaffolds fabricated by microcellular injection molding,

Mater. Sci. Eng. C Mater. 33 (8) (2013) 4767–4776.
[20] J.Y. Cherng, T.Y. Hou, M.F. Shih, H. Talsma, W.E. Hennink, Polyurethane-based drug delivery systems, Int. J. Pharm. 450 (1–2) (2013) 145–162.
[21] C. Vitale-Brovarone, G. Ciapetti, E. Leonardi, N. Baldini, O. Bretcanu, E. Verne, F. Baino, Resorbable glass-ceramic phosphate-based scaffolds for bone tissue engineering: Synthesis, properties, and in vitro effects on human marrow stromal cells, J. Biomater. Appl. 26 (4) (2011) 465–489.
[22] J. Grzesiak, K. Marycz, D. Szarek, P. Bednarz, J. Laska, Polyurethane/polylactide-based biomaterials combined with rat olfactory bulb-derived glial cells and adipose-derived mesenchymal stromal cells for neural regenerative medicine applications, Mat. Sci. Eng. C Mater. 52 (2015) 163–170.
[23] H. Janik, M. Marzec, A review: fabrication of porous polyurethane scaffolds, Mat. Sci. Eng. C Mater. 52 (2015) 586–591.
[24] B. Imre, D. Bedő, A. Domján, P. Schön, G.J. Vancso, B. Pukánszky, Structure, properties andinterfacial interactions in poly(lactic acid)/polyurethane blends prepared by reactive processing, Eur. Polym. J. 49 (10) (2013) 3104–3113.
[25] C. Prisacariu, Polyurethane Elastomers: from Morphology to Mechanical Aspects, Springer-Verlag Wein, 2011.
[26] J. Brzeska, A. Heimowska, W. Sikorska, L. Jasinska-Walc, M. Kowalczuk, M. Rutkowska, Chemical and enzymatic hydrolysis of polyurethane/polylactide blends, Int. J. Polym. Sci. (2015). Article Number: 79598.
[27] K.A. Barrera-Rivera, L. Peponi, A. Marcos-Fernandez, J.M. Kenny, A. Martinez-Richa, Synthesis, characterization and hydrolytic degradation of polyester-urethanes obtained by lipase biocatalysis, Polym. Degrad. Stabil. 108 (2014) 188–194.
[28] P. Król, B. Król, P. Chmielarz, J. Wojturska, Assesment of susceptibility to hydrolytic degradation of different types of polyurethanes in terms of their use a biomaterials, Polimery 58 (4) (2013) 282–291.
[29] G.R. da Silva, A. da Silva-Cunha, F. Behar-Cohen, E. Ayres, R.L. Orefice, Biodegradation of polyurethanes and nanocomposites to non-cytotoxic degradation products, Polym. Degrad. Stabil. 95 (4) (2010) 491–499.
[30] M. Ramirez, K.R. Miller, M.D. Soucek, Linking of oligoesters hydrolysis to polyurethane coatings, J. Appl. Polym. Sci. 131 (9) (2014) 40198.
[31] X.H. Kong, G.G. Liu, J.M. Curtis, Novel polyurethane produced from canola oil based poly(ether ester) polyols: synthesis, characterization and properties, Eur. Polym. J. 48 (12) (2012) 2097–2106.
[32] M.C. Tanzi, S. Fare, P. Petrini, In vitro stability of polyether and polycarbonate urethanes, J. Biomater. Appl. 14 (4) (2000) 325–348.
[33] M. Sobczak, C. Debek, E. Oledzka, G. Nalecz-Jawecki, W.L. Kolodziejski, M. Rajkiewicz, Segmented polyurethane elastomers derived from aliphatic polycarbonate and poly(ester-carbonate) soft segments for biomedical applications, J. Polym. Sci. A Polym. Chem. 50 (18) (2012) 3904–3913.
[34] D.K. Dempsey, C. Carranza, C.P. Chawla, P. Gray, J.H. Eoh, S. Cereceres, E.M. Cosgriff-Hernandez, Comparative analysis of in vitro oxidative degradation of poly(carbonate urethanes) for biostability screening, J. Biomed. Mater. Res. A 102 (10) (2014) 3649–3665.
[35] L.H. Chan-Chan, R. Solis-Correa, R.F. Vargas-Coronado, J.M. Cervantes-Uc, J.V. Cauich-Rodriguez, P. Quintana, P. Bartolo-Perez, Degradation studies on segmented polyurethanes prepared with HMDI, PCL and different chain extenders, Acta Biomater. 6 (6) (2010) 2035–2044.
[36] K.A. Chaffin, X.J. Chen, L. McNamara, F.S. Bates, M.A. Hillmayes, Polyether urethane hydrolytic stability after exposure to deoxygenated water, Macromolecules 47 (15) (2014) 5220–5226.
[37] L. Rueda, B.F. d'Arlas, M.A. Corcuera, A. Eceiza, Biostability of polyurethanes. Study from the viewpoint of microphase separated structure, Polym. Degrad. Stabil. 108 (2014) 195–200.
[38] E.M. Christenson, J.M. Anderson, A. Hittner, Biodegradation mechanisms of polyurethane elastomers, Corros. Eng. Sci. Techn 42 (4) (2007) 312–323.
[39] J.H. Zhu, Z.R. Shen, L.T. Wu, S.L. Yang, Invitro degradation of polylactide and poly(lactide-co-glycolide) microspheres, J. Appl. Polym. Sci. 43 (11) (1991) 2099–2106.
[40] B. Ochiai, H. Amemiya, H. Yamazaki, T. Endo, Synthesis and properties of poly(carbonate-urethane) consisting of alternating carbonate and urethane moieties, J. Polym. Sci. A Polym. Chem. 44 (9) (2006) 2802–2808.
[41] Y.W. Tang, R.S. Labow, J.P. Santerre, Isolation of methylene dianiline and aqueous-soluble biodegradation products from polycarbonate-polyurethanes, Biomaterials 24 (17) (2003) 2805–2819.
[42] M. Špírková, J. Pavličević, A. Strachota, R. Poręba, O. Bera, L. Kapráková, J. Baldrian, M. Šlouf, N. Lazić, J. Budinski-Simendić, Novel polycarbonate-based polyurethane elastomers: composition-property relationship, Eur. Polym. J. 47 (5) (2011) 959–972.
[43] M. Špírková, R. Poręba, J. Pavličević, L. Kobera, J. Baldrian, M. Pekárek, Aliphatic polycarbonate-based polyurethane elastomers and nanocomposites. I. The influence of hard-segment content and macrodiol-constitution on bottom-up self-assembly, J. Appl. Polym. Sci. 126 (3) (2012) 1016–1030.
[44] R. Poręba, M. Špírková, L. Brožová, N. Lazić, J. Pavličević, A. Strachota, Aliphatic polycarbonate-based polyurethane elastomers and nanocomposites. II. mechanical, thermal, and gas transport properties, J. Appl. Polym. Sci. 127 (1) (2013) 329–341.
[45] M. Špírková, L. Machová, L. Kobera, J. Brus, R. Poręba, M. Serkis, A. Zhigunov, Multiscale approach to the morphology, structure, and segmental dynamics of complex degradable aliphatic polyurethanes, J. Appl. Polym. Sci. 132 (10) (2015) 41590.
[46] R. Poręba, J. Kredatusová, J. Hodan, M. Serkis, M. Špírková, Thermal and mechanical properties of multiple-component aliphatic degradable polyurethanes, J. Appl. Polym. Sci. 132 (2015) 41872.
[47] R. Poręba, M. Špírková, J. Pavličević, J. Budinski-Simendić, K.M. Szecsenyi, B. Hollo, Aliphatic polycarbonate-based polyurethane nanostructured materials. The influence of the composition on thermal stability and degradation, Compos. Part B Eng. 58 (2014) 496–501.
[48] C. Zhang, X.J. Jiang, Z.Y. Zhao, L.X. Mao, L.Q. Zhang, P. Coates, Effects of wide-range gamma-irradiation doses on the structures and properties of 4,4'-dicyclohexyl methane diisocyanate based poly(carbonate urethane)s, J. Appl. Polym. Sci. 131 (22) (2014) 41049.
[49] J. Kozakiewicz, G. Rokicki, J. Przybylski, K. Sylwestrzak, P.G. Parzuchowski, K.M. Tomczyk, Studies of the hydrolytic stability of poly(urethane-urea) elastomers synthesized from oligocarbonate diols, Polym. Degrad. Stabil. 95 (12) (2010) 2413–2420.
[50] M. Serkis, M. Špírková, R. Poręba, J. Hodan, J. Kredatusová, D. Kubies, Hydrolytic stability of polycarbonate-based polyurethane elastomers tested in physiologically simulated conditions, Polym. Degrad. Stabil. 119 (2015) 23–34.
[51] L. Tatai, T.G. Moore, R. Adhikari, F. Malherbe, R. Jayasekara, I. Griffiths, A. Pathiraja, P.A. Gunatillake, Thermoplastic biodegradable polyurethanes: The effect of chain extender structure on properties and in-vitro degradation, Biomaterials 28 (36) (2007) 5407–5417.
[52] C.G. Pitt, M.M. Gratzl, G.L. Kimmel, J. Surles, A. Schindler, Aliphatic polyesters 2. The degradation of poly(DL-lactide), poly(epsiloncaprolactone), and their copolymerss in vivo, Biomaterials 2 (4) (1981) 215–220.
[53] J.W. Leenslag, A.J. Pennings, R.R.M. Bos, F.R. Rozema, G. Boering, Resorbable materials of poly(L-lactide). 7. In vivo and in vitro degradation, Biomaterials 8 (4) (1987) 311–314.
[54] A. Saiani, C. Rochas, G. Eeckhaut, W.A. Daunch, J.W. Leenslag, J.S. Higgins, Origin of multiple melting endotherms in a high hard block content polyurethane. 2. Structural investigation, Macromolecules 37 (4) (2004) 1411–1421.
[55] M. Serkis, R. Poręba, J. Hodan, J. Kredatusová, M. Špírková, Preparation and characterization of thermoplastic water-borne polycarbonate-based polyurethane dispersions and cast films, J. Appl. Polym. Sci. 132 (42) (2015) 42672.
[56] M. Wojdyr, Fityk: a general-purpose peak fitting program, J. Appl. Crystallogr. 43 (5) (2010) 1126–1128.